SCIENCE APPLICATIONS, INC.

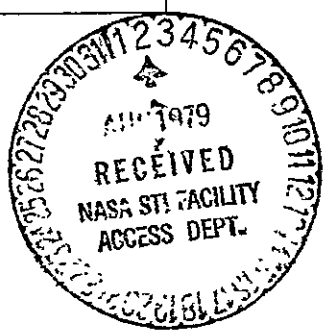

FIRST PRINCIPLES NUMERICAL MODEL OF AVALANCHE-INDUCED ARC DISCHARGES IN ELECTRON-IRRADIATED SPACECRAFT DIELECTRICS

SAI-102-79-002

MARCH 1979

SAI

ATLANTA • ANN ARBOR • BOSTON • CHICAGO • CLEVELAND • DENVER • HUNTSVILLE • LA JOLLA
LITTLE ROCK • LOS ANGELES • SAN FRANCISCO • SANTA BARBARA • TUCSON • WASHINGTON

1 Report No.	2. Government Accession No.	3. Recipient's Catalog No.
CR 159560		

4. Title and Subtitle	5. Report Date
First Principles Numerical Model of Avalanche-Induced Arc Discharges in Electron-Irradiated Dielectrics	March, 1979
	6. Performing Organization Code SAI-102-79-002

7 Author(s)	8. Performing Organization Report No
B. L. Beers, V. W. Pine, H. C. Hwang, H. W. Bloomberg, D. L. Lin, M. J. Schmidt and D. J. Strickland	

9. Performing Organization Name and Address	10. Work Unit No.
Science Applications, Inc. Radiation and Electromagnetics Division 8330 Old Courthouse Road, Suite 510 Vienna, VA 22180	YOS 7059
	11. Contract or Grant No. NAS3-21378
	13. Type of Report and Period Covered Final, July 1978 ti Feb. 1979

12. Sponsoring Agency Name and Address	14. Sponsoring Agency Code
NASA-Lewis Research Center 21000 Brookpark Road Cleveland, OH 44135	6124

15. Supplementary Notes

16 Abstract

A first principles numerical model of avalanche-induced arc discharges in electron-irradiated dielectrics is developed. The model consists of four phases: single electron dynamics, single electron avalanche, negative streamer development, and tree formation. Numerical algorithms and computer code implementations are presented for the first three phases. An approach to developing a code description of fourth phase is discussed. Numerical results are presented for a crude material model of Teflon.

Single electron dynamics are described using a linear Boltzmann equation for the single electron distribution function. The equation is solved using a single scatter Monte Carlo code SEMC. The scattering processes include electron-acoustic phonon, electron-optical phonon, and electron induced electron-hole pair creation. Numerical results include mobility, diffusion coefficients, ionization length, and distribution of ionization sites as a function of field strength. These results are used to develop a single-electron induced avalanche using a simple individual particle Monte Carlo code CASCAD. Numerical results include the electron, hole, and net charge distributions, as well as the space-charge field generated by the charges. Further evolution of the avalanche is followed in a continuum approximation. A code, ACORN, has been developed which solves for the self-consistent evolution of the electron distribution and the electric field as a function of time. Numerical results suggest that a growing, propagating ionization front develops which leaves behind a conducting channel. Strong field ennancement is seen.

17. Key Words (Suggested by Author(s))	18. Distribution Statement
dielectric breakdown, dielectric, spacecraft charging, streamer, avalanche, discharge, Lichtenberg Figure, collision ionization	Publicly Available.

19. Security Classif (of this report)	20. Security Classif. (of this page)	21. No. of Pages	22. Price*
Unclassified	Unclassified	202	

* For sale by the National Technical Information Service, Springfield, Virginia 22161

TABLE OF CONTENTS

APPENDICES

Section 1

INTRODUCTION

This report describes the initial attempts by the Radiation and Electromagnetics Division of SCIENCE APPLICATIONS, INC. to develop a detailed model of the dynamics of arc discharges in electron-irradiated dielectrics. This work, which was sponsored by the NASA Lewis Research Center, will be described in detail in the following sections. In this introduction, we note the requirements which we feel a detailed model of arc discharges must possess. These requirements and observations have motivated our attack on the problem — we have chosen a first principle's approach to provide a basic physics model of the process. We summarize this model briefly after reviewing the general requirements.

Any model of the breakdown and discharge of electron irradiated dielectrics should possess most of the following features — features which have been gleaned from the extensive literature on observations of such phenomena.

(1) The model should admit permanent damage patterns (Lichtenberg figures) in the discharged sample.

(2) It should also provide for the preferential channeling of current.

(3) The propagation of the discharge with speeds of the order of 10^5 m/sec is also required.

(4) The model should be capable of explaining the optical luminosity of discharges.

(5) Discharge propagation and damage should preferentially occur in regions of large trapped charge density.

(6) The model should contain intrinsically statistical features to account for the apparent statistical nature of discharges.

(7) The overall features of the model should be generic and not material specific, as similar phenomena are observed in many different materials.

(8) A discharge, once initiated, appears to continue to propagate independently of the field level at which initiation occurred, and into regions in which predischarge fields are substantially below breakdown levels. A discharge model should be capable of explaining this fact.

(9) The model should provide quantitative information about most of the important physical quantities: propagation velocity, current density, current, temperature, channel size, and discharge time. These should be parametrically explainable (in principle) in terms of material type, sample dimensions, and prebreakdown trapped charge conditions.

(10) Quantitative predictions should be in agreement with experiment.

In this report, we present a model which satisfies all the above requirements, with the possible exception of (10). Requirement (10) should not be applied too rigorously in testing the reported model. The reasons for this are simple: while the model is generic, its application to any specific material and material configuration requires the specification of a large number of materials specific parameters — parameters which to a major degree are relatively unknown. Detailed numerical predictions of the model will reflect the uncertainty in these parameters. Detailed agreement cannot be expected when these uncertainties are large.

This is not to say that the predictions reported herein are in disagreement with existing data — we do not believe they are — but rather that the model should be judged first on its generic features. Thus, the qualitative features should be judged, the various scaling features addressed, and the order of magnitude of the predictions should be consistent. When detailed numerical comparisons are to be performed, they should be performed on well categorized materials. This type of comparison remains for the future.

With this caveat, the model conforms to the requirements. Our approach to the problem utilizes a first principles physical description of the underlying electron dynamics. The model inputs are descriptions of the basic electron scattering processes in the solid. With this information, the model consists of the following:

(1) A description of the single electron distribution function in the conduction band in the presence of high fields. This includes a specification of drift velocity, diffusion, and avalanche length, as well as mean energy — all as a function of electric field.

(2) A description of the primary spatially and temporally coherent process of electron multiplication by avalanche.

(3) A description of the self-consistent evolution of the electron avalanche into a primary negative tip streamer which propagates with the field, leaving a high conductivity charge neutral region behind.

(4) A description of the propagation of the positive tip of the neutral region by successive electron avalanche/streamers, this phase occurring in three dimensions.

(5) A description of the current flow, channel evolution, charge release, and temperature rise associated with the above process.

The above model, whose physical implementation is described below, provides for a complete description of the discharge process from single electron dynamics to Lichtenberg figure formation. It provides for a quantitative description of all relevant physical quantities. Code implementation of the descriptions of (1-3) are described in this report. Their names are, respectively, SEMC, CASCAD, and ACORN. A description of the processes involved in (4-5) is also given, and a possible code implementation is described. A detailed application of the model is presented for a rough material model of Teflon.

Section 2

SINGLE ELECTRON DYNAMICS

In this section we give a discussion of our approach to the motion of individual conduction band electrons of a dielectric in the presence of an impressed external electric field $\vec{E}$. The discussion is organized by presenting the details of the theoretical structure which has been assumed, followed by a brief discussion of the limitations of the approach. This ordering of the discussion allows the limitations to be viewed against the concrete framework which is presented. Once the theoretical basis has been established, we present our computational approach to solving the problem which has been posed. A final section discusses computational results for two particular materials, gaseous molecular Nitrogen and FEP Teflon. The material models employed in these calculations are discussed in Appendices.

2.1 THEORY

The fundamental assumption of our approach to breakdown dynamics is that the dynamics of the electrons of interest may be followed with a linear Boltzman equation.

We assume that the behavior of a single electron may be described with a distribution function $f(\vec{x},\vec{v},t)$, where $\vec{x}$ denotes the position of the particle, $\vec{v}$ its velocity and t is time. The distribution function f is interpreted as the probability of finding the electron at position $\vec{x}$, with velocity $\vec{v}$, at time t. The distribution is assumed to evolve in phase space $(\vec{x},\vec{v})$ according to the Boltzman equation

$$\frac{\partial f}{\partial t} + \vec{v}\cdot\vec{\nabla}_{\vec{x}} f - \frac{e\vec{E}}{m}\cdot\vec{\nabla}_{\vec{v}} f = \left(\frac{\delta f}{\delta t}\right)_{scatt} \qquad (2.1)$$

The left hand side represents the evolution in phase space of the distribution function according to the ordinary phase space trajectories of an ensemble of non-interacting particles under the influence of the external force $\vec{F} = -e\vec{E}$. (The Louiville theorem.) The right hand side represents the changes in these trajectories due to various scattering processes. The linearity assumption requires that the interaction of various conduction band electrons may be neglected so that the scattering is specified by the interaction of the electron of interest with the remainder of the solid. Specifically, the assumption requires that the rate of change of f due to collisions be given by a linear collision integral,

$$\left(\frac{\delta f}{\delta t}\right)_{scatt} = \int d\vec{v}_o \; K(\vec{v},\vec{v}_o) \; f(\vec{x},\vec{v}_o,t) \qquad (2.2)$$

where $K(\vec{v},\vec{v}_o)$ is the scattering kernel. The scattering kernel $K(\vec{v},\vec{v}_o)$ consists of two parts, that due to gain K_+, and that due to loss K_-. Thus $K_+(\vec{v},\vec{v}_o)$ is equal to the rate at which an electron of velocity $\vec{v}_o$ will scatter into the new velocity $\vec{v}$, while $K_-(\vec{v},\vec{v}_o)$ is the rate at which electrons of velocity $\vec{v}$ are scattered into velocity $\vec{v}_o$. The scattering rate is normally thought of in terms of the sum of several rates due to individual elementary scattering processes. We denote the differential rate for the i'th scattering process as

$$K_i(\vec{v},\vec{v}_o) = \frac{d\nu_i}{d\vec{v}} \; (\vec{v}_o \longrightarrow \vec{v}) \qquad (2.3)$$

where $\frac{d}{d\vec{v}}$ indicates partial differentiation with respect to all elements of the volume element $d\vec{v}$. The notation implies that the rate in general depends not only on the initial state $\vec{v}_o$ but also the final state $\vec{v}$. The total rate for the i^{th} process $\nu_i(\vec{v}_o)$ is obtained by integrating over final scattering states

$$\nu_i(\vec{v}_o) = \int d\vec{v} \; \frac{d\nu_i}{d\vec{v}} \; (\vec{v}_o \longrightarrow \vec{v}) \qquad (2.4)$$

The rate for the i'th process is normally related to a mean free time $\tilde{\tau}_i(\vec{v}_o)$ for the i'th process by the equation $\tilde{\tau}_i = \nu_i^{-1}$. The total rate for all scattering ν is the sum of all the individual rates. With these definitions, we have

$$K_+(\vec{v},\vec{v}_o) = \sum_i \frac{d\nu_i}{d\vec{v}} \; (\vec{v}_o \longrightarrow \vec{v}) \qquad (2.5)$$

$$K_-(\vec{v},\vec{v}_o) = \nu(\vec{v}_o) \; \delta^3(\vec{v}_o - \vec{v}) \qquad (2.6)$$

and $K(\vec{v},\vec{v}_o) = K_+(\vec{v},\vec{v}_o) - K_-(\vec{v},\vec{v}_o)$ (2.7)

where δ^3 is the usual Dirac delta function.

The interpretation of equation (2.1) together with eqs. (2.2 - 2.7) requires some explanation. We are interested in processes in which the electron of interest (described by f) induces a transition from a bound state (trap or valence band) into the conduction band. If we were to attempt to describe this multiparticle situation with the Boltzman equation (multiparticle distribution function described by a mean single particle distribution function), then equation (2.1) would require the addition of a source term which takes into account the changing particle number. Likewise, sink terms would need to be added for processes taking an electron out of the conduction band (trapping, recombination). We expressly ignore these processes in Eq. (2.1), and assume that we can meaningfully follow the evolution of a single distinguishable electron. Thus, the effect of the ionization process on the motion of this single electron is taken into account, but the multiparticle, multi-band nature of the actual configuration is ignored. The limitations of this assumption will be explored after further development of the theoretical framework.

Our discussion indicates that we are considering the Boltzman equation under the circumstances in which particle number is conserved. This follows from our description of the scattering kernel given by equation (2.7). With the usual interpretation, we may define the total number of particles N described by f to be

$$N(t) = \int d\vec{x}d\vec{v}\ f(\vec{x},\vec{v},t) \qquad (2.8)$$

Using the Boltzman equation (2.1) together with the scattering kernel property

$$\int d\vec{v}\ K(\vec{v},\vec{v}_o) = 0 \qquad (2.9)$$

which follows from eqs. (2.5 - 2.7) it is easily verified that $\frac{dN}{dt} = 0$. Thus, N is a constant in time which may conveniently be chosen to be unity.

Our use of the Boltzman equation to describe the motion of the electron is demanded not because there are many electrons to describe, but rather because we do not know the precise state of the solid during the electron interaction. Thus, the ensemble average implied in the use of the Boltzman equation is the average over the ensemble of solid configurations. The usual statistical mechanical interpretation permits the use of the Boltzman equation for the description of the single electron.

We have assumed in eq. (2.2) that the scattering kernel does not depend on position -- the assumption of a homogeneous material. For the time and distance scales of interest, this is an excellent assumption. For kernels of this variety, the usual velocity space form of the Boltzman equation may be derived. Defining the velocity space probability distribution $g(\vec{v},t)$ by

$$g(\vec{v},t) = \int d\vec{x}\ f(\vec{x},\vec{v},t) \qquad (2.10)$$

we find

$$\frac{\partial g}{\partial t}(\vec{v},t) - \frac{e\vec{E}}{m} \cdot \nabla_{\vec{v}} g(\vec{v},t) = \int d\vec{v}_o\ K(\vec{v},\vec{v}_o) g(\vec{v}_o,t) \qquad (2.11)$$

Discussions of transport in solids (and gases) normally involve eq. (2.11) rather than eq. (2.1). In fact, most attacks on transport properties specialize even further by considering the equilibrium solution $g_o(\vec{v})$ (time independent) of eq. (2.11).

The relation of these various functions and approaches is best seen by considering various moments of the distribution function. In the usual fashion, define the mean value of a function of position and velocity ρ (denoted $<\rho>$) by

$$<\rho> = \int d\vec{x}d\vec{v}\ \rho(\vec{x},\vec{v})\ f(\vec{x},\vec{v},t) \tag{2.12}$$

The following relations may then be easily established from eq. (2.1);

$$\frac{d<\vec{x}>}{dt} = <\vec{v}> \tag{2.13}$$

$$\frac{d}{dt}<x_i x_j> = <x_i v_j + v_i x_j> \tag{2.14}$$

$$\frac{d<\vec{v}>}{dt} = \frac{-e\vec{E}}{m} + \frac{\vec{F}_c}{m} \tag{2.15}$$

$$\frac{d}{dt}<v_i v_j> = \frac{-e}{m}\left(E_i<v_j> + E_j<v_i>\right) + \frac{2}{m}T_{ij} \tag{2.16}$$

where

$$\vec{F}_c = m\int d\vec{v}_o \int d\vec{v}\ \vec{v}\ K(\vec{v}_o,\vec{v}_o)\ g(\vec{v}_o,t) \tag{2.17}$$

and

$$T_{ij} = \frac{m}{2}\int d\vec{v} \int d\vec{v}_o v_i v_j\ K(\vec{v},\vec{v}_o)\ g(\vec{v}_o,t) \tag{2.18}$$

The important point to note is that the evolution of the various velocity moments $\{\langle v_i \rangle, \langle v_i v_j \rangle\}$ depends only on the evolution of the velocity space distribution function g. In particular, if equilibrium has been obtained ($\frac{\partial g}{\partial t} = 0$), the mean velocity and energy are constant, and the mean position increases linearly with $\langle \vec{v} \rangle$. Thus, the drift velocity $\vec{v}_D$ is easily identified from the equilibrium solution

$$\vec{v}_D = \langle \vec{v} \rangle_o = \int d\vec{v}\ \vec{v}\ g_o(\vec{v}) \quad , \qquad (2.19)$$

Define the displacement $\vec{\xi}$ from the mean position $\langle \vec{x} \rangle$ by $\vec{\xi} = \vec{x} - \langle \vec{x} \rangle$. What is not quite so apparent from eqs. (2.12 - 2.19) is that $\langle \xi_i \xi_j \rangle$ also evolves linearly in time when g has reached equilibrium. The proof of this fact requires a somewhat delicate application of the Chapman-Enskog theory and is relegated to Appendix 9. Suffice it to say here that the coefficient of time in the evolution of $\langle \xi_i \xi_j \rangle$ is interpreted as a diffusion coefficient. Let $\hat{e}_{\parallel}$ be a unit vector in the direction of the electric field, and define the parallel and perpendicular components of $\vec{x}$ by $\vec{x}_{\parallel} = (\hat{e}_{\parallel} \cdot \vec{x})\hat{e}_{\parallel}$, $\vec{x}_{\perp} = \vec{x} - \vec{x}_{\parallel}$. For diffusive motion, we have the definition of the parallel and perpendicular diffusion coefficients by the relations

$$\langle \hat{\xi}_{\parallel} \cdot \hat{\xi}_{\parallel} \rangle = 2D_{\parallel} t \qquad (2.20)$$

$$\langle \hat{\xi}_{\perp} \cdot \hat{\xi}_{\perp} \rangle = 4D_{\perp} t \qquad (2.21)$$

These terms may be isolated from the solution f of the Boltzman equation using equation 2.12 - 2.19. Formulae for the D's in terms of the equilibrium solution g_o may be found in Appendix 9.

Another averaged quantity of primary concern in our discussion is the mean distance between ionizing collisions, variously called the avalanche length or the first Townsend coefficient α. Let $\nu_{ion}(v_o)$ be ionization rate for electrons of speed v_o. Then the rate $\dot{n}(\vec{x},t)$ at which ionizing collisions are occurring at a particular point in space $\vec{x}$ at time t is given by (#/unit volume/unit time)

$$\dot{n}(\vec{x},t) = \int d\vec{v}_o \nu_{ion}(\vec{v}_o)\, f(\vec{x},\vec{v}_o,t) \qquad (2.22)$$

The rate at which ionizing events are occurring at all locations $\dot{N}(t)$ is obtained by integrating $\dot{n}(x,t)$ over all space,

$$\dot{N}(t) = \int d\vec{x}\, \dot{n}(\vec{x},t) = \int d\vec{v}_o\, \nu_{ion}(\vec{v}_o)\, g(\vec{v}_o,t) \qquad (2.23)$$

The total number of ionizing collisions which have occurred to up time t, N(t) is obtained by integration $\dot{N}$ in time. When g has reached equilibrium, N increases linearly with time. Let t_I be the time period required for N to change by unity. The inverse of t_I is of course the ionization rate β. The mean distance between ionizations is related to t_I by $\alpha = v_D t_I$.

The spatial probability distribution $n(\vec{x},t)$ of ionizing events is obtained by integrating $\dot{n}(\vec{x},t)$ in time. A convenient way to disentangle the many ionizing events is restrict attention to the first event. Let t_1 be a time such that $N(t_1) = 1$. The spatial distribution $n(\vec{x},t=t_1) \equiv n_1(\vec{x})$ may then be interpreted as the probability that the first ionization

occurs at $\vec{x}$. The mean location of the first ionization is then

$$\langle \vec{x}_I \rangle = \int d\vec{x}\; n_1(\vec{x})\; \vec{x} \qquad (2.24)$$

The temporal evolution of the ionization may then be thought of in terms of a sequence of events identical to the first event, with spatial probability given by $n_1(\vec{x})$, and temporal probability of occurrence N(t) [cumulative]. In so far as $t_1 \approx t_I$, the definition of $\langle \vec{x}_I \rangle$ may be identified with α. This has been the standard procedure in the literature [Baraff, 1964].

Experimentally, the mean quantities α, v_D, $D_{\parallel}$ and $D_{\perp}$ are the quantities which have been measured. We will refer to specifics of such measurements below in discussing our computational results. Quantities such as these are also the natural quantities to use in proceeding to a macroscopic description of multi-electron dynamics, which will be discussed in Section 4 below. Note that a specification of a material model requires a model for the various scattering processes which occur in the description of the scattering kernel $K(\vec{v},\vec{v}_o)$.

2.1.1 LIMITATIONS

The description of single electron dynamics implied by the use of the Boltzman equation is purely classical. That is, the probability distributions which are obtained are related to the classical averaging over ensembles which is customary in statistical mechanics. These probability distributions are in no way directly related to the probability distribution associated with the quantum mechanical description of the electron. The fundamental limitation of the method is therefore related to the fundamental domain of applicability of classical statistical techniques. For a general problem involving electronic transport properties in solids, density matrix techniques of quantum statistical mechanics are required, leading the Kubo theory of transport phenomena (Kubo, 1959).

We believe, however, that the classical description which we have invoked for the calculation of the electron transport properties is adequate for the problem of interest. This technique is not unique to our approach and has been invoked by essentially all authors who have studied this problem at reasonably high temperatures ($\sim$ room temperature). A somewhat detailed justification may be found in Ziman's book (Ziman, 1960) and references cited therein, while a review of the literature may be found in O'Dwyer's book (O'Dwyer, 1973). Though the details of the argument can become complex, the underlying idea is quite simple. The correspondence principle demands that wave packet solutions of the Schroedinger equation obey the classical equations of motion. The fundamental limitation of the

classical methods comes only when attempting to provide more localization in phase space than is allowed by the Uncertainty Principle. If, for the energies and times of interest, the classical averaging provides an uncertainty greater than that demanded by the Uncertainty Principle, then the quantum uncertainty is masked by these effects, and classical techniques may be expected to be applicable. For example, if we wish to discuss (free) electrons of roughly thermal energy ($\sim$ 0.025 e.v.), then we are justified in applying classical techniques if we do not try to localize the electron any more than $\Delta x \sim \frac{\hbar}{\Delta p}$, or about 25 Å. For higher energy electrons, this length becomes smaller.

The problem may roughly be factored, with classical techniques being used for distances large compared to $\Delta x \sim \frac{\hbar}{\Delta p}$, and quantum techniques being used over smaller distance scales (with corresponding statements about time scales). If the fundamental scattering processes are specified using quantum techniques (description of the scattering kernel), the longer distance scale transport properties should then be describable by classical techniques. That this approach is adequate for the problem of concern is taken as a working hypothesis, a hypothesis consistent with those of other workers in the field.

A second limitation of the approach is more severe. In applying a Boltzman type transport equation to the problem, we require that the interactions which are occurring in the quantum regime are describable in terms of a scattering formalism. This roughly requires that the electronic states of the conduction band be

describable with quasi-free wave functions (i.e., that a quadratic relation exist between electron energy and Bloch wave number). While this is probably a reasonable assumption for a perfect crystalline insulator (trap-free), it is decidedly not true for non-crystalline polymeric trap-dominated insulators. Shown in Figure 2.1 is a schematic representation of the electronic energy levels expected in solid insulators with a large degree of non-crystallinity (Mott and Davis, 1971). We can see that the crystalline concept of a forbidden gap has been replaced by a minimum in the density of states. Near the top and bottom of what would normally be thought of as the valence and conduction bands respectively are a group of states which are normally called "trap" states. These states correspond to localized wavefunctions, and hence do not have a translational wave number associated with them. Localized states such as these (so-called Anderson states (Anderson, 1958) cannot be represented as quasi-free electrons, so that a scattering formalism is inapplicable for a description of their properties. In particular, the states just below the "conduction band," the shallow trapping states, are the lowest lying levels above the "valence band." Statistical arguments at ordinary temperatures suggest that most electrons which are not in the valence band in fact occupy these states. Because of this, the normal conduction properties of a material with an energy level structure of the type shown in Figure 2.1 are dominated by the behavior of electrons in these states. The normal description of the conduction process is then by "hopping" conduction; that is, successive detrapping and retrapping. Techniques other than Boltzman equation techniques are required to describe this type of transport. The

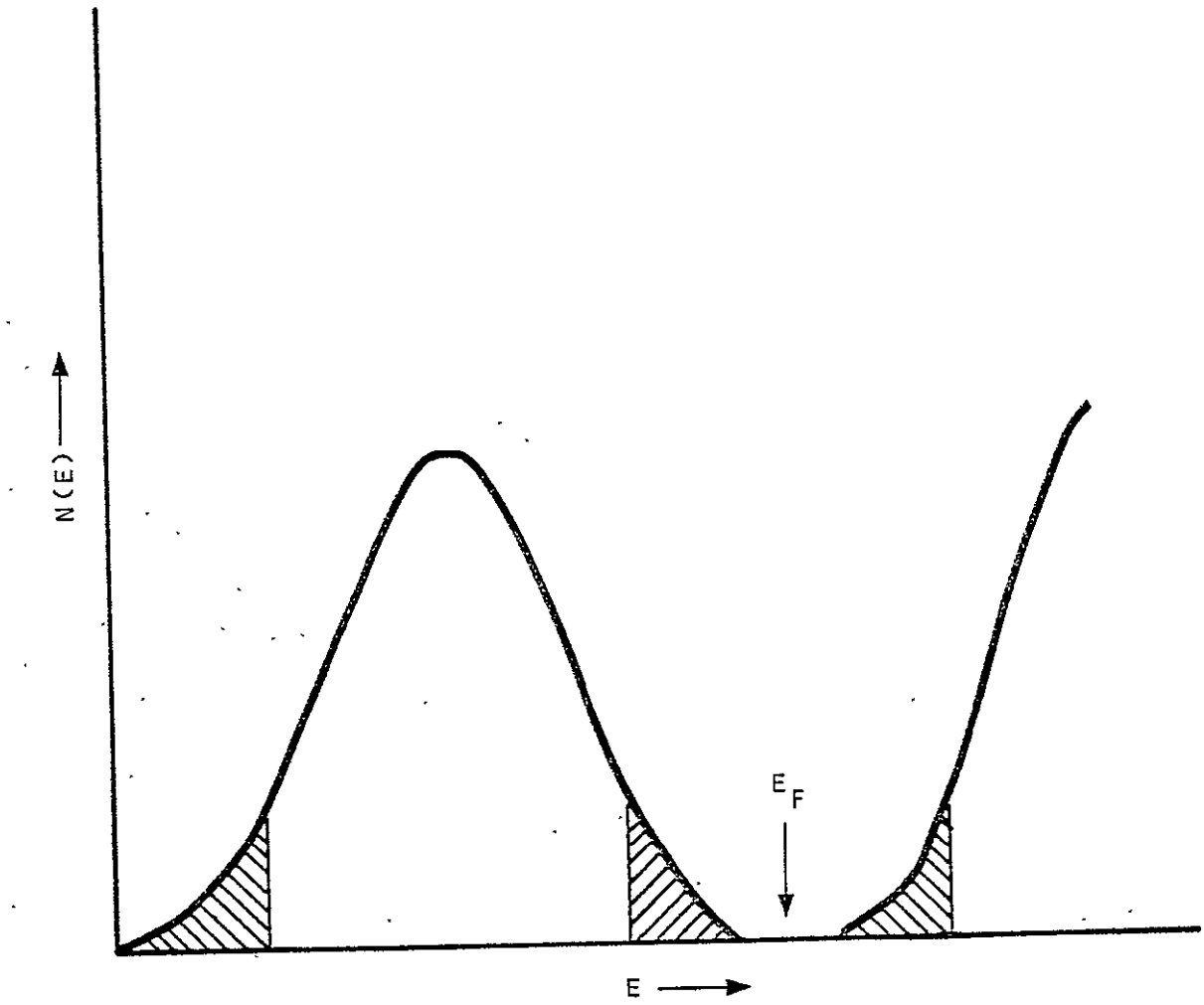

FIGURE 2.1. SCHEMATIC ENERGY LEVEL DIAGRAM FOR NON-CRYSTALLINE INSULATOR

background on the required techniques may be found in the book by Mott and Davis (1971).

Despite the above remarks, we persist in the use of the Boltzman equation for our model of avalanche induced breakdown. Our reasons are as follows. We are only interested in performing electron transport calculations at or near breakdown fields. It is our working hypothesis that in this regime an electron which is initially in the conduction "band" (above the trap states of Figure 2.1) will undergo significant "heating." That is, the rate of energy loss to the solid will not equal the gain from the field until the electron has an energy substantially greater than typical thermal energies. The presence of the field, therefore, induces an effective transition rate upwards in the conduction "band." This effective shift of the energy of conducting electrons effectively removes electrons from those states which have the greatest probability of trapping (within kT of the trap states). Thus, if the heating rate is substantially faster than the trapping rate, we are well-justified in concentrating attention on the conduction "band" dynamics, and treating the trapping as a perturbation on these processes.

The validity of the above assumption is clearly a function of field strength. It is our working hypothesis that for the field strengths associated with breakdown this condition is satisfied. Once a calculation of the electron distribution function has been performed, an a posteriori check of the assumption should serve to check its adequacy. With this assumption, it is reasonable to expect that a quasi-free

electron description of the conduction "band" electrons should be adequate, that a scattering formalism is appropriate, and that the Boltzman equation is applicable. In fact, the results below suggest mean electron energies in the eV range. Because we are well up into the "band" in this regime, we expect potential energy effects to be less important than kinetic energy effects. We uniformly assume therefore that $M_e^* \approx M_e$ in relating energy and momentum.

We have suggested above that we are well justified in treating trapping as a perturbation of the energy gain rate is substantially greater than the trapping rate. There are a whole host of other limitations of our approach which are based on a similar comparison of rates (of energy gain and conduction band scattering). In particular, the deep trapping and recombination rates must also be negligible compared to the energy gain rate. The electron-electron energy-momentum exchange rate must be negligible compared to the electron-lattice scattering rate. Finally, the electric field must be sufficiently small that the details of the ionization process (energy/angle) do not determine the evolution of the distribution function (scattering rate much greater than ionization rate). We believe all the above restrictions to be satisfied for the fields of interest.

2.2 COMPUTATIONAL APPROACH

A great deal of detailed work has been performed on methods for computing the equilibrium solution of the Boltzman equation for gases. In fact, the low energy cross-sections for gases have been determined from measurements of macroscopic parameters as a function of electric field by inverting the process discussed above, i.e., by adjusting cross-sections in the calculations until an adequate fit of the measured macroscopic data is obtained. We refer the reader particularly to the work of Phelps [see e.g. Hake and Phelps (1967) and Frost and Phelps (1962) and references cited therein]. Further references to the literature may be found in the compendium of data prepared by Dutton (1975) and, the recent book of Meek and Craggs (1978), while the older literature may be found from Loeb's book [Loeb (1955)]. The techniques developed by these workers are quite adequate for the proposed problem. Unfortunately, they are rather specialized, in that various electric field regions are distinguished, various approximations employed, and specialized solution techniques are employed in the several regions. Further, the application of any of these solutions to the spatial and temporal variation of the distribution function requires the application of the macroscopic diffusion theory.

In solid dielectrics, much less work has been performed on developing numerical transport techniques. The state of the art appears to be represented by the work of Baraff (1962), who determined a universal set of curves for the avalanche length under a constant mean

free path assumption. Earlier work, and more complete descriptions of the various competing processes may be found in Heller (1951), Wolff (1954) and Shockley (1951), while a summary may be found in O'Dwyer's book (1974). Again, the techniques employed have either been very specialized, or very difficult to employ for general circumstances.

Rather than rely on any of the specialized techniques which have been developed, we have chosen to attack the computational problem by a brute force Monte Carlo technique. This method (to be described below) has several strong advantages: There are essentially no restrictions on the type, number or character of scattering processes which can be considered; as the technique involves path tracing, it can readily solve problems associated with both the real space and velocity space positions of the distribution function simultaneously; the technique is conceptually simple to implement – resulting codes are quite small; the technique may be used in principle to determine any information desired about the evolution of the distribution function; finally, SAI is well-versed in implementation of such codes. The technique has several disadvantages; Monte Carlo codes are inefficient – they are expensive to execute compared to comparable codes using other techniques; Monte Carlo codes provide essentially no basis for intuitive understanding of the results computed; without special sampling techniques, quantities depending on low probability events are impossible to compute; the statistical nature of the Monte Carlo output often requires that special fitting routines be developed for data smoothing. Our decision

to go with Monte Carlo techniques was driven by ease of implementation and generality.

The basic concept of Monte Carlo transport is extremely simple. The left hand side of the Boltzman equation describes the evolution of the distribution function in the absence of collisions. It is well known that this evolution is described by individual particles following their mechanical trajectories, i.e., f is constant on phase space trajectories. The scattering integral represents the scattering of individual particles from one velocity to another. This occurs at a rate of $\nu(\vec{v}_o)$. Thus, on the average, an individual particle will undergo free motion for a time $\tau(\vec{v}_o) = 1/\nu_e(\vec{v}_o)$. This mean free time may be associated with a mean free path $\lambda(\vec{v}_o)$ by the standard relation $\lambda(\vec{v}_o) = |\vec{v}_o|\ \tau(\vec{v}_o)$. Thus, the picture is that of individual particles undergoing free motion, together with successive scatters at a mean time increment of $\tau(\vec{v}_o)$. The scattering events of the scattering integral may be described according to single particle scattering theory – which is precisely in accord with the method by which the scattering integral was developed. The scattering events themselves are random events chosen according to the differential rate $\frac{d\nu}{d\vec{v}}(\vec{v}_o \longrightarrow \vec{v})$, again in accord with the meaning of the scattering integral. Averaging the results over many particle paths chosen as above yields the distribution function. That the above procedure indeed yields a solution to the Boltzman equation is intuitively apparent (the Boltzman equation was developed from this picture). The rigorous mathematical demonstration of the equivalence is much more difficult. A discussion of the proof of this

equivalence would take us too far from our goals — we accept the equivalence and refer the reader to the literature for further discussion.

We have chosen to implement the above picture for the transport of electrons in the presence of an electric field. The method chosen is a single-scatter Monte Carlo method (to distinguish it from other Monte Carlo algorithms), i.e., each individual scattering event is modeled. The method as implemented is brute force — no special sampling techniques have been employed. The restrictions resulting from this are discussed after a description of the algorithm. The algorithm is as follows:

- A set of differential rates $\frac{d\nu_i}{d\vec{v}}(\vec{v}_o \rightarrow \vec{v})$ is prescribed, i=1,..., N, where N is the number of scattering processes to be included.
- The total scattering rate $\nu(\vec{v}_o)$ is determined, together with the mean free path $\lambda(\vec{v}_o) = |\vec{v}_o|/\nu(\vec{v}_o)$.
- The differential scattering probability functions are determined according to the rule $$\frac{dP_i}{d\vec{v}}(\vec{v}_o \rightarrow \vec{v}) = \frac{\frac{d\nu_i}{dv}(\vec{v}_o \rightarrow \vec{v})}{\nu(\vec{v}_o)}$$
- Cumulative probability functions $P_i(\vec{v}_o, \vec{v})$ are determined by appropriately defined integrals of $\frac{dP_i}{d\vec{v}}$
- An initial velocity space distribution function $f_o(\vec{v})$ is specified. The cumulative distribution function, $C(\vec{v})$ is determined from $f_o(\vec{v})$ by appropriate integration.

- Particles are started from a preassigned position in space $\vec{x}_o$.

- A single particle path is constructed by the following sequence.

  (1) An initial velocity $\vec{v}_o$ is chosen randomly according to the distribution function $C(\vec{v}_o)$.

  (2) The mean free path $\lambda(\vec{v}_o)$ is noted.

  (3) A free path ℓ is chosen according to an exponential distribution of paths with mean λ.

  (4) The particle is allowed to traverse a path length ℓ under the influence of the external field, with initial conditions $\vec{x}_o$, $\vec{v}_o$. This requires the determination of the time δt required to travel a path length ℓ (this depends on $\vec{v}_o$, $\vec{E}$ and $\vec{v}_o \cdot \vec{E}$). The particle position and velocity are updated according to the equations of motion

  $$\vec{x} = \vec{x}_o + \vec{v}_o \delta t - 1/2\left(\frac{e\vec{E}}{m}\right)(\delta t)^2$$

  $$\vec{v} = \vec{v}_o - \frac{e\vec{E}}{m}\delta t$$

  (5) A scattering event is described at the new location For velocity $\vec{v}$, a new velocity $\vec{v}_o'$ is randomly selected according to the probability distributions $P_i(\vec{v}, \vec{v}_o')$. The particle now has position $\vec{x}$, and velocity $\vec{v}_o'$.

  (6) The steps (2) - (5) are repeated for the new position and velocity. This process is repeated until prespecified conditions (e.g., fixed number of steps) are satisfied.

  (7) The above sequence of path increments represents one Monte Carlo History. The sequence is repeated for a prespecified number of histories.

(8) Various quantities are scored during the course of each history. These quantities are averaged over the number of histories.

The first four steps of the above algorithm have been programmed into a FORTRAN code called XSCPRP. The remaining steps have been programmed into a FORTRAN code called SEMC (Single-scatter Electron Monte Carlo). The operational features of XSCPRP are described in Appendix 3. The operational features of SEMC are described in Appendix 4. Some general features of the codes are as follows:

- SEMC is designed to operate in the high electric field region where collision ionization is important. Many of the scoring and path stopping flags are keyed to these events. For low electric fields, such events become very improbable. The code is not meant to operate in this regime without special directives.

- The initial distribution of electrons for the computation is assumed to lie in the low energy domain (thermal energies). Under high fields, the exact form of this initial distribution is immaterial to the ultimate development of the distribution function. It was consequently specified to be monoenergetic and unidirectional.

- SEMC only follows each individual electron trajectory up until its first ionization event. It therefore assumes that the electron loses essentially all of its energy in this encounter, so that its further history is undistinguished from starting with the initial distribution. This requires that the electric field not be so large that a substantial fraction of the ionization energy be gained in a mean free path.

- Sampling on free paths, rather than free times was chosen because the mean free path is more nearly constant in energy than mean free time. SEMC samples from the mean free path distribution of the electron prior to the time step. In principle, the distribution should be integrated along the trajectory, and an energy weighted path distribution sampled from. If the fields are not too large, this approximation should be adequate.

- The path length traversed ℓ, is related to the time required to traverse that distance by the formula

$$\ell' = 1/2 \left\{ \cos\theta + (t'-\cos\theta)\sqrt{t'^2-2t'\cos\theta+1} + \sin^2\theta \ln\left[\frac{t'-\cos\theta+\sqrt{t'^2-2t'\cos\theta+1}}{(1-\cos\theta)}\right]\right\} \quad (2.24)$$

where

$$\ell' = \frac{e|\vec{E}|\ell}{mv_o^2} \quad (2.25)$$

$$t' = \frac{e|\vec{E}|t}{m|\vec{v}_o|} \quad (2.26)$$

and,

$$\cos\theta = \frac{\vec{E}\cdot\vec{v}_o}{|\vec{E}||\vec{v}_o|} \quad (2.27)$$

For a choice of path length ℓ, eq. (2.24) s inverted, and the new velocity and position are up- ated with the equations of motion for elapsed time t.

- The location of the i'th ionization event $\vec{x}_i$ is scored together with the time of occurrence t_i. These results are binned to provide the spatial distribution of ionization events.

- At the end of each history, the following particle attributes are scored. The mean value of the component of $\vec{x}$ along the field provides the ionization length. The mean value of $(\vec{x}_i/t_i)$ provides the drift velocity. The RMS speed of the final positions perpendicular to the field provides the diffusion coefficient perpendicular to the field $D_\perp$. Because of the strong correlation between ionization time and distance traversed, the RMS speed of the ionization location about the mean ionization location does not provide a good measure of the longitudinal diffusion coefficient $D_{\parallel}$. Instead a computation of mean dispersion is scored for a fixed time (to be specified on input). This provides the longitudinal diffusion coefficient.

- The scattering distributions required for performing the random walk are required input parameters for the code.

- The angular dependence of the inelastic processes is currently being neglected. This is a reasonable approximation so long as acoustic phonon scattering (elastic scattering) dominates.

2.3 RESULTS

In this section we present the results of the single electron dynamics calculation for two materials, N_2 and CF_2. One of the features which makes the Monte Carlo appealing is ease with which a running computer code may be developed. Unlike finite difference methods, for example, the Monte Carlo method does not have stability criteria and in general convergence is assured. For this reason it is imperative that the Monte Carlo codes be checked, if at all possible, against experimental data. As our test case we have chosen N_2, primarily because of the abundance of experimental data available.

2.3.1 N_2 RESULTS

The model for the cross section set used for N_2 is presented in Appendix 1. For all results presented for N_2 the solid curves are from an electron swarm data compilation (Dutton, 1975) and the points are data calculated by the SEMC code. All N_2 results are for a gas density of 2.7×10^{25} molecule/m^3. In Figure 2.2 the ionization length is plotted as a function of electric field. The ionization length is the reciprocal of α, the first Townsend coefficient. In Figure 2.3 the electron mobility (ratio of drift velocity to electric field) is plotted as a function of electric field. In Figure 2.4, the longitudinal diffusion coefficients (the coefficient in a direction along the applied electric field) is plotted as a function of electric field. And finally, in Figure 2.5 the transverse diffusion coefficient (the coefficient in a direction normal to the applied electric field) is plotted as a function of electric field.

On two of the curves, data was not available for high values of the electric field. The curves have been extended (dashed position of the curve) for comparison purposes. The generally excellent agreement of the code calculated results with experimental data validate the code.

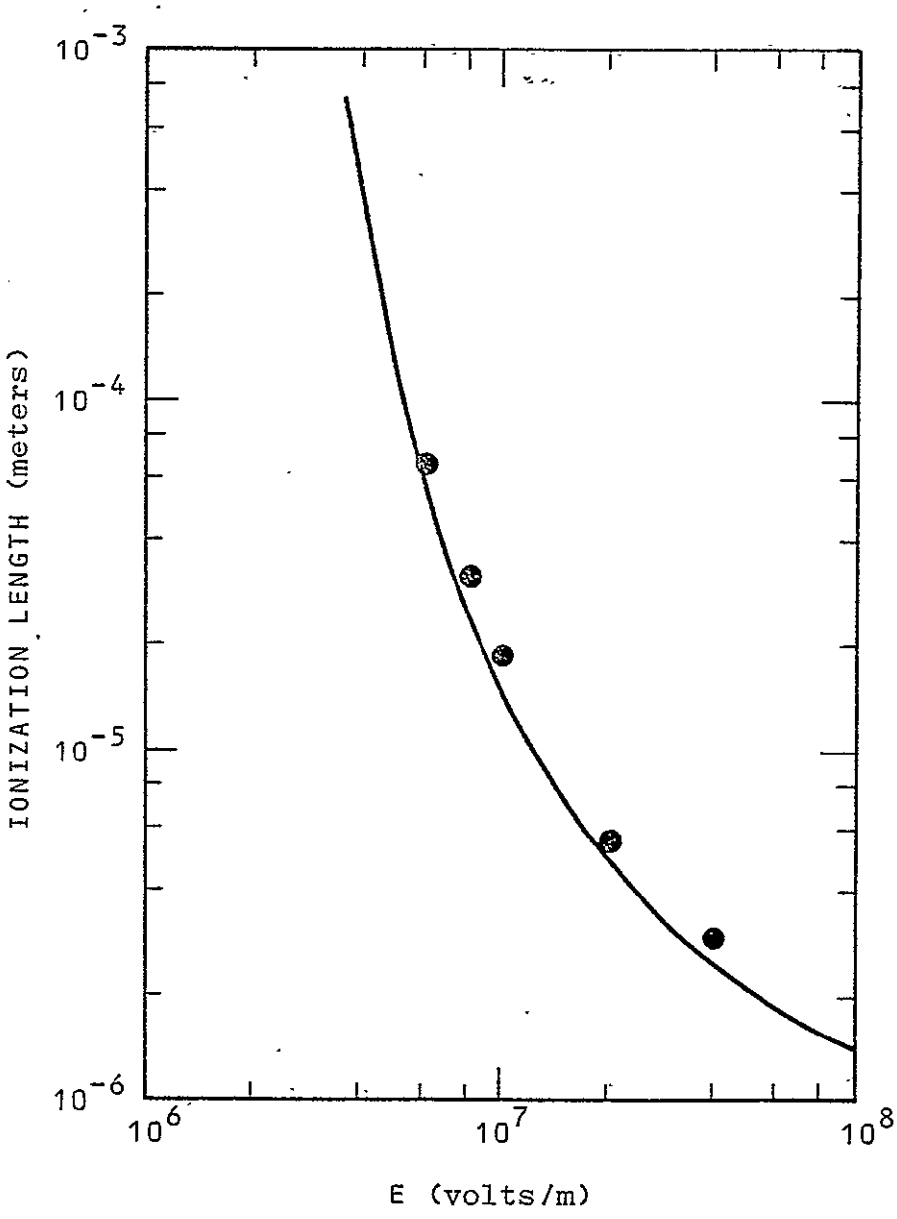

FIGURE 2.2. IONIZATION LENGTH AS A FUNCTION OF APPLIED ELECTRIC FIELD FOR N_2

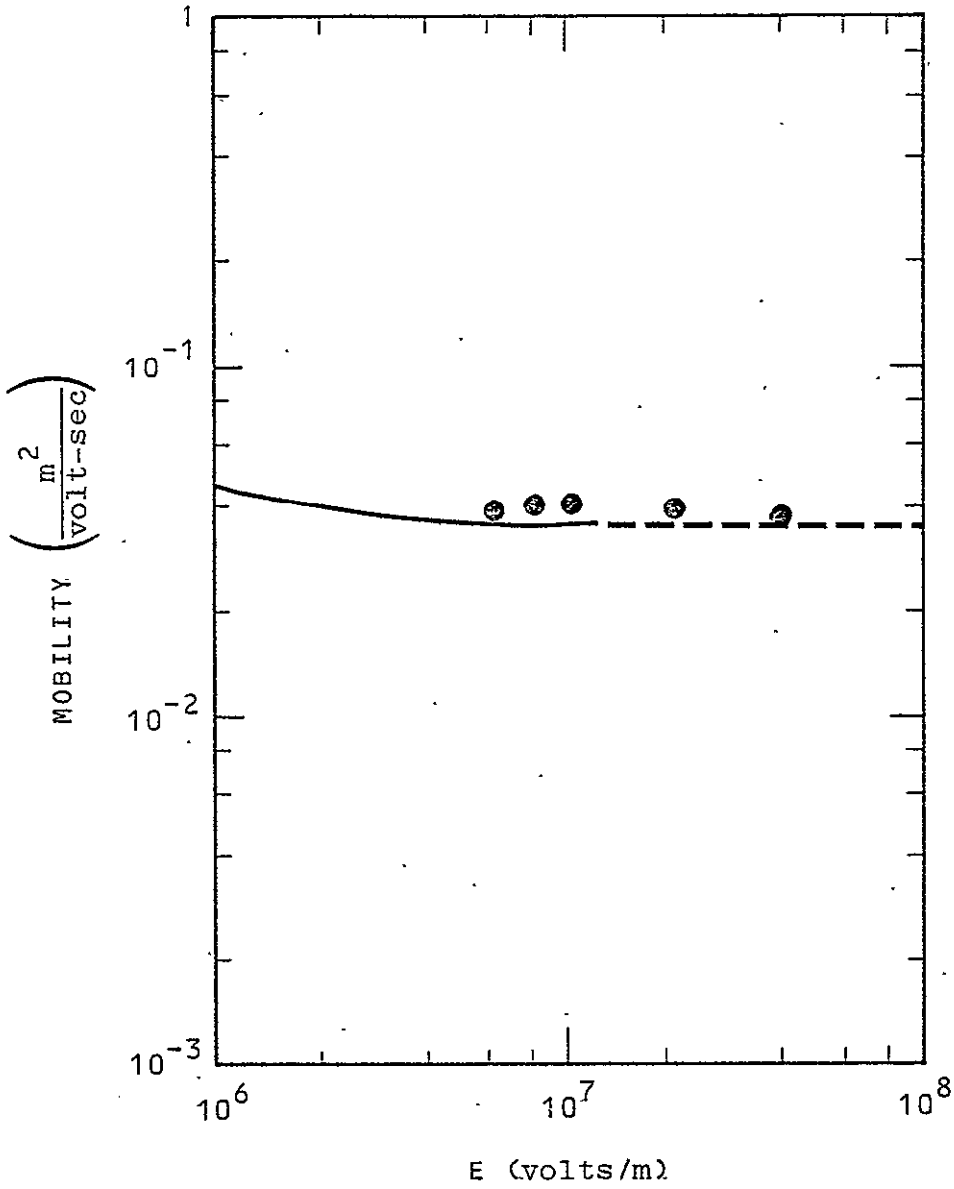

FIGURE 2.3. ELECTRON MOBILITY AS A FUNCTION OF APPLIED ELECTRIC FIELD IN N_2

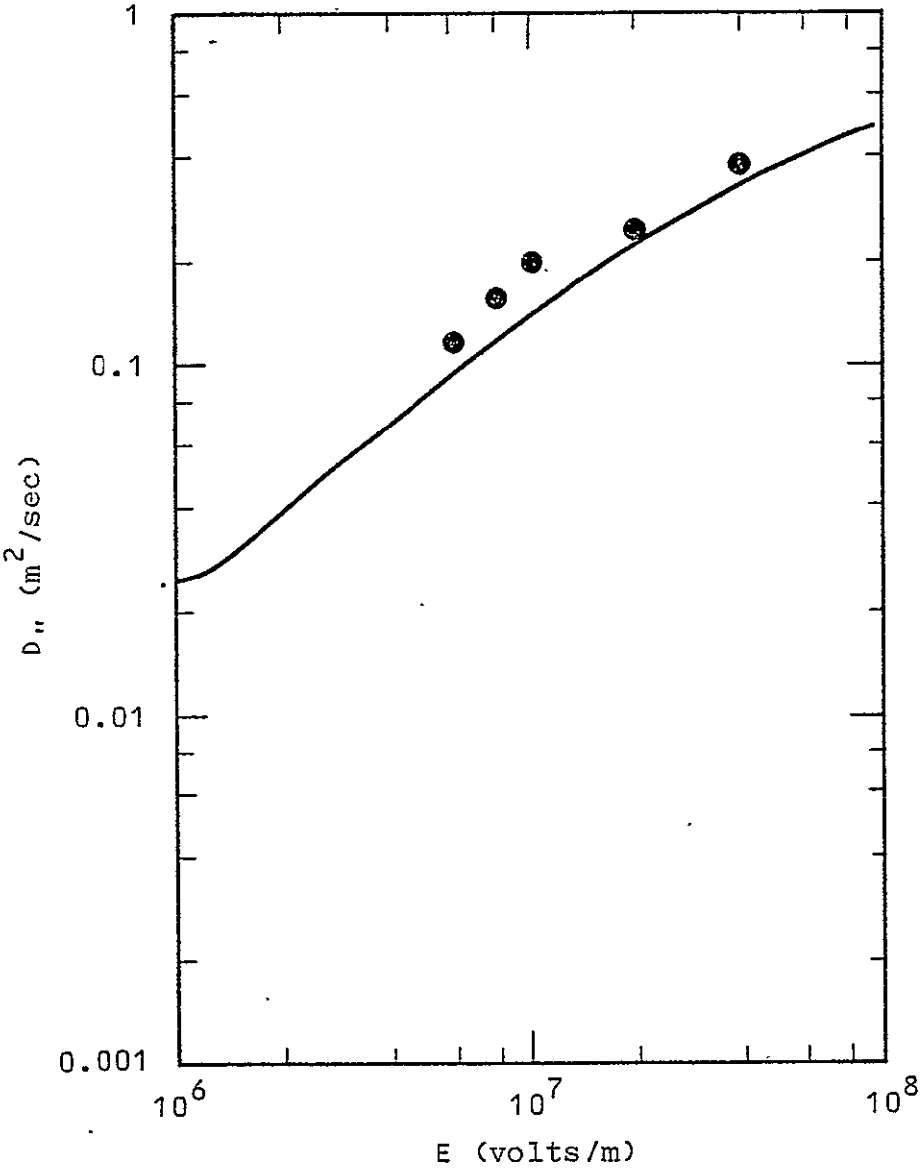

FIGURE 2.4. LONGITUDINAL DIFFUSION COEFFICIENT AS A FUNCTION OF APPLIED ELECTRIC FIELD IN N_2

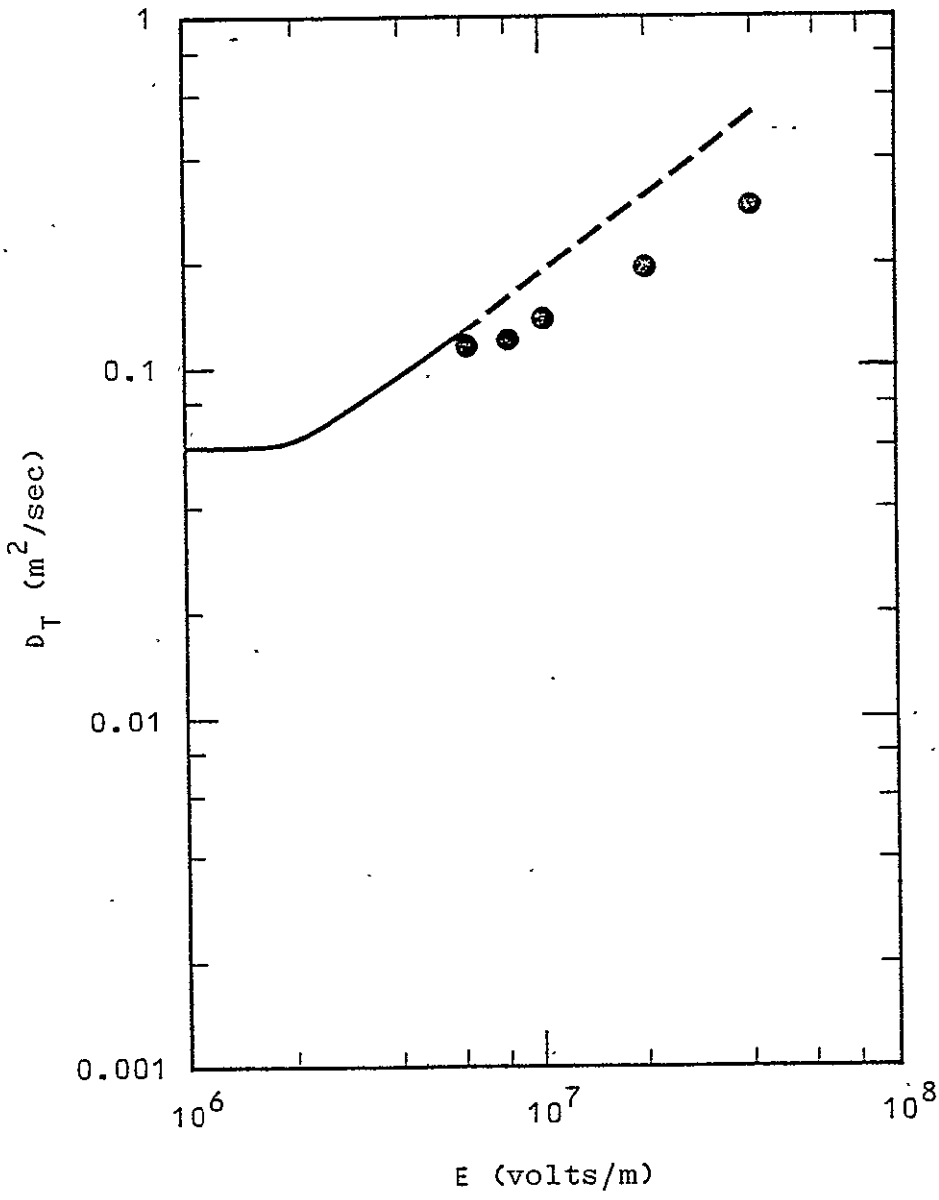

FIGURE 2.5. TRANSVERSE DIFFUSION COEFFICIENT AS A FUNCTION OF APPLIED ELECTRIC FIELD IN N_2

2.3.2 TEFLON

SEMC has been exercised for a material model of Teflon which is described in Appendix 2. The model is necessarily crude. Shown in figure 2.6 is mean distance for e-folding the number of electrons (inverse first Townsend coefficient). This quantity equals the mean ionization length divided by ln (2). For an applied field of 8×10^8 V/m, this corresponds to a distance of 1.5×10^{-8} m (130 Å). As for Nitrogen, the quantity increases exponentially as the field is decreased. The extremely small distance scale associated with these high fields should be noted, as it will determine the scale of later computations. These results are consistent with an analytic estimate of the avalanche length presented in Appendix 7. Shown in figure 2.7 is the electronic mobility μ. Its remarkably flat value of about 1.6×10^{-4} m^2/V-sec can be ascribed to the small constant acoustic phonon collision mean free path, and is consistent with simple estimates. Shown in figures 2.8 and 2.9 are the longitudinal and transverse diffusion coefficients. While the order of magnitude of these coefficient is consistent with analytic estimates, the rather strong increase in D_T at low fields seems a bit peculiar. This behavior remains to be explained. This feature does coincide with the onset of significant ionization. The equations of Section 4 require the ionization rate $\beta = \alpha V_D$. This quantity is plotted in figure 2.10. Its variation with electric field is extremely sharp, and reflects the properties of μ and α noted above. Finally, figure 2.11 shows the marginal distributions for the locations of ionization events parallel and perpendicular to the field. It should be

noted that these distributions show a somewhat greater width than would be expected from diffusion alone. This is a reflection of the correlation between ionization location and ionization time, and was discussed in Section 2.2 above.

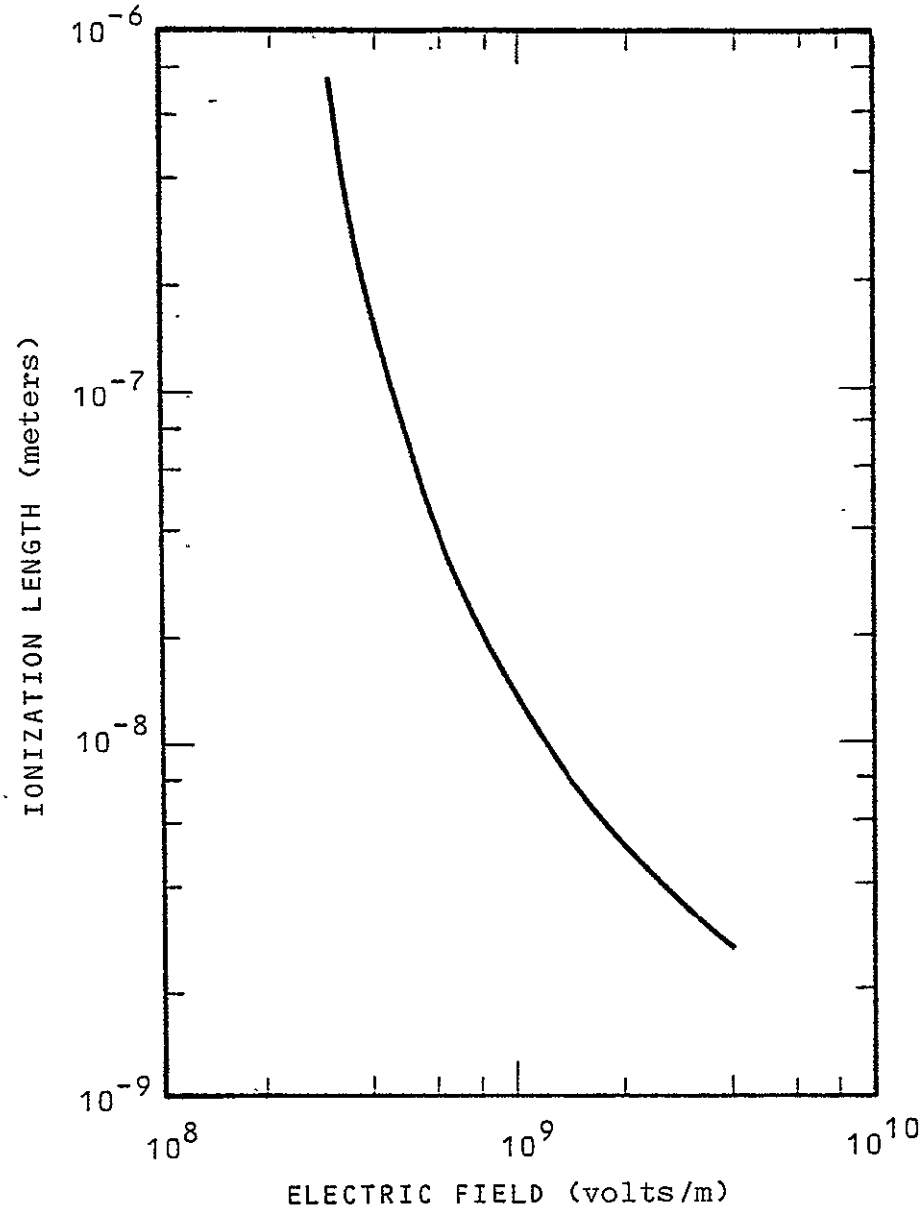

FIGURE 2.6. IONIZATION LENGTH AS A FUNCTION OF APPLIED ELECTRIC FIELD FOR CF_2

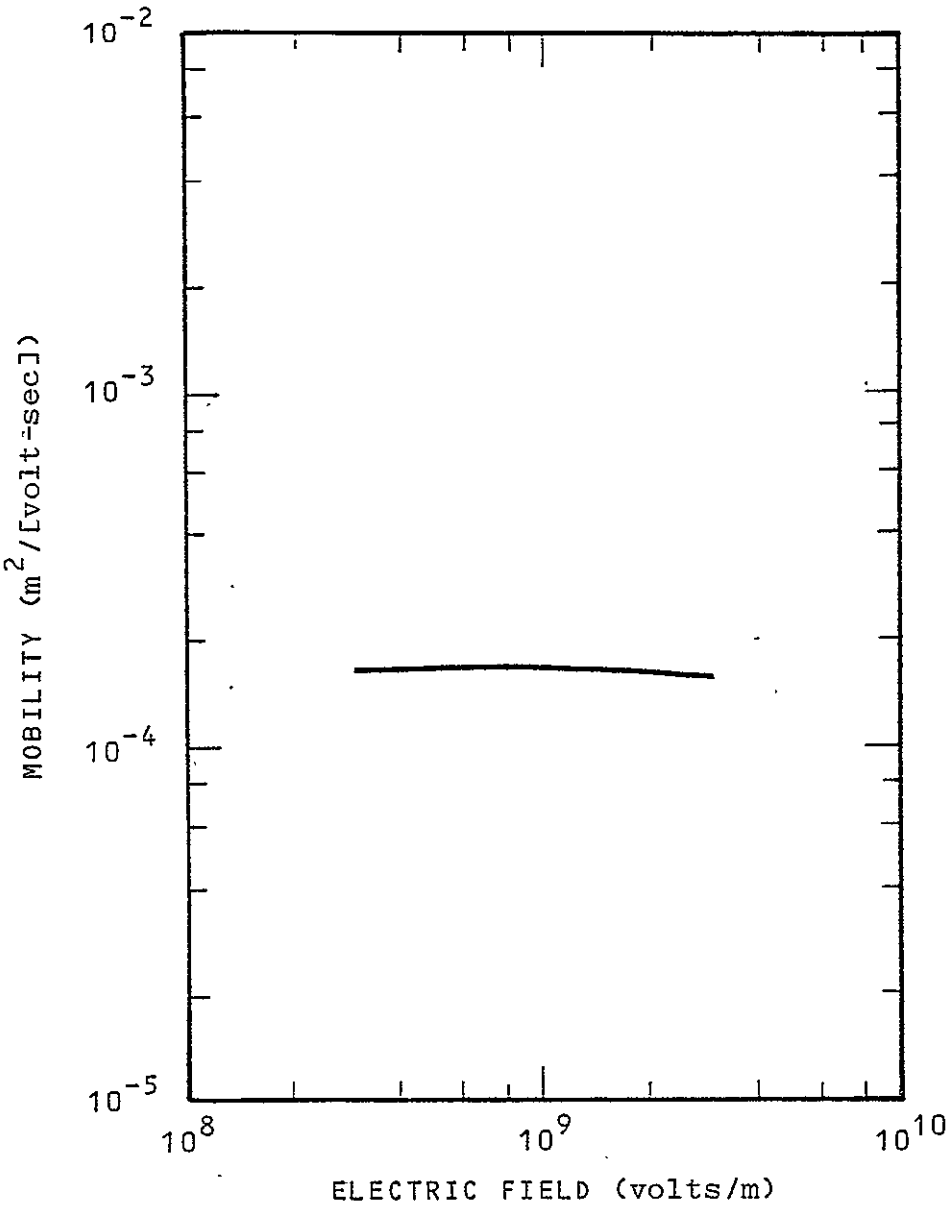

FIGURE 2.7. ELECTRON MOBILITY AS A FUNCTION OF APPLIED ELECTRIC FIELD IN CF_2

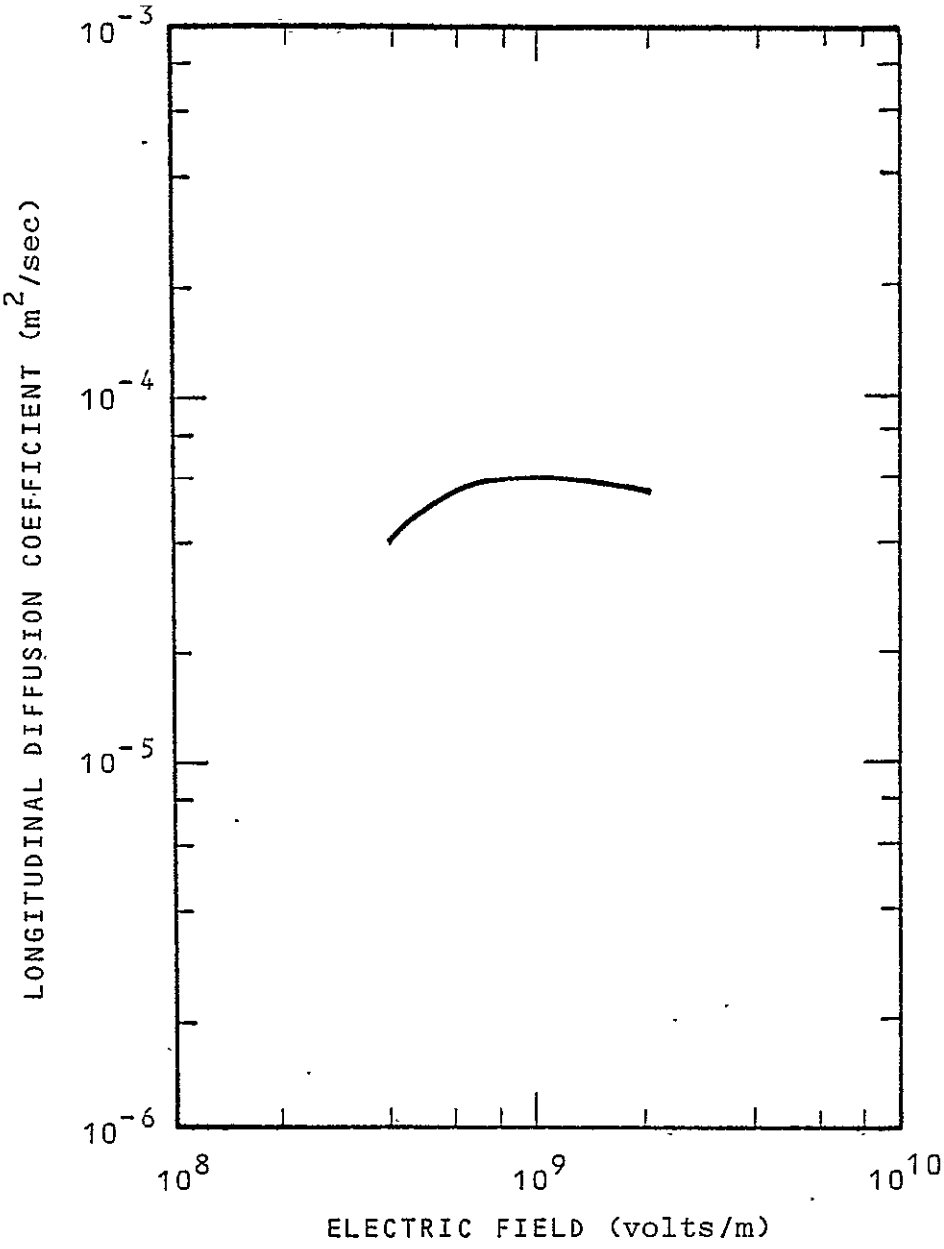

FIGURE 2.8. LONGITUDINAL DIFFUSION COEFFICIENT AS A FUNCTION OF APPLIED ELECTRIC FIELD IN CF_2

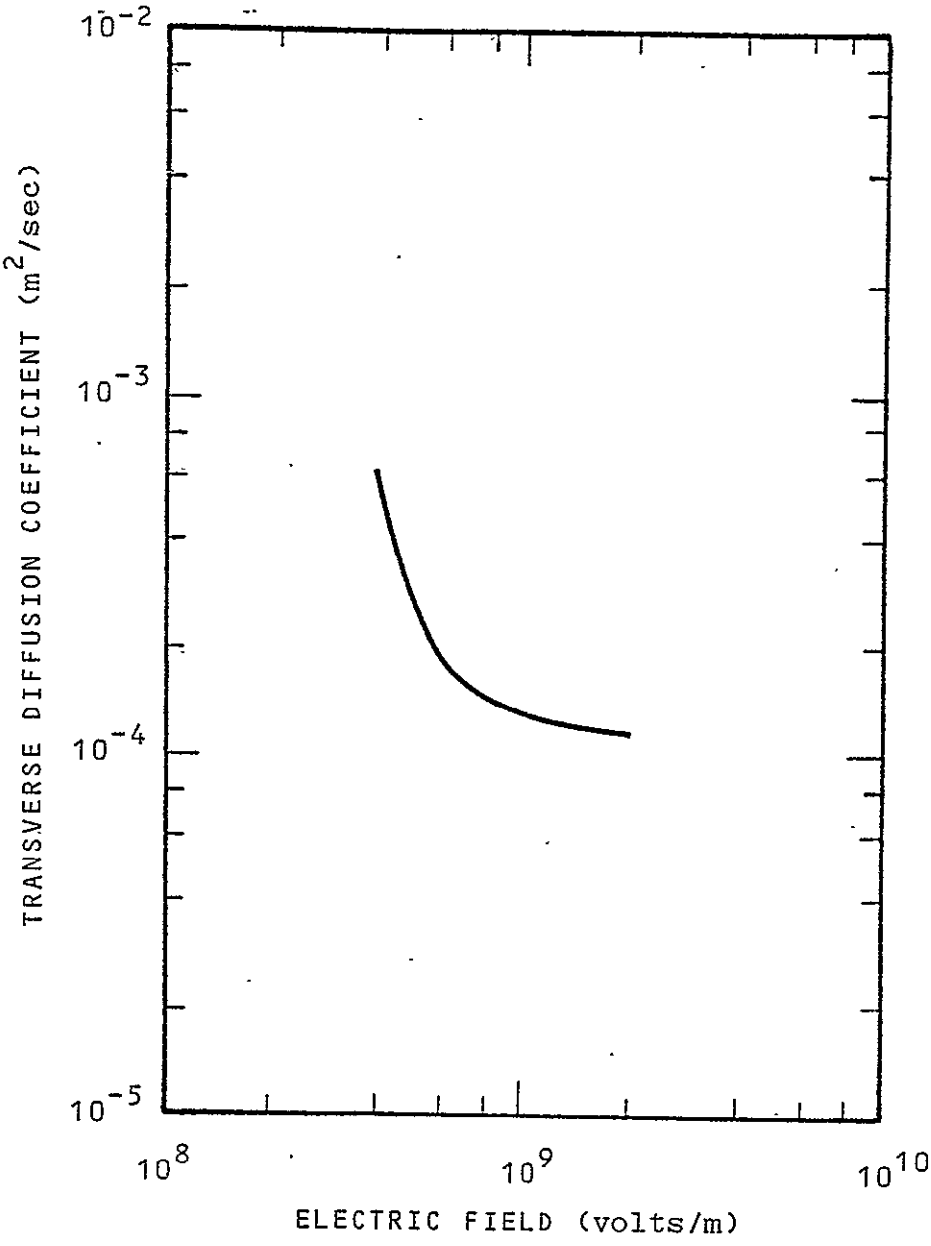

FIGURE 2.9. TRANSVERSE DIFFUSION COEFFICIENT AS A FUNCTION OF APPLIED ELECTRIC FIELD IN CF_2

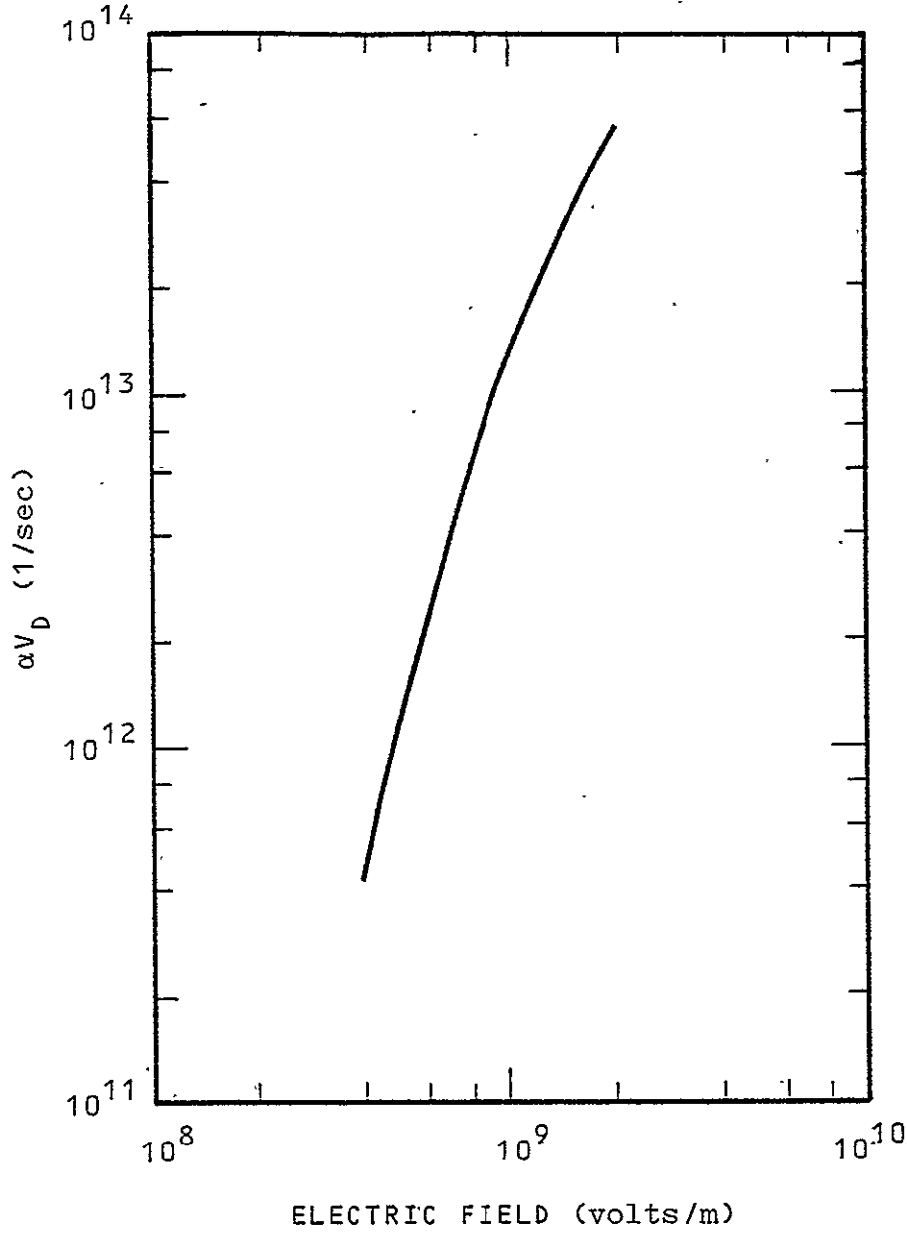

FIGURE 2.10. IONIZATION FREQUENCY AS A FUNCTION OF APPLIED ELECTRIC FIELD IN CF_2

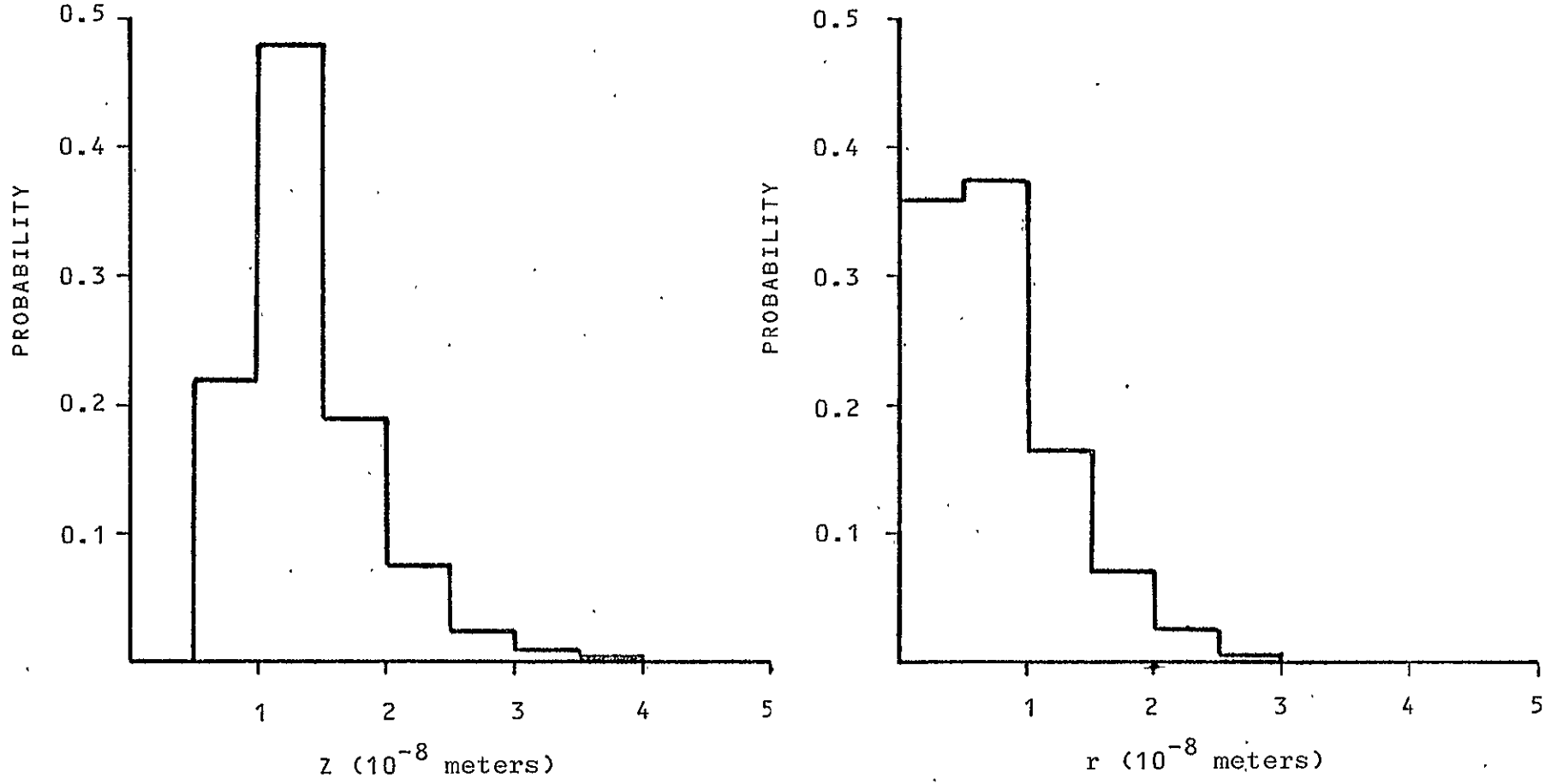

FIGURE 2.11. PROBABILITY DISTRIBUTION FUNCTION IN r AND Z FOR FIRST IONIZATIONS FOR AN APPLIED ELECTRIC FIELD OF 8 x 10^8 volts/m

Section 3

ELECTRON AVALANCHE

In the previous section we developed the computational apparatus for calculating the production of a second conduction band electron due to impact ionization by an existing conduction band electron. The newly created electron is expected to undergo the same acceleration process due to the electric field, i.e., its dynamics should be identical to those of the first electron. An electron multiplication (avalanche) with drift is expected (the Townsend mechanism). For an avalanche generated by a single initial electron, we envision the evolution of the avalanche to be a spatially and temporally coherent process (within the confines of the Uncertainty Principle discussed in Section 2.1). In this section we discuss this phenomenon, our approach to computing its evolution, and some numerical results for Teflon.

3.1 THEORY

Extensive cloud chamber and electrical observations in gases have demonstrated that spatially and temporally coherent electron avalanches can be generated by a single electron. We refer the reader to the excellent book by Raether (1960) which describes the foundations of this research, and to the recent book by Meek and Craggs (1978) for a current survey of the literature. Shown in Figure 3.1 is a schematic representation of such an avalanche. A single electron was freed at the tail of the figure. As the electron drifted with the field, it created a second electron – this pair of electrons in turn generated four electrons, and so on. As the electrons drift with the field, they also diffuse due to collisions with the background gas, while the relatively immobile ions remain more or less stationary.

This picture of single-electron induced avalanche is conceptually precise. Neglecting complications due to other rate processes (attachment, recombination, etc.) it admits, on the average, a simple description. The total number of electrons N in the avalanche is given by

$$N = e^{\alpha x} \tag{3.1}$$

where α is the inverse ionization length (first Townsend coefficient) computed in Section 2 above, and x is the drift distance along the avalanche direction, given by

$$x = v_D t \tag{3.2}$$

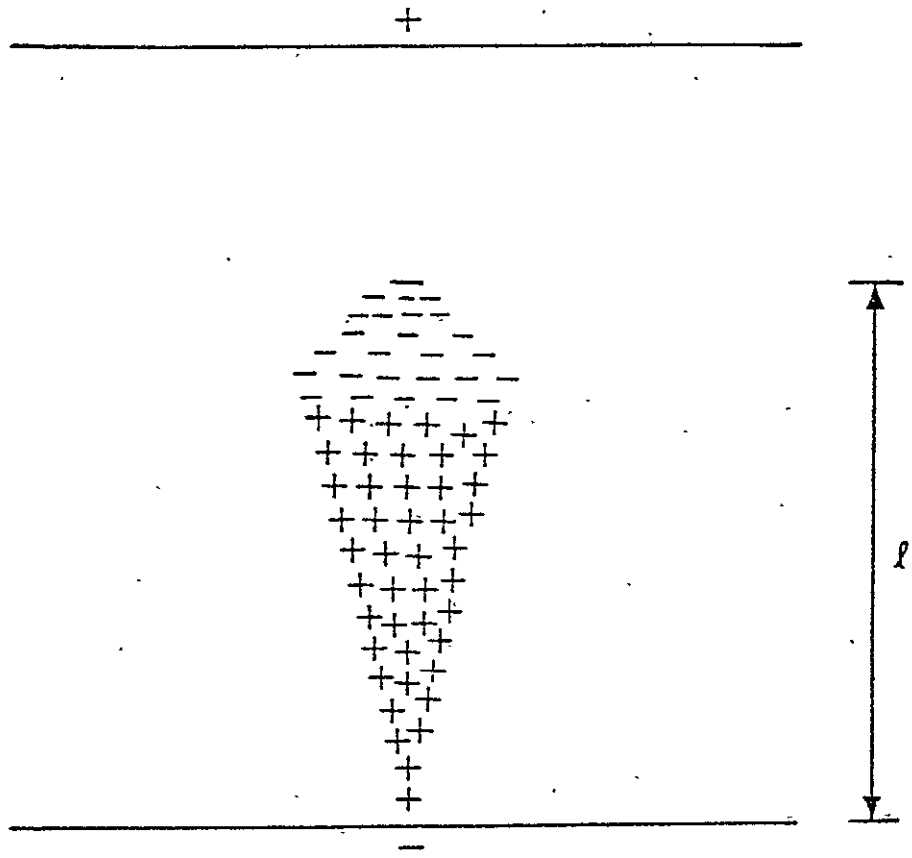

FIGURE 3.1 CONCEPTUAL MODEL OF A SINGLE-ELECTRON INDUCED AVALANCHE

where v_D is the drift velocity and t is time. The volume occupied by this number of electrons is roughly spherical (centered at x) and grows in radius r by diffusion as

$$r^2 = r_o^2 + 6Dt \tag{3.3}$$

where D is the diffusion coefficient. Thus, the electron density as a function of distance is given by

$$n_e(x) = \frac{e^{\alpha x(t)}}{4/3\pi r^3(t)} \tag{3.4}$$

while the positive ion density n_+ may be obtained by integrating the equation

$$\frac{dn_+}{dt} = \alpha n_e \tag{3.5}$$

Insofar as a continuum description of the avalanche development is adequate, the above description is essentially complete (of course we have only computed mean values, the actual description requires solution of the drift and diffusion equations). These formulae provide the basis with which the phenomena may be analytically treated. Extensive analysis for gaseous avalanches may be found in Raether's book (1960) as well as many other places (e.g., Meek and Craggs, 1978). We merely note here the availability of this formulation which may be called upon as needed.

The above process continues until either the avalanche encounters a conducting boundary, or secondary effects become important. The major secondary effects which have been observed are those due to attachment and

recombination, photoionization and space charge. Attachment and recombination both tend to quench the avalanche. They must be accounted for if either effect is important at the field strength of interest. Photoionization of both the ambient gas and the electrodes can be caused by photons generated during radiative deexcitation of molecules excited by the drifting electrons. While this process is extremely important in gas breakdown, it has little impact on the evolution of the avalanche until space charge effects become important. The major effect at high amplification is to make the avalanche head somewhat more diffuse.

The major secondary effect which alters the development of the avalanche from the above simple picture is the space charge effect. The effective drift and multiplication of the electrons, together with the immobility of the ions leads to charge separation. This separated charge has a self-field which grows as the amount of free charge in the avalanche grows. When this self-field becomes comparable to the applied field, the further motion of the electrons is influenced by the total field. Further development requires the self-consistent evolution of the field and drift motions. While it is relatively easy to give estimates of this self-field (Raether, 1960), we will content ourselves here with some general observations, as we present a numerical prescription and evaluation of the self-field in results below. For gas pressures typical of laboratory experimentation ($\sim$ 1 Torr), it has been observed that space-charge effects do not become important until the avalanche has reached an amplification of 10^6-10^8. For parameters characteristic of solids, however, one expects

self-field effects to become important at much smaller amplifications, of the order to 10^2-10^4. Some reflection on Figure 3.1 together with inspection of figures given in the next section demonstrate that the space charge fields are rather complicated. In particular, a one dimensional description (as has often been used for estimates) is far from adequate to describe its features. Qualitatively, the field is that of a dipole, so that outside the charge distribution the electric field is enhanced over its ambient value, while internal to the distribution the field tends to oppose the applied field. These features of the space charge field (enhancement outside, decrease inside) are the characteristics which determine the further evolution of the avalanche.

It is our working hypothesis that single-electron induced avalanches of the type described above also take place in solids, and that these avalanches may ultimately evolve into breakdown channels. In the next section we describe our approach to computing the properties of these avalanches up until the time that space-charge effects become important. Further evolution in the space-charge dominated regime is described in Section 4.

3.2 COMPUTATIONAL APPROACH

As with the solution of the Boltzman transport equation, we have opted to simulate the electron avalanche with a Monte Carlo method. Also as before, a "crude" Monte Carlo has been used. The algorithm is

(1) The set of distribution functions for the location of ionization sites is integrated giving cumulative distribution functions for ionization sites.

(2) A 2-D cylindrical (r,z) grid is defined and a single electron initiated at 1 point in the volume.

(3) The site of the next ionization is randomly selected from the cumulative function defined in (1).

(4) The electron is moved to the selected position, the location of the ionized atom and the incident and newly released electron are separately recorded.

(5) The newly released electron is added to the aggregate of free electrons.

(6) The process (steps 3-5) is repeated for each electron in the current generation.

(7) After updating the electrons in the current generation, the charge density is calculated.

(8) The potential at the outer boundary of the grid is set via a multipole expansion.

(9) The potential within the volume is solved with a relaxation scheme.

(10) The fields are calculated and if the fields are less than an input value, the next generation of electrons is followed.

(11) If the fields exceed the maximum input value, the positive ion density and electron density are printed and written to disk. The net charge density, potential and electric fields are also printed.

The implementation of the above algorithm is uncomplicated except for the Poisson solution. Poisson's equation in cylindrical coordinates (r,z) (with $0 \leq r \leq a$, $0 \leq z \leq L$) is

$$\frac{\partial^2 \phi}{\partial r^2} + \frac{1}{r}\frac{\partial \phi}{\partial r} + \frac{\partial^2 \phi}{\partial z^2} = -\rho/\varepsilon \qquad (3.1)$$

where ρ is the charge density and ε is the dielectric constant of the material.

A grid can be imposed on the region $0 \leq r \leq a$, $0 \leq z \leq L$ as follows. Let I,J be the number of grid points in the r-z directions, respectively, and define

$$\Delta r = \frac{2a}{2I-1} \qquad \Delta z = \frac{L}{J-1} \qquad (3.2)$$

The grid coordinates are

$$r_i = (i-1/2)\Delta r \qquad Z_j = (j-1)\Delta z \qquad (3.3)$$

for $1 \leq i \leq I$, $1 \leq j \leq J$. Note that $r_I = a$, $z_J = L$. Let the notation $f_{ij} = f(r_i, z_j)$ be used and let $F = -\rho/\varepsilon$. The differential equation is anchored to the grid by

$$\left(\frac{\partial^2\phi}{\partial r^2}\right)_{ij} + \left(\frac{1}{r}\frac{\partial\phi}{\partial r}\right)_{ij} + \left(\frac{\partial^2\phi}{\partial z^2}\right)_{ij} = F_{ij} \qquad (3.4)$$

where $1<i<I$, $1<j<J$. The potential on the $z=o$, $z=z_{max}$ and $r=r_{max}$ boundaries is set by a multipole expansion.

The derivatives are approximated by

$$\left(\frac{\partial\phi}{\partial r}\right)_{ij} = \frac{\phi_{i+1,j} - \phi_{i-1,j}}{2\Delta r} \qquad (3.5)$$

$$\left(\frac{\partial^2\phi}{\partial r^2}\right)_{ij} = \frac{\phi_{i+1,j} - 2\phi_{ij} + \phi_{i-1,j}}{\Delta r^2} \qquad (3.6)$$

$$\left(\frac{\partial^2\phi}{\partial z^2}\right)_{ij} = \frac{\phi_{i,j\ 1} - 2\phi_{ij} + \phi_{i,j-1}}{\Delta r^2} \qquad (3.7)$$

for $1<i<I$, $1<j<J$. The radial derivatives at $i = 1$ are derived as follows. Consider the regular grid points (r_i,z_j) as lying in the Θ plane and let the grid points (r_o,z_j) lie in the $\Theta + \pi$ plane, where $r_o = -\Delta r/2$. The symmetry condition requires that $\phi_{oj} = \phi_{1j}$, $1\leq j\leq J$. If these conditions are imposed for $i = 1$ the result is

$$\left(\frac{\partial \phi}{\partial r}\right)_{ij} = \frac{\phi_{2j} - \phi_{1j}}{2\Delta r} \tag{3.8}$$

$$\left(\frac{\partial^2 \phi}{\partial r^2}\right)_{1j} = \frac{\phi_{2j} - \phi_{1j}}{\Delta r^2} \tag{3.9}$$

The above difference framework can be anchored to a simultaneous relaxation scheme. Let the residual R_{ij} be given by

$$R_{ij} = \left(\frac{\partial^2 \phi}{\partial r^2}\right)_{ij} + \left(\frac{1}{r}\frac{\partial \phi}{\partial r}\right)_{ij} + \left(\frac{\partial^2 \phi}{\partial z^2}\right)_{ij} - F_{ij} \tag{3.10}$$

where $1 \leq i < I$, $1 < j < J$. The relaxation scheme must converge which means the residuals should become smaller as the iteration process proceeds. Suppose the influence of all points surrounding the ij^{th} point be neglected and let k denote the coefficient of ϕ_{ij}. Then k is given by

$$k = -2\left(\frac{1}{\Delta r^2} + \frac{1}{\Delta z^2}\right) \tag{3.11}$$

and

$$R_{ij} = k\phi_{ij} - F_{ij} \tag{3.12}$$

Let $\delta\phi_{ij}$ be a small change in ϕ_{ij} and δR_{ij} the corresponding change in R_{ij}. Then

$$R_{ij} + \delta R_{ij} = k\phi_{ij} + k\delta\phi_{ij} - F_{ij} \tag{3.13}$$

Combining the above yields

$$\delta R_{ij} = k\delta\phi_{ij} \tag{3.14}$$

The new residual $R_{ij} + \delta R_{ij}$ is zero provided $R_{ij} = -\delta R_{ij}$. Thus

$$\delta\phi_{ij} = -R_{ij}/k \tag{3.15}$$

Let $\phi'_{ij} = \phi_{ij} + \delta\phi_{ij}$. Then, $\phi'_{ij} = \phi_{ij} + cR_{ij}$, where $c = -1/k$.

In order to put the preceding results into an iterative scheme let n denote the number of the iteration, $1 \leq n \leq N$. The simultaneous relaxation scheme can be written

$$\phi^{n+1}_{ij} = \phi^{n}_{ij} + \alpha\, cR^{n}_{ij} \tag{3.16}$$

where α is a convergence parameter which under relaxes or over relaxes the scheme. Note that ϕ^{1}_{kj}, $1 \leq i \leq I$, $1 < j < J$, denotes a starting state that must be specified.

The simultaneous relaxation scheme can be considerably improved relative to computer run time by using all new information immediately after it is computed. Thus, if the computations for all j are performed for each i as i increases, the quantities $\phi^{n+1}_{i-1,j}$, $\phi^{n+1}_{i,j-1}$ are available in the computation for ϕ^{n+1}_{ij}. Such a scheme incorporating this new information is a sequential relaxation iteration procedure, and is the scheme used in CASCAD.

The convergence criteria used for the sequential scheme is

$$\max_{ij} \left| \frac{\phi_{ij}^{n+1} - \phi_{ij}^{n}}{\phi_{ij}^{n}} \right| \leq \varepsilon \qquad (3.17)$$

Convergence is influenced by starting state, convergence parameter and spatial grid size.

The above procedure has been implemented in a FORTRAN code called CASCAD. The operational features of CASCAD are described in Appendix 5. Some features of the code are:

- the distributions of first ionization sites, calculated by SEMC are required as input.
- the size of the grid must be large enough so that the multipole expansion of the potential on the boundary will converge with a few terms (<10).
- maximum number of generations is limited by central memory available ($<2^{14}$).

3.3 - RESULTS

3.3.1 N_2 RESULTS

Using the N_2 parameters calculated by the SEMC code, we have calculated the avalanche history through 12 generations (4096 electrons). As expected, the electric field remained small (550 volts/meter). Estimates indicate that 20 to 30 generations would be necessary for field to approach 10^7 volts/m.

3.3.2 TEFLON RESULTS

Employing the SEMC code results for Teflon, the electron avalanche time history in Teflon was computed using CASCAD. The computation was terminated when the space charge field reached 50% of the applied field. For an applied field of 8×10^8 V/m, this occurred after 12 generations. This is entirely consistent with the following analytical estimate of the space-charge field:

$$E = E_o \frac{e^{\zeta}}{\zeta^{3/2}}$$

where ζ is the number of generations, and E_o is related to the problem parameters by:

$$E_o = \frac{e}{4\pi\varepsilon_o X_I^2} \left(\frac{X_I}{r_o}\right)^3$$

X_I is the ionization length, and r_o is the elementary diffusion radius given by:

$$r_o = \sqrt{\frac{6DX_I}{v_D}}$$

Figure 3.2 shows the net charge density for the avalanche after twelve generations. Note its essentially dipole character. The positive and negative charge densities are shown in Figures 3.3 and 3.4. Note their very similar nature, and the delicate cancellation which gives rise to the net charge density of figure 3.2. These charge densities are consistent with the estimates given by equations 3.4 and 3.5. Shown in figure 3.5 is the electric field after 12 generations in Teflon. Note that it is rather complicated, but that external to the charge distribution, it is dipole in character. These results form the initial conditions for the computations of Section 4. No surprises are apparent.

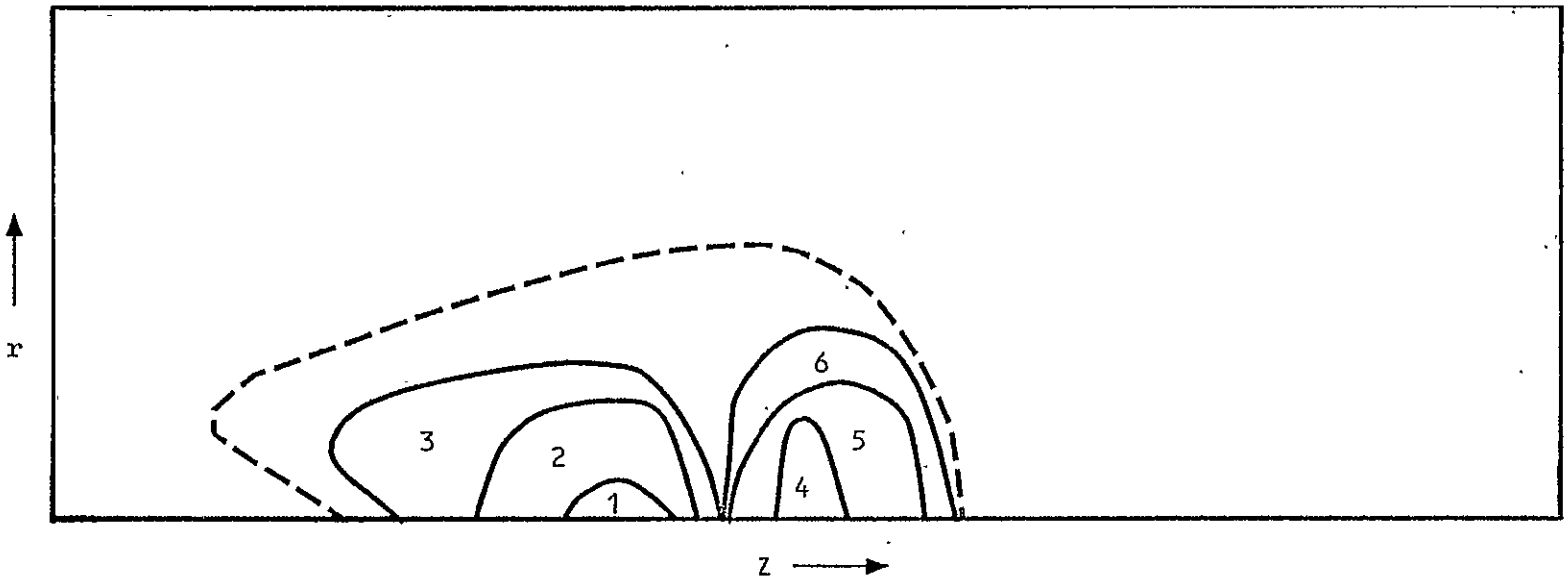

ALL CHARGE CONTAINED WITH DASHED BOUNDARY.

REGION	DENSITY (coul/m^3)	SIGN OF CHARGE
1	$> 5 \times 10^5$	+
2	$> 1 \times 10^5$	+
3	$> 5 \times 10^4$	+
4	$> 5 \times 10^5$	-
5	$> 1 \times 10^5$	-
6	$> 5 \times 10^4$	-

FIGURE 3.2. CHARGE DENSITY AS A FUNCTION OF SPACE FOR AN APPLIED ELECTRIC FIELD OF 8×10^8 volts/m AFTER 12 GENERATIONS

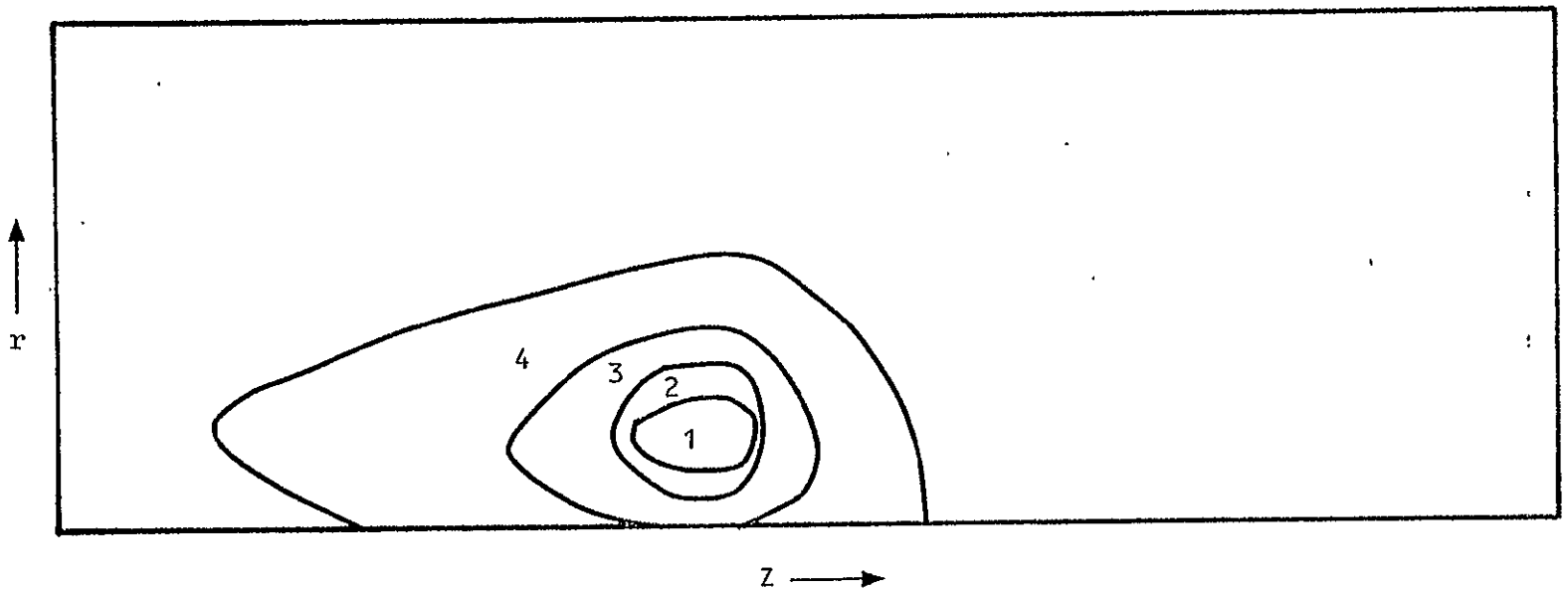

REGION	FRACTION OF POSITIVE CHARGE WITHIN REGION
1	0.34
2	0.50
3	0.88
4	1.00

FIGURE 3.3. POSITIVE CHARGE DISTRIBUTION FOR AN APPLIED ELECTRIC FIELD OF 8 X 10^8 volts/m AFTER 12 GENERATIONS

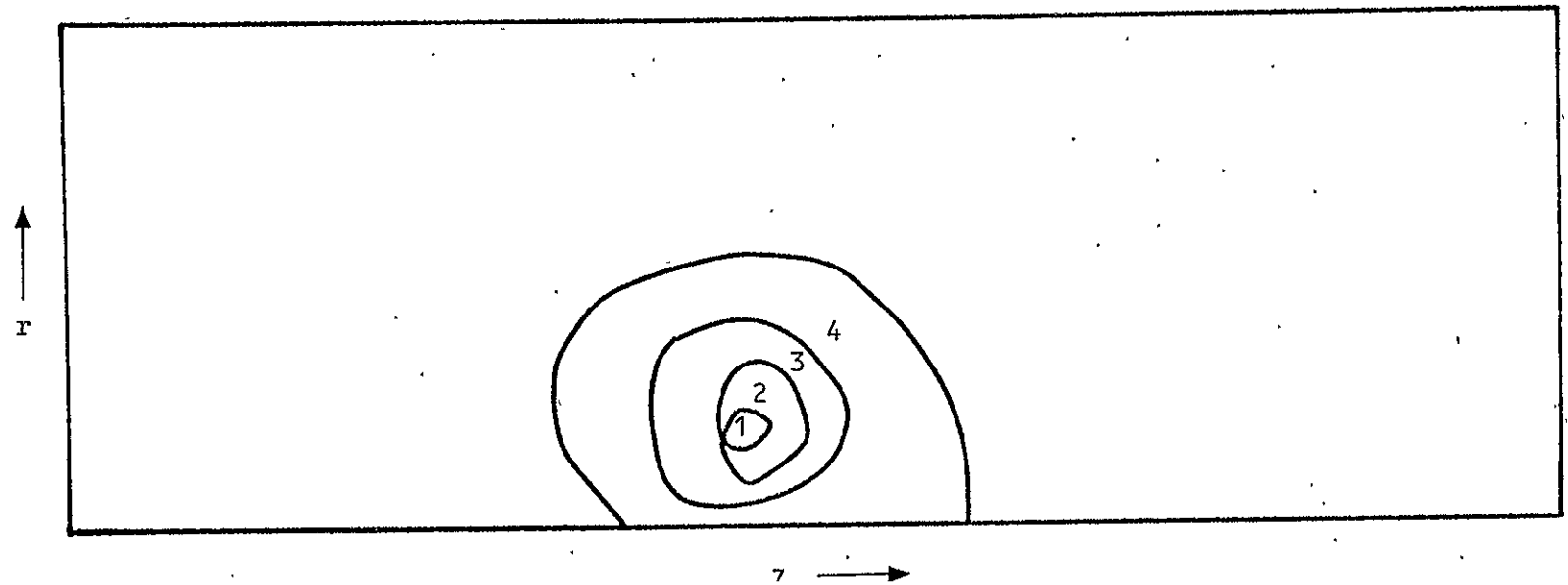

REGION	FRACTION OF NEGATIVE CHARGE WITHIN REGION
1	0.12
2	0.40
3	0.84
4	1.00

FIGURE 3.4. NEGATIVE CHARGE DISTRIBUTION FOR AN APPLIED ELECTRIC FIELD OF 8 X 10^8 volts/m AFTER 12 GENERATIONS

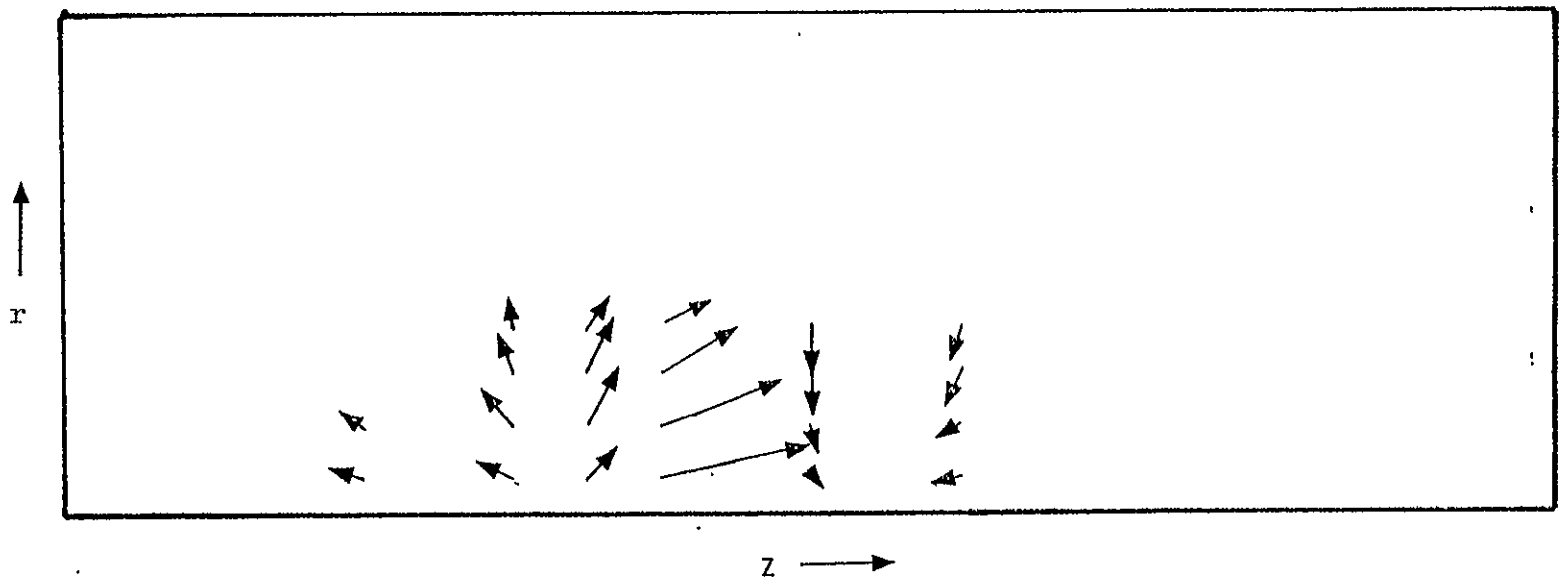

MAXIMUM VALUE: 4.7×10^8 volts/m

FIGURE 3.5. ELECTRIC FIELD DISTRIBUTION FOR AN APPLIED ELECTRIC FIELD OF 8×10^8 volts/m AFTER 12 GENERATIONS

Section 4

NEGATIVE STREAMER DEVELOPMENT

In the previous section we have developed computations of the evolution of single electron avalanches up until the time when space-charge fields become comparable to the applied field. Further development requires a description of the self-consistent evolution of both the fields and the electronic motions. We describe this phenomenon, our computational approach to calculating its evolution, and some model results for Teflon.

4.1 THEORY

In Figures 3.2-3.5 we have shown the electron, hole, total charge and electric field distributions due to a single electron induced avalanche in Teflon. We see that a negatively charged region appears near the front of the avalanche, while a positively charged region appears at the tail. In front of the negative tip, the field is enhanced over its ambient value. Behind the positive tip a similar situation prevails. Between the positive and negative charge regions, the field is diminished from its impressed value. Further, the field begins to develop a significant radial component.

In gases [Raether (1960), Meek and Craggs (1978)] it has been observed that when the conditions of strong space-charge prevail, a different set of physical phenomena occur. At both ends of the charge distribution the configuration distorts from the simple picture of Section 3 above, and a rapid propagation phase sets in. One end of the distribution propagates toward the anode, the other toward the cathode. Though the terminology is not completely uniform, these are usually called the "anode-directed streamer," and the "cathode-directed streamer." The anode-directed streamer evolves from the negatively charged tip, while the cathode-directed streamer evolves from the positively charged tip. It is our working hypothesis that similar phenomena can occur in solids. In this section we develop the theory of negative streamer development. A discussion of positive streamer development may be found in Section 5 below.

For the purposes of this discussion, we will assume a single trapping level. We will further assume that only electrons can be trapped — that hole trapping is not of importance. The generalization to include more complicated carrier kinetics will be apparent. We will further assume that the time scale of interest is long enough that all microscopic parameters are in local equilibrium, i.e., that macroscopic parameters may be used to describe the relevant physics. This should be an excellent assumption. For the conceptual purposes of isolation of effects, we will also assume the dielectric to be locally neutral, with the impressed electric field given by some distant sources.

Let us define the following symbols:

n_e - number density of conduction "band" electrons

n_+ - number density of holes

n_t - number density of trapped electrons

N_t - number density of trap sites

μ_e - electronic mobility of conduction band electrons

μ_+ - hole mobility

μ_t - "effective" mobility of trapped electrons

$\vec{v}_e$ - drift velocity of conduction band electrons

$\vec{v}_+$ - drift velocity of holes

$\vec{v}_t$ - "effective" drift velocity of trapped electrons

ρ - net charge density

$\vec{E}$ - Electric field

Φ - Electrostatic Potential

With these definitions, let us consider the various processes which can alter the basic number densities (n_e, n_+, n_t) [we label this as n_i respectively]. Each species may be transported by drift with the electric field, and diffusion due to number density gradients. The basic transport equation (derivable from Boltzman equation arguments) is

$$\frac{\partial n_i}{\partial t} + \nabla \cdot \vec{J}_i = \text{sources} \tag{4.1}$$

where

$$\vec{J}_i = n_i \vec{v}_i - D_i \vec{\nabla} n_i \tag{4.2}$$

The quantity $\vec{J}_i$ is the flux of particles of type i, $n_i \vec{v}_i$ is the flux due to field drift, $-D_i \vec{\nabla} n_i$ is the flux due to diffusion, and D_i is the diffusion coefficient for the i'th species. Each of the species number densities may also change due to sources, i.e., due to transitions from one type to the other. The number of electrons in the conduction band may increase due to creation of electron-hole pairs (valence band ionization), and thermal and collision induced detrapping, while it may decrease due to trapping, and electron-hole recombination. Assuming that all number densities are small compared to the valence band number density (an excellent assumption), these terms contribute sources βn_e, $\delta_1 n_t$, $\delta_2 n_e n_t$, $-a n_e (N_t - n_t)$, and $-b n_e n_+$, where β is the avalanche rate, δ_1 the thermal detrapping rate, δ_2 the collision induced detrapping rate, a the trapping rate, and b the recombination rate. Similarly, the number of trapped electrons may increase by trapping $[a n_e (N_t - n_t)]$ and decrease by detrapping $[-\delta_1 n_t - \delta_2 n_e n_t]$,

while the number of holes may increase by pair creation [βn_e] and decrease by recombination [$-bn_e n_+$].

The coefficients in these kinetic source terms are in general a function of the electric field strength $|\vec{E}|$, and the lattice temperature T, as are the mobilities and diffusion coefficients. The charge density $\rho = e(n_+ - n_e - n_t)$ determines the space charge field through Poisson's equation, while the impressed field $\vec{E}_o$ is assumed invariant. The lattice temperature is determined by the ambient conditions together with the joule heating of the lattice $\vec{J}\cdot\vec{E}$, where $\vec{J}$ is the net electrical current. It is assumed that the time scale is sufficiently fast that all energy deposition is instantaneous, that is, lattice thermal diffusion, and mechanical pressure relief are assumed much too slow to allow for energy transport away from the deposition site during the times of interest. The heating is therefore a strictly local process, the lattice internal energy increasing with the Joule heating, and the temperature increasing as a constant volume process.

With this background, we have the following equations describing the evolution of the system:

$$\frac{\partial n_e}{\partial t} + \nabla\cdot\vec{J}_e = \beta n_e + (\delta_1 + \delta_2 n_e)\, n_t - a n_e (N_t - n_t) - b n_e n_+ \qquad (4.3)$$

$$\vec{J}_e = n_e \vec{v}_e - D_e \vec{\nabla} n_e \qquad (4.4)$$

$$\vec{v}_e = -\mu_e \vec{E} \tag{4.5}$$

$$\frac{\partial n_+}{\partial t} + \nabla \cdot \vec{J}_+ = \beta n_e - b n_e n_+ \tag{4.6}$$

$$\vec{J}_+ = n_+ \vec{v}_+ - D_+ \vec{\nabla} n_+ \tag{4.7}$$

$$\vec{v}_+ = \mu_+ \vec{E} \tag{4.8}$$

$$\frac{\partial n_t}{\partial t} + \nabla \cdot \vec{J}_t = a n_e (N_t - n_t) - (\delta_1 + \delta_2 n_e) n_t \tag{4.9}$$

$$\vec{J}_t = n_t \vec{v}_t - D_t \vec{\nabla} n_t \tag{4.10}$$

$$\vec{v}_t = -\mu_t \vec{E} \tag{4.11}$$

$$\rho = e(n_+ - n_e - n_t) \tag{4.12}$$

$$\vec{J} = e(\vec{J}_+ - \vec{J}_e - \vec{J}_t) \tag{4.13}$$

$$\frac{\partial \rho}{\partial t} + \nabla \cdot \vec{J} = 0 \tag{4.14}$$

$$\nabla^2 \Phi = \frac{\rho}{\varepsilon} \tag{4.15}$$

$$\vec{E} = -\nabla \vec{\Phi} + \vec{E}_o \tag{4.16}$$

$$C_v \frac{\partial T}{\partial t} = \vec{J} \cdot \vec{E} \tag{4.17}$$

C_v is the specific heat at constant volume for the substance.

A substantial simplification of these equations is possible for the conditions of interest. Trap densities N_t in most solids are usually at most of the order of $10^{16}/cm^3$. As we saw in Section 3 above, electron avalanches quickly reach densities of the order of $10^{18}/cm^3$. The effect of the trapping is therefore expected to be of the order of 1% at most. We may therefore neglect trapping kinetics entirely, unless *a posteriori* inspection of the solutions suggests otherwise. Formally, we require $n_t=N_t=\delta_1=\delta_2=a\equiv 0$. For the highly mobile electrons well up in the conduction band, we also have the inequality $\mu_+ << \mu_e$. Thus, for the time scales of interest (10^{-12}-10^{-11} secs) we may neglect hole drift. This same inequality, together with the Einstein relation implies that we may neglect hole diffusion as well.

In the results presented in Section 4.3 below, the computations also assume that $b\equiv 0$, that is, recombination has been ignored. This is justified *a posteriori* by noting that the maximum hole densities reached are of the order of $10^{19}/cm^3$. The recombination coefficient for Teflon is thought to be $\approx 10^{-9}$ cm^3/sec [Gross (1978)], so that the maximum value of this term is $\approx 10^{-10} n_e$. For the time scales of the calculations ($\approx 10^{-11}$) this term may be neglected. For the larger times associated with the discussion of Section 5, this neglect is no longer justified. The subject will be readdressed during that discussion.

The above set of equations, together with the simplifications provide the basic model for the description of the development of the negative streamer. These equations should be good if:

a) there are sufficient numbers of particles available that a continuum description of the particle properties is justified

b) the time scale is sufficiently long ($>10^{-13}$ sec) that microscopic equilibrium has been achieved, and

c) the time scale is sufficiently short ($>10^{-10}$ sec) that the conditions on trapping and recombination noted above are valid.

All the above conditions are thought to be satisfied for computations given below.

What is the behavior of such a streamer expected to be? The literature associated with the computational modeling of this phenomena is fairly limited, and has been limited to investigations of gaseous discharges. Further, most of the work has been either one-dimensional, or quasi-two dimensional. Only the recent work of Davies, Evans and Woodson (1978) and Geary and Penney (1978) [see also Geary (1973)] appear to treat the fully two-dimensional problem. Earlier work may be traced from these references, as well as Bayle and Bayle (1974), Kline (1975), Ward (1965), Ward (1976), Kline and Sianbis (1971), Reininghaus (1973), Yoshida and Tagashira (1976) and Meek and Cragg (1978). These results are a bit difficult to interpret because of complications due to photoionization, parallel plate circuitry, secondary cathode ionization processes and an emphasis on the cathode

directed streamer. The results suggest that a thin shell of space charge develops which propagates at essentially a uniform velocity, and that an essentially neutral conducting region is left behind. The space charge distortion of the field reaches an equilibrium at a field substantially higher than the impressed field, and the effective velocity of propagation is consequently larger than would be expected from drift in the ambient field. Features such as these are best seen in the paper of Geary and Penney (1978). We will not discuss these qualitative features further here, as numerical results will be presented in Section 4.3 below. We merely note that it is the propagation of an ionizing space charge wave which we are attempting to model. We concentrate in this section on the negative tip alone.

4.2 COMPUTATIONAL APPROACH

In this section, we write down the specific equations for streamer propagation and describe the numerical methods used in the solutions. The system under consideration is axially symmetric and the equations are solved in 2-D cylindrical coordinates. A description of the operational feature of the code is given in Appendix 6. The code is an adaptation of the code SPARK2 which is publicly available from the CPC Program Library of the Queen's University of Belfast. This code has been documented by Davis, et al. (1978) in Computer Physics Communications. The reader is referred to this primary reference for a detailed discussion of several of the major algorithms. Our version of the code is called ACORN. The equation of basic interest is that for electron charge continuity and is obtained by combination of equations (4.3) and (4.4):

$$\frac{\partial n_e}{\partial t} + \nabla \cdot n_e \vec{v}_e = \beta n_e + D_e \nabla^2 n_e \qquad (4.18)$$

To complete the set of equations, we require equation (4.5) and specification μ_e, β, and D_e. The space charge part of the electric field is formally given in terms of a potential (equation 4.16), which, in turn, is obtained through solution of equation (4.15), the Poisson equation. The net charge density ρ in this equation can be obtained equivalently in two ways. We may solve eq. (4.6), along with eq. (4.3), to obtain the net density given by equation (4.12). Alternately, we can solve the net charge continuity equation (4.14) directly. The latter is the procedure we have taken in the numerical algorithm. The expression for the positive density can then be found from equation (4.12).

In summary, the equations ancillary to equation (4.18) are:

$$\vec{V}_e = -\mu_e \vec{E} \quad ; \quad (4.19)$$

$$\rho = e(n_+ - n_e) \quad ; \quad (4.20)$$

$$\vec{J} = -e\vec{J}_e = en_e\vec{V}_e + eD_e\vec{\nabla}n_e \quad ; \quad (4.21)$$

$$\frac{\partial \rho}{\partial t} + \nabla \cdot \vec{J} = 0 \quad ; \quad (4.22)$$

$$\nabla^2 \Phi = \frac{\rho}{\varepsilon} \quad ; \quad (4.23)$$

$$\vec{E} = -\vec{\nabla}\phi + \vec{E}_o \quad ; \quad (4.24)$$

The derivations for μ_e, β, and D_e have been discussed previously. In principle, the equations can admit arbitrary functions of the electric field. We have found for the Teflon case that μ_e and D_e are nearly independent of the field, and we have programmed simple constants into the code. On the other hand, β is found to take on the form

$$\beta = \alpha_o |\vec{V}_e| \exp(-\alpha_E / |E|)$$

where α_o and α_E are constants.

Equation (4.18) is solved numerically by a time-splitting process. The diffusion part of the equation is first stepped forward over a trial time step. The diffusion equation is solved implicitly so that the result is stable. The Peacemen-Rachford ADI method was used to solve the equation. The advantage of the scheme is that the diffusion equation can be written in tridiagonal form, thus simplifying the matrix inversion required for the solution. The remaining part of equation (4.18) is solved in the last frame of reference moving at the electron drift velocity, that is along the characteristic curve. This concept implies that the velocity during the time interval for the calculation must be known, and this is determined by an iterative scheme. At the beginning of the iteration, the drift velocity corresponding to the electric field found at the end of the previous time interval is used to estimate the characteristic derivative during the trial time interval. Then the continuity equation is integrated along the characteristic. The net change density equation is then found by an implicit solution of equation (4.21). Once the charge density is determined, Poisson's equation is solved to find the potential from which the electric field and corresponding electron drift velocities are obtained. These new values of the electron drift velocities are fed back into the beginning of the iteration sequence to find better estimates for the characteric curves. The solution along characteristic curves, as well as the diffusion solution, are calculated at least twice. Convergence tests are employed after solution of the potentials and after determination of the electric fields. A failure in these tests means that the solution along characteristics, as well as the time split

diffusion solution, must undergo at least two more iterations. When appropriate, a time step reduction is made before a new set of iterations on the characteristics is carried out.

The Poisson equation is solved in the z-direction by a method similar to Hockney's fast Fourier transform method. The remaining ordinary differential equations in the r-direction depend on the Fourier variable K and are solved by standard methods. The prescribed boundary conditions are introduced into the equations as pseudo charge sources.

The boundary potentials for the streamer problem correspond to free boundaries enclosing a charge distribution. With each iteration step where a new charge distribution is computed, a new set of boundary potentials is also determined. The boundaries are placed far away from the region of charge, so that a multipole expansion is appropriate. This technique is especially valuable for axisymmetric charge distributions because the azimuthal angle integration can be carried out analytically. There remain a set of two-dimensional charge moment integrals to solve. In order to make the resulting series converge as fast as possible, the origin for the moment calculations is taken to be midway between the positions of positive and negative charge centers, respectively.

Convergence of the iterative scheme was determined through two major tests. The first test was that no "fluid" element would drift more than halfway across a cell in one time step. This is the standard Courant check required for the stability of explicit solutions of the continuity equation. This technique is used to ensure that the trial time interval at the beginning of the iteration is indeed sufficiently small. Another check requires that the change of electric field over

the time interval did not exceed a prescribed value. This criterion is a measure of the conductivity of the system, for an electric field relaxes very quickly in a highly conductive medium. Since the conductivity is easily shown to be proportional to the electron density, the highest electron density in the system determines the smallest time step according to this criterion. In practice, this test was conservative and gave a smaller time step then was actually necessary, and a different stability criterion described below has been implemented. The reason that this criterion is overly strict is that the highest electron number densities occur behind the head of the anode streamer in a "passive" region where electric fields are small and near charge neutral conditions prevail. Under these conditions, some overshoot of the electric field relaxation can be permitted without harming the overall streamer solution. It is important, however, that only a fractional change of the electric field be allowed during a time step in the streamer head where the net charge density is negative. Since the electron density is usually smaller here than in the neutral region, the time increment will be larger when the relaxation criterion is applied only to the head of the streamers.

4.3 COMPUTATIONAL RESULTS

We have exercised ACORN to compute the evolution of the electron avalanche in Teflon when self-electric fields are important. The computation was performed for an applied field of 8×10^8 V/m. The parameters used for the electron drift quantities were those reported in Section 2.3.2. The initial conditions were those taken from Section 3.3.2. The computation was performed on a 21 x 64 grid with both radial and axial grid sizes of about 7.5×10^{-9} m (75 Å). The computations were carried out for a total evolved time of 0.73 ps. By this time in the calculation, the initial distribution has reached very near the boundary of the grid, and the required time steps have become quite small. Longer time computations have been performed (~2 ps) using slightly different material parameters on a grid with twice the above spacing. Though these results (meant to represent Lucite) are for a different material, they indicate that the results given above are indicative of the general features of the evolution. We will present these results elsewhere, and restrict our attention to the above noted Teflon computation.

Shown in Figure 4.1 and 4.2 are the time evolution of the high density ($>10^5$ C/m^3) regions of electron and hole concentrations. Note that the radial scale on these (and many subsequent) figures has been expanded to better display this variation. This region can be seen to be increasing in size by drift with the field and diffusion radially. A somewhat better feel for the spatial dependence of these densities may be seen by considering the contour plots of these quantities at the end of the calculation shown in figures 4.3 and 4.4. Note the sharp variation in profile near the axis in the direction of propagation. A better feel for the propagation can be obtained by considering the regions of

high net charge density. Shown in figure 4.6 is the region of large net negative charge density ($>10^5$ C/m^3), as a function of time. This region shows clearly the propagation of this "active" region to the right. This region propagates to the right and grows radially by diffusion and field distortion. The growth of the positive charge region which is left behind is shown in figure 4.7. Note its growth in both the radial and axial directions. Between the two regions of positive and negative charge, an essentially neutral region develops which grows as the active space charge head propagates to the right. This may be seen in the net charge density contour plot of figure 4.5. Note particularly the sharp variations in net charge density in the axial direction, in rough conformance with the results given in Appendix 8. An intuitive feel for the evolution of the field and charge density may be obtained from figure 4.8 which shows both the field and high charge density regions at the end of the calculation. Note the enhancement of the field over the ambient field both near the negative charge region and the positive charge region. In the internal essentially neutral region between the two charge regions, the field has been relaxed to a small value. External to this region, the field points either toward or away from the region, i.e., the fields are like those around a conductor. This type of feature is continuously evolving in the calculation.

A quantitative feel for these results will be obtained from figure 4.9, which shows the axial electric field and net charge density as a function of position along the axis at the end of the calculation. The enhanced fields at either end are clearly associated with the exposed charge regions. Note a factor of two increase in field near the positive tip, with not quite so large an increase near the negative tip. The time evolution of the field along the

axis is shown in figure 4.10. Note the clear propagation of the negative head, and the continuing increase in enhanced field.

Some feeling for the variation in the radial field may be obtained from figure 4.11, which shows this variation on two fixed radii as a function of axial distance. Note the correlation with the exposed charge regions. The radial variation of the radial field may be seen in figure 4.12, where several fixed Z profiles are displayed. The profile at Z=0.1 μ coincides with the positive charge region, that at 0.3 μ with the negative charge region, while the Z=0.2 μ profile falls in between.

The peak value of the axial electric field on axis is shown in figure 4.13 as a function of time. It is apparent that this is not nearly saturated. Ohmic heating of the lattice gives rise to a temperature change of the solid material in the avalanching regions. Shown in figure 4.14 is the maximum temperature as a function of time. While this does not represent a temperature rise nearly sufficient to cause major alteration of the solid, it does represent a significant temperature rise for so small a period of time. A profile of the temperature change is shown in figure 4.15. Note the sharp variation near the avalanche head.

Shown in figure 4.16 is the axial centroid of electron density as a function of time. While the data is not accurate enough to determine adequately the acceleration of the head, the mean velocity from the slope of 1.65×10^5 m/s is larger than the drift velocity in the ambient field. Another useful diagnostic on the propagation is given in figure 4.17, which gives the length of the effective dipole

as a function of time. The calculated results indicate an expanding dipole with acceleration. The strength of that same dipole can be seen as a function of time in figure 4.18. Note its rapid growth. Finally, the total number of electrons involved in the entire process is shown in figure 4.19. Note that this number is significantly smaller than that which would be obtained by unretarded avalanche.

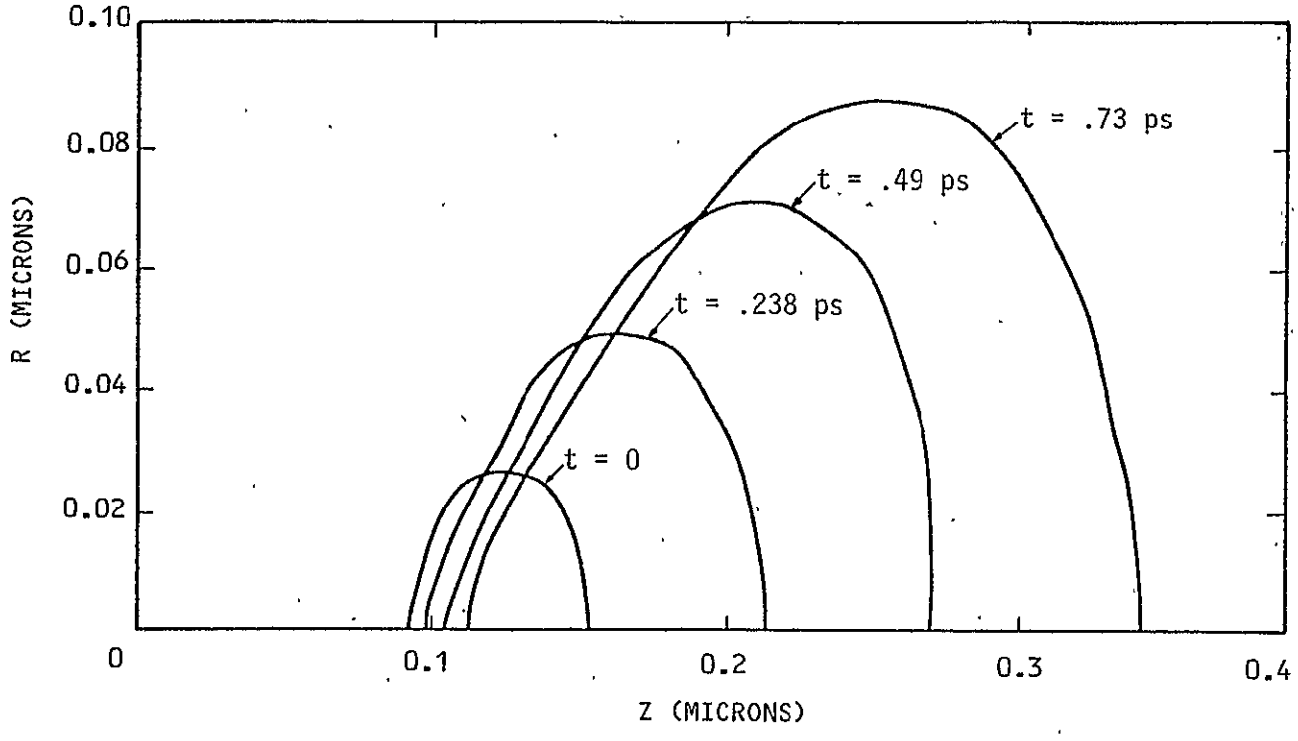

FIGURE 4.1. REGION FOR WHICH ELECTRON DENSITY > 10^5 coul/m^3 IN TEFLON

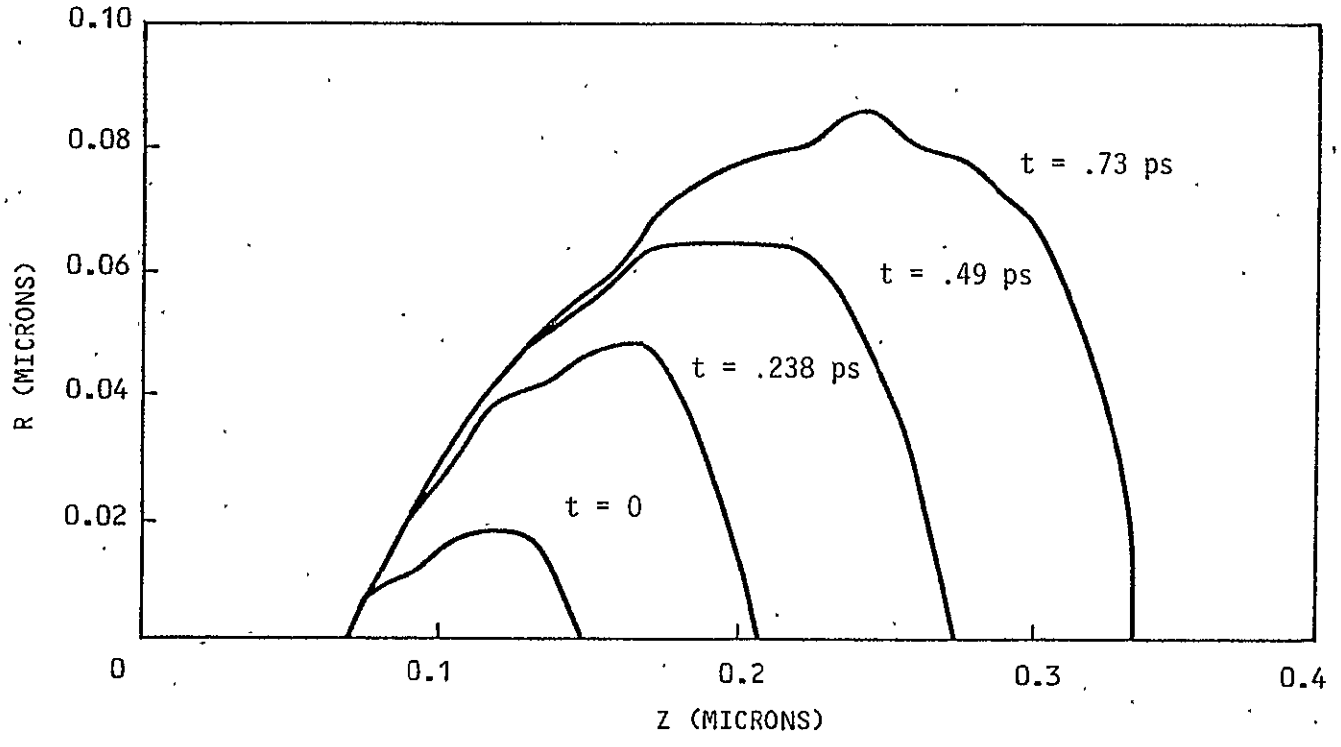

FIGURE 4.2. REGION FOR WHICH $N_p > 10^5$ coul/m^3 IN TEFLON

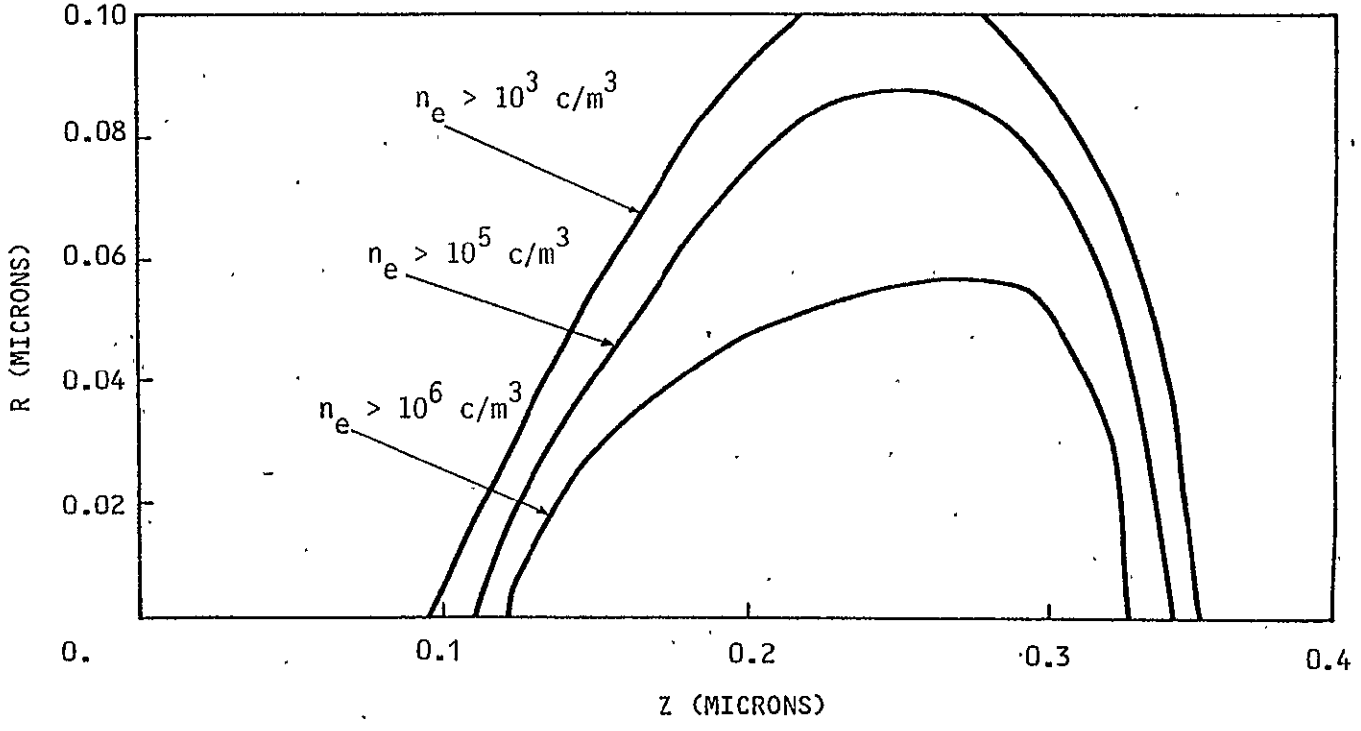

FIGURE 4.3. ELECTRON NUMBER DENSITY CONTOURS AT .73 ps IN TEFLON

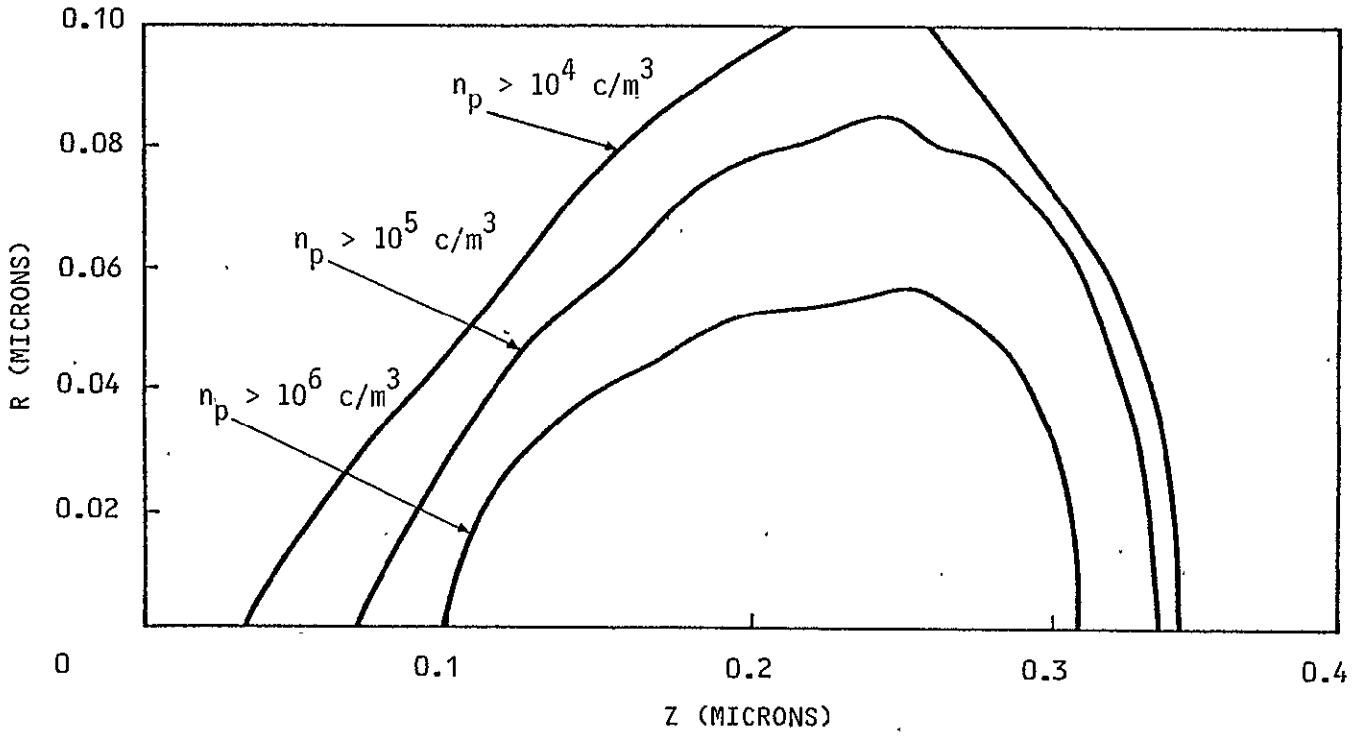

FIGURE 4.4. POSITIVE CHARGE DENSITY CONTOURS AT .73 ps IN TEFLON

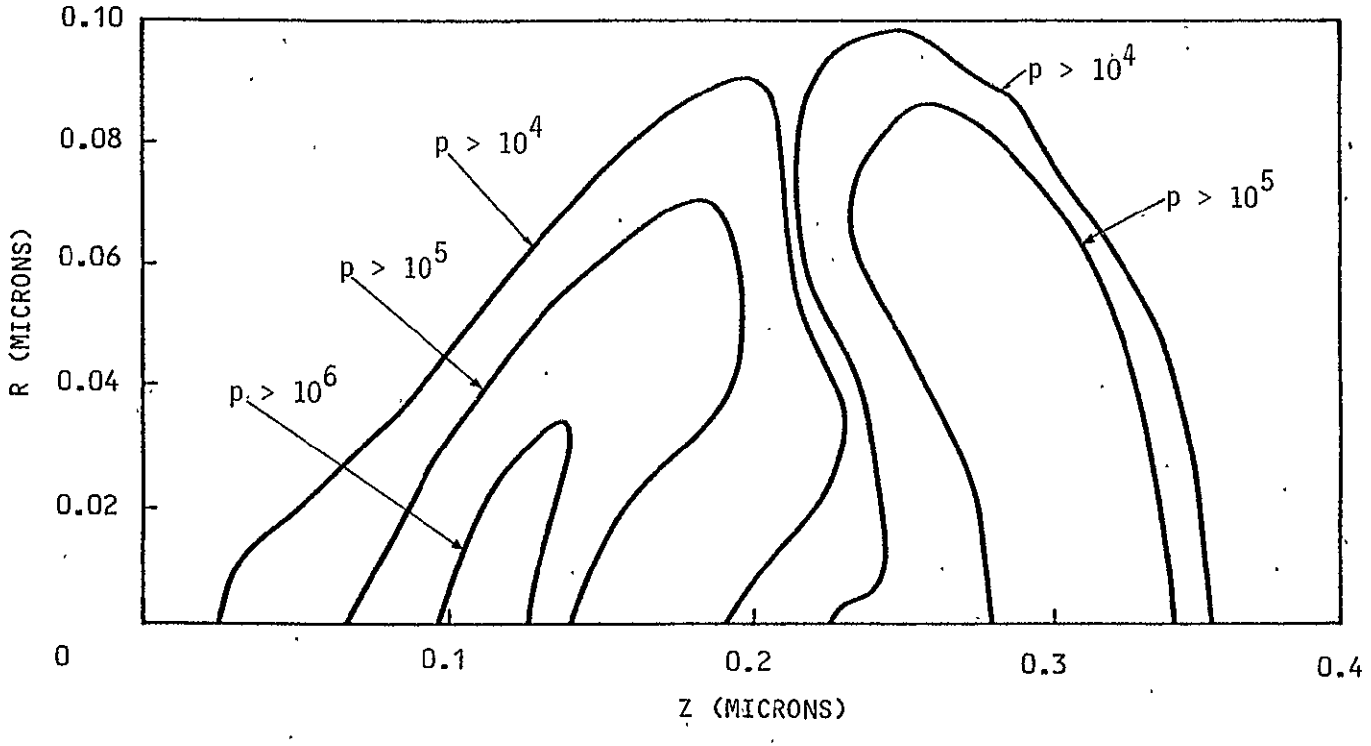

FIGURE 4.5. NET CHARGE DENSITY CONTOURS AT .73 ps IN TEFLON

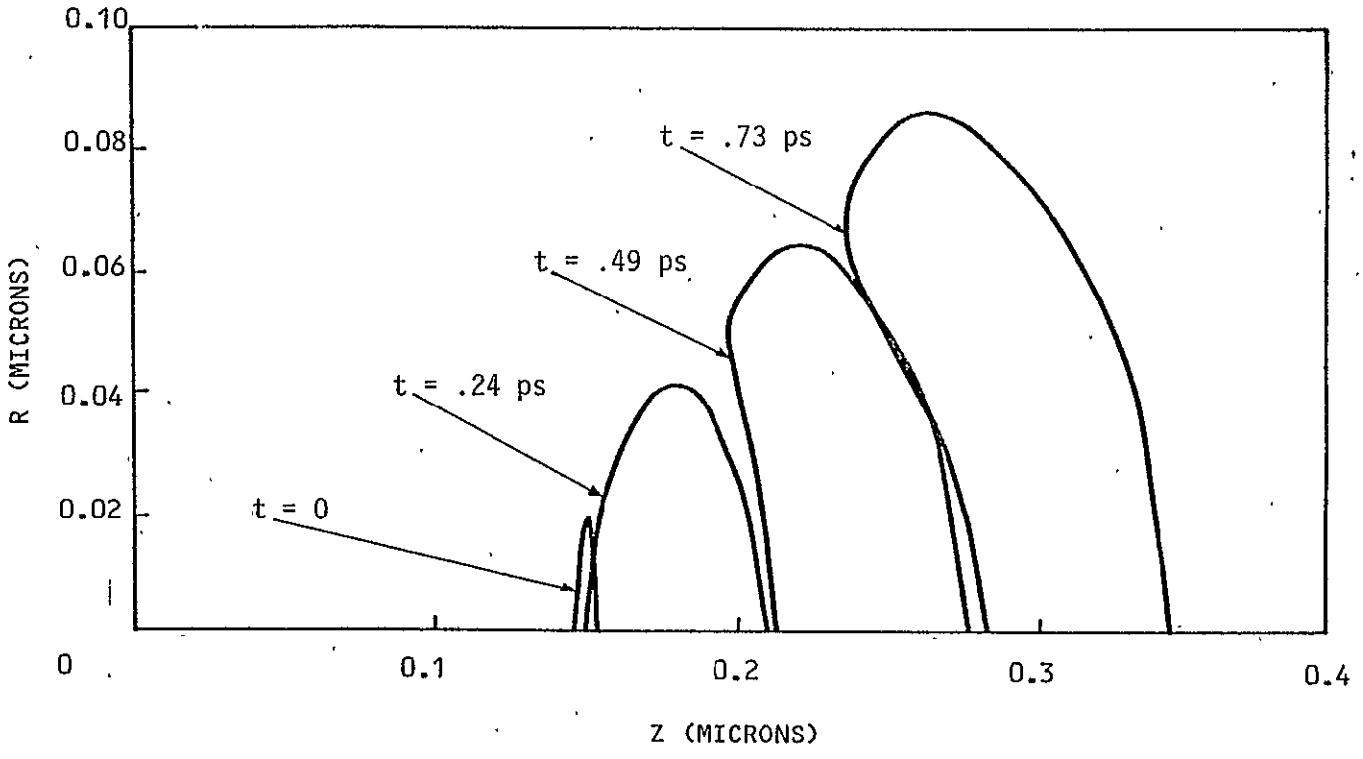

FIGURE 4.6. PROPAGATION OF THE REGION OF NEGATIVE CHARGE DENSITY > 10^5 coul/m^3 IN TEFLON

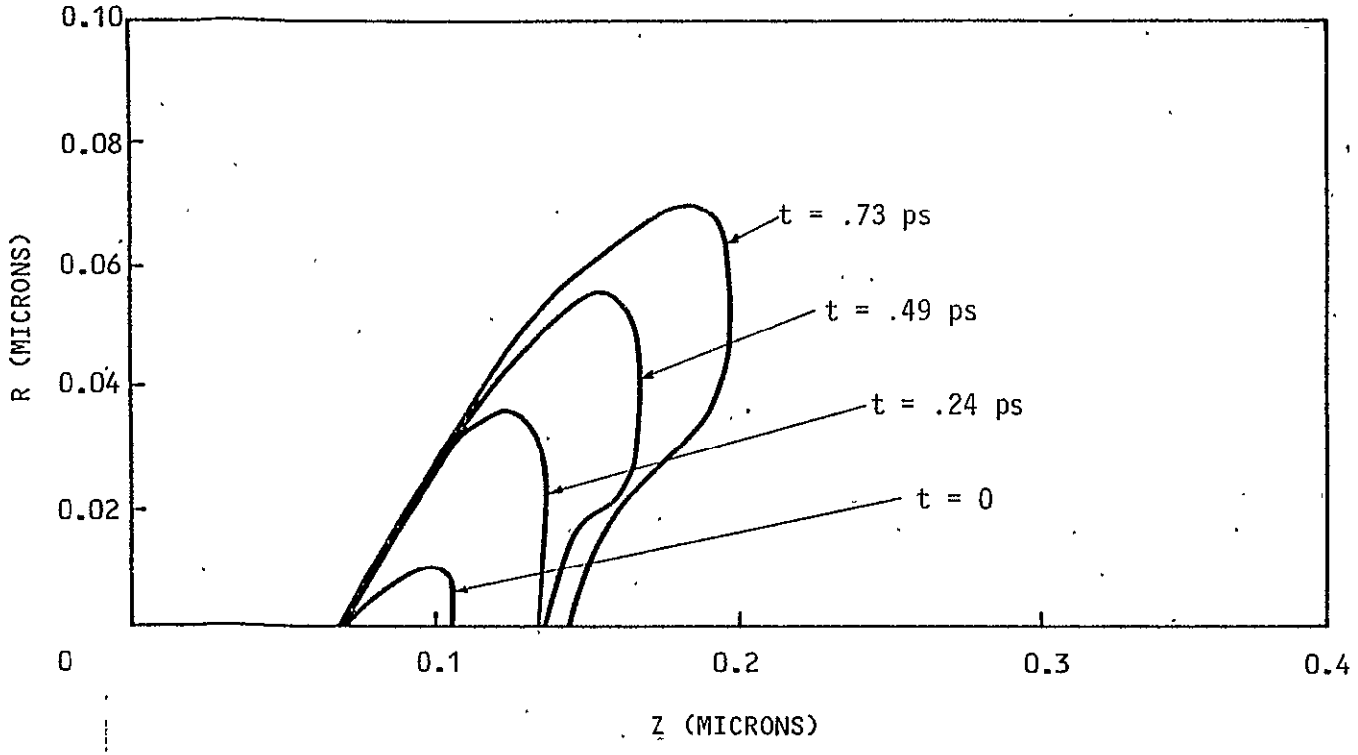

FIGURE 4.7. PROPAGATION OF THE REGION OF POSITIVE CHARGE DENSITY > 10^5 coul/m^3 IN TEFLON

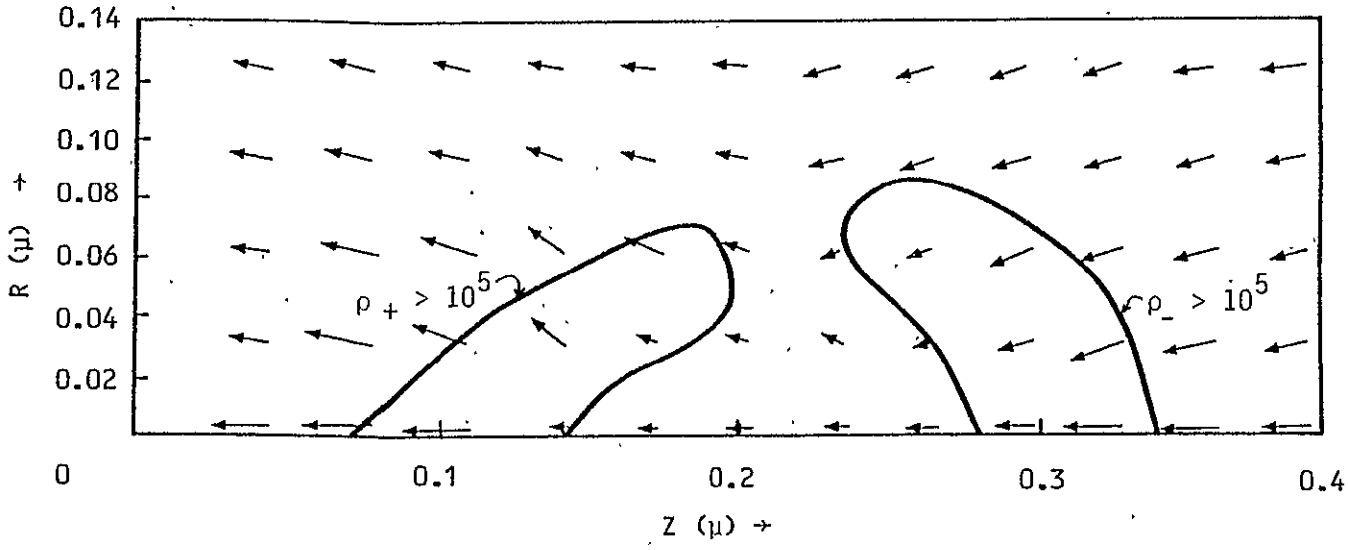

FIGURE 4.8. VECTOR FIELD AND ACTIVE CHARGE CONTOUR AT t = .73 ps

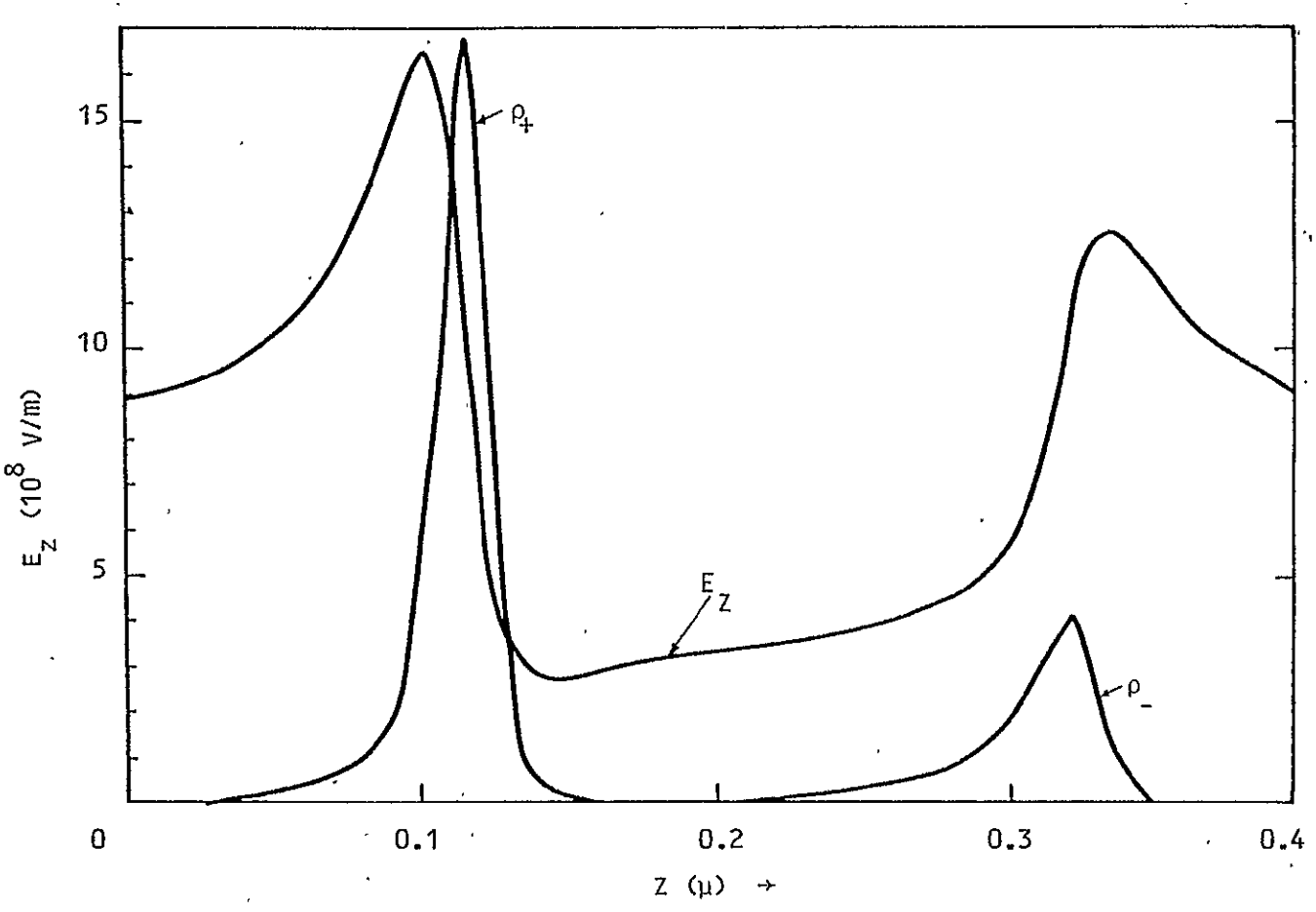

FIGURE 4.9. AXIAL FIELD AND NET CHARGE DENSITY ON AXIS TEFLON AT t = .73 ps

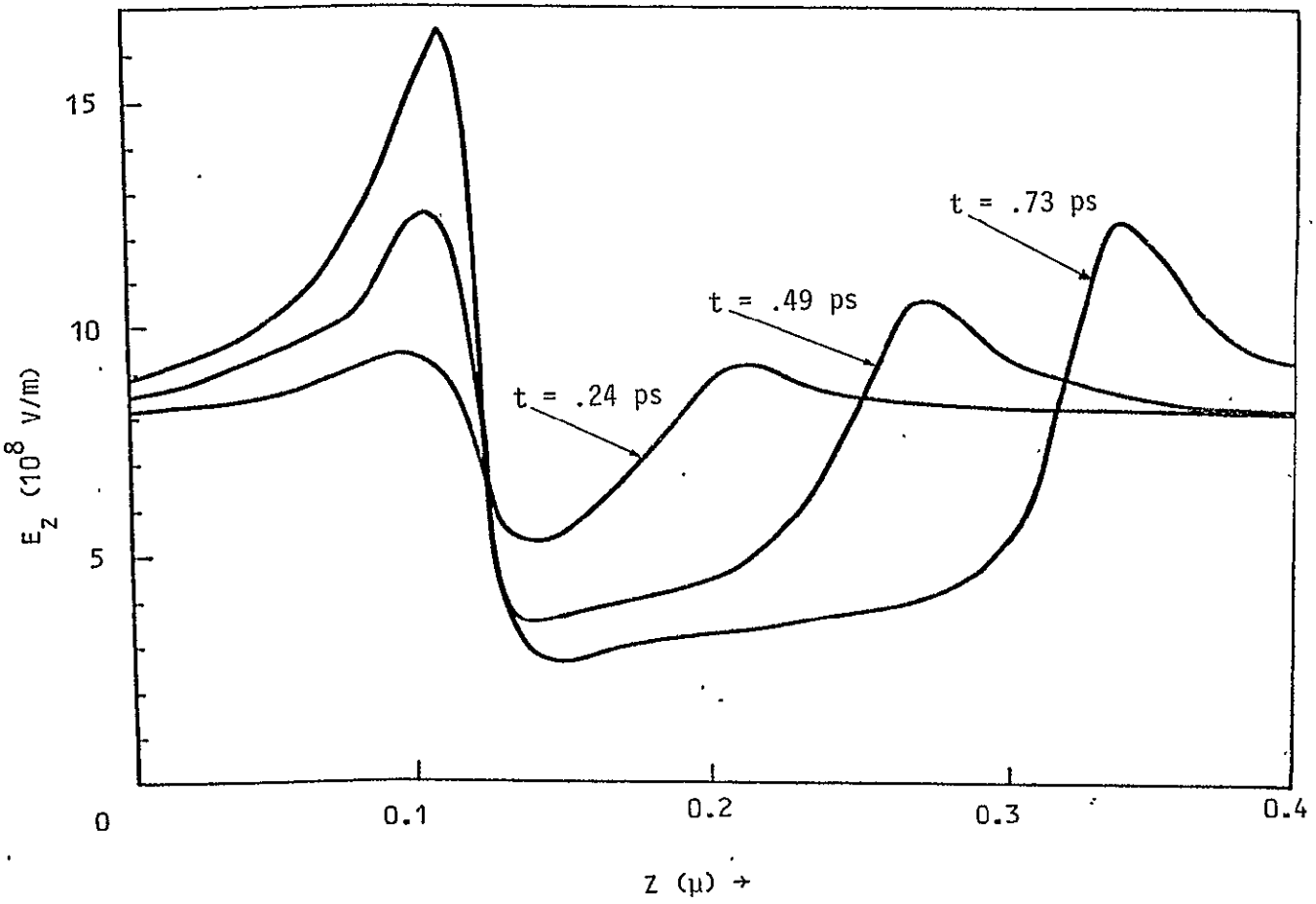

FIGURE 4.10. AXIAL FIELD ON AXIS vs. TIME-TEFLON

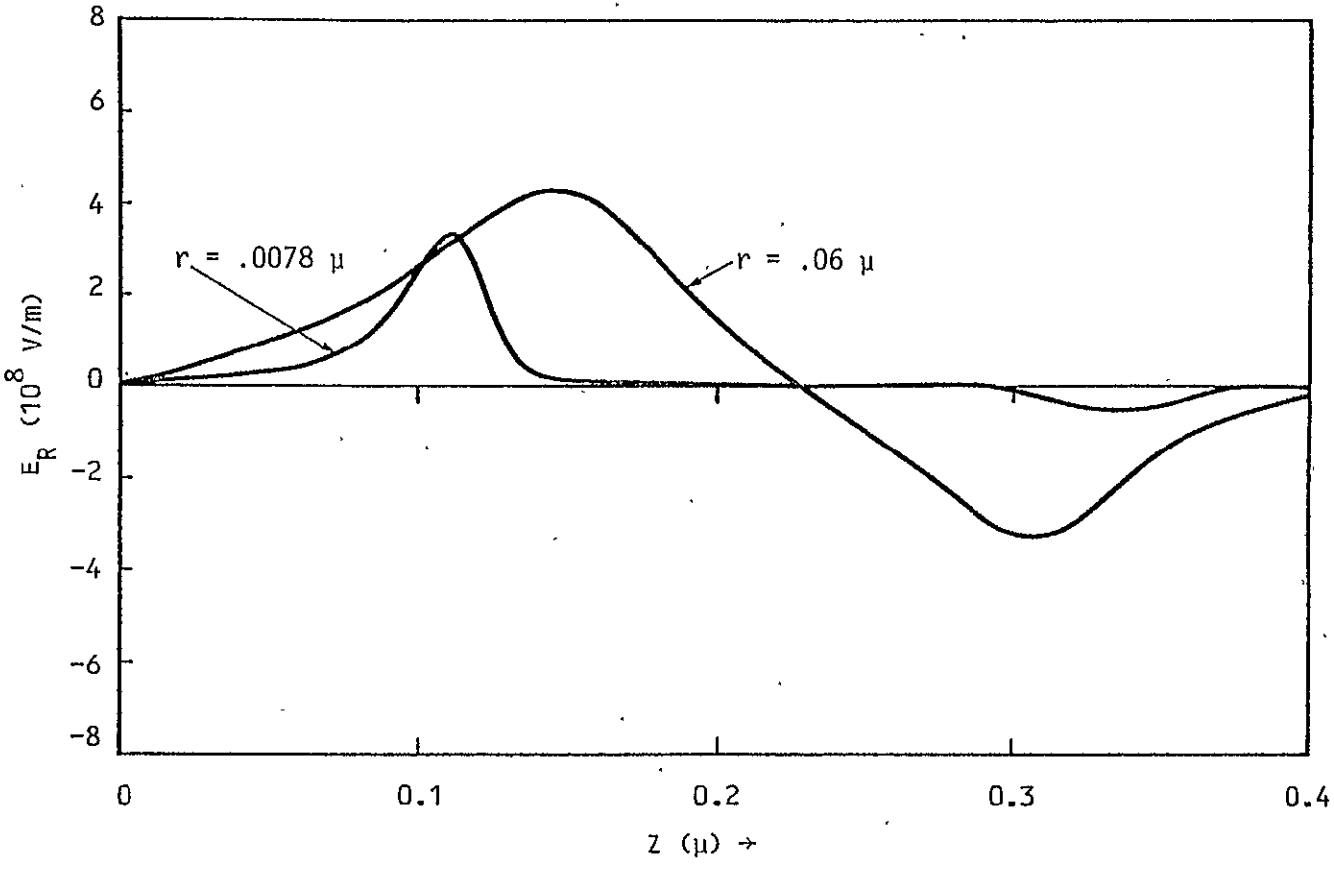

FIGURE 4.11. RADIAL FIELD ON TWO SLICES AT t = .73 ps-TEFLON

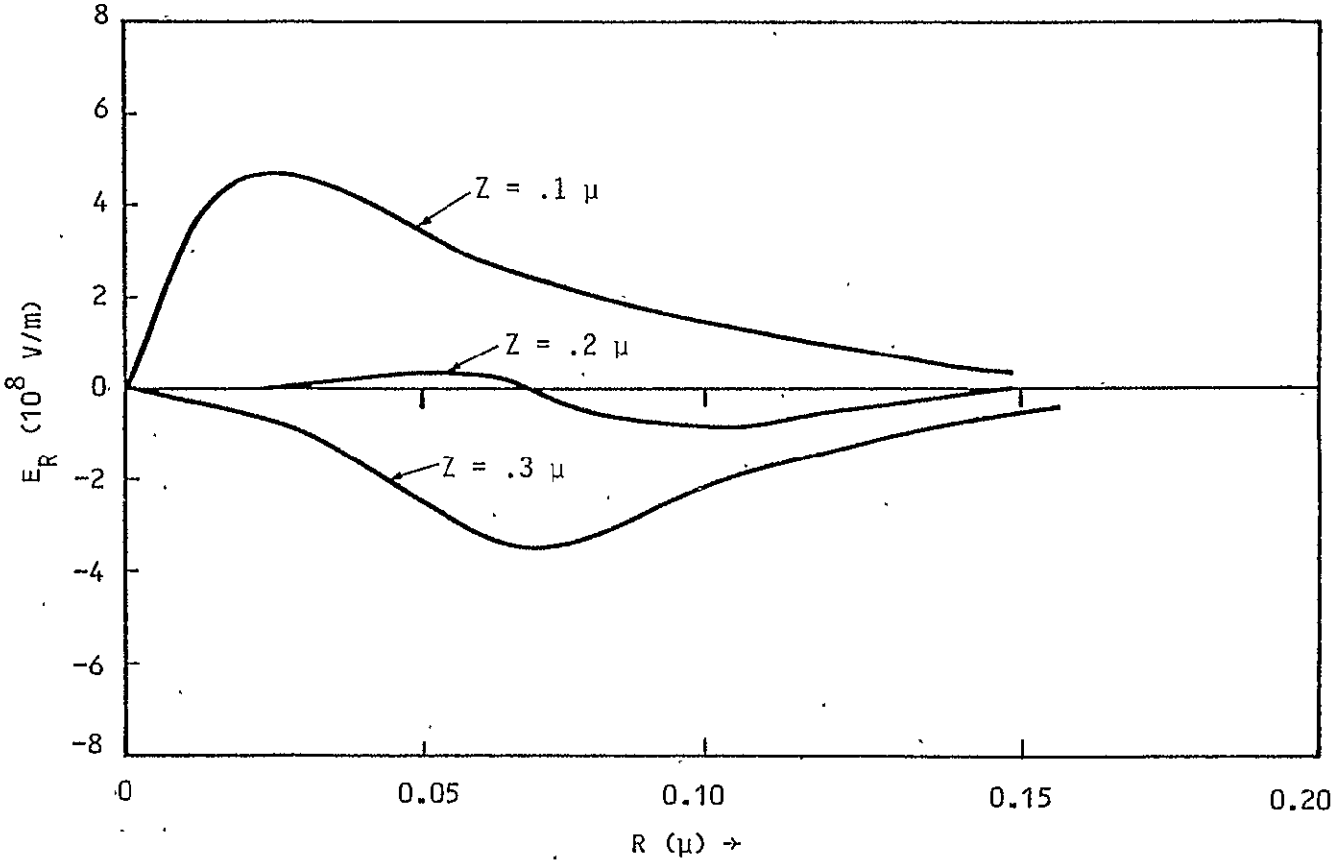

FIGURE 4.12. RADIAL FIELD vs. RADIUS AT t = .73 ps-TEFLON

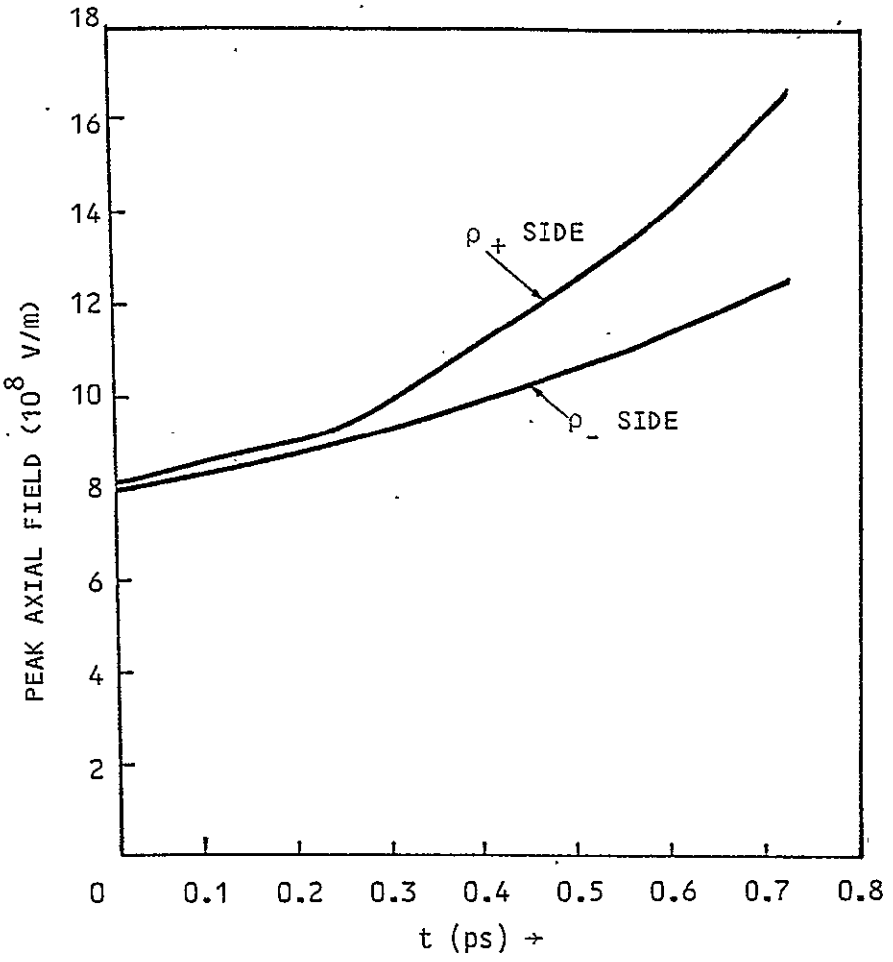

FIGURE 4.13. PEAK AXIAL FIELD ON AXIS vs. TIME-TEFLON

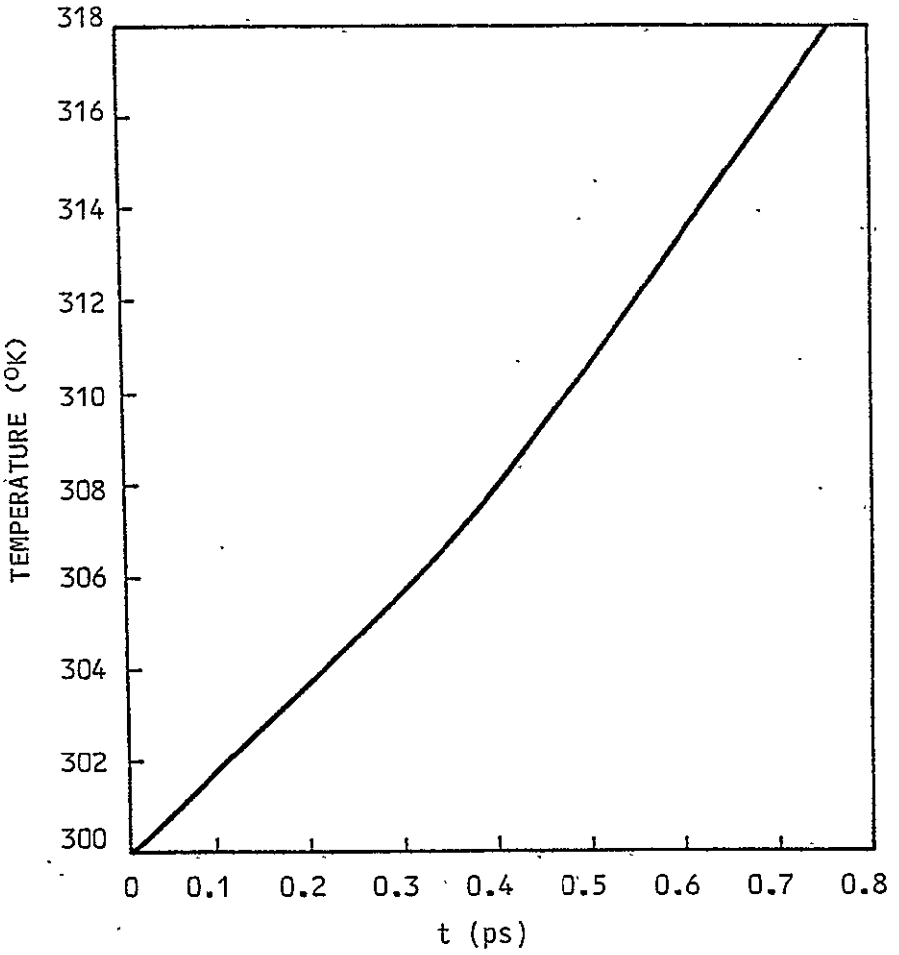

FIGURE 4.14. MAXIMUM TEMPERATURE vs. TIME-TEFLON

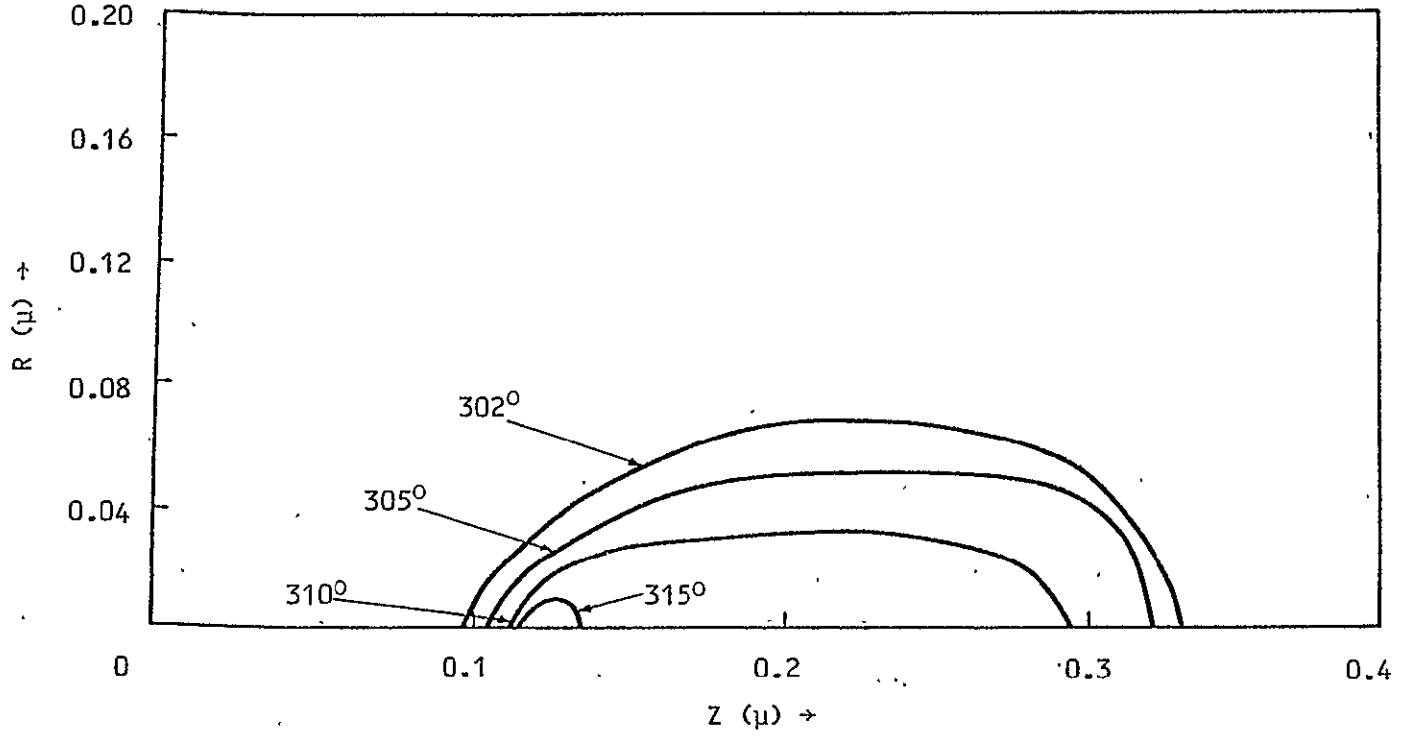

FIGURE 4.15. TEMPERATURE CONTOURS AT t = .73 ps-TEFLON

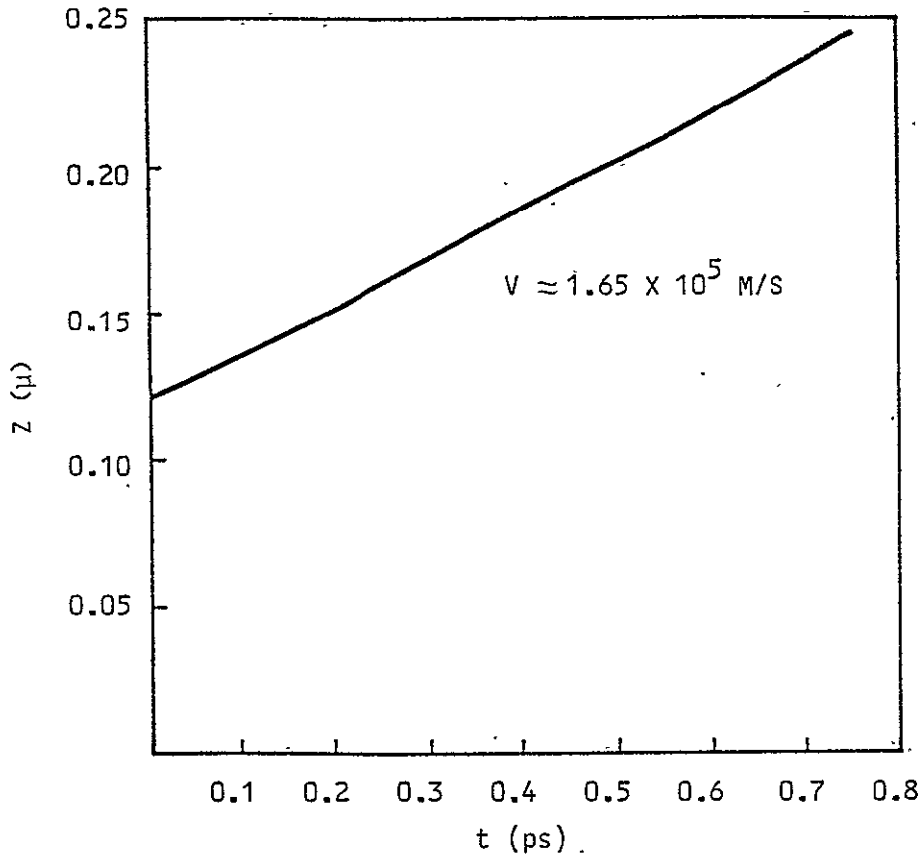

FIGURE 4.16. POSITION OF ELECTRON CLOUD CENTER vs. TIME-TEFLON

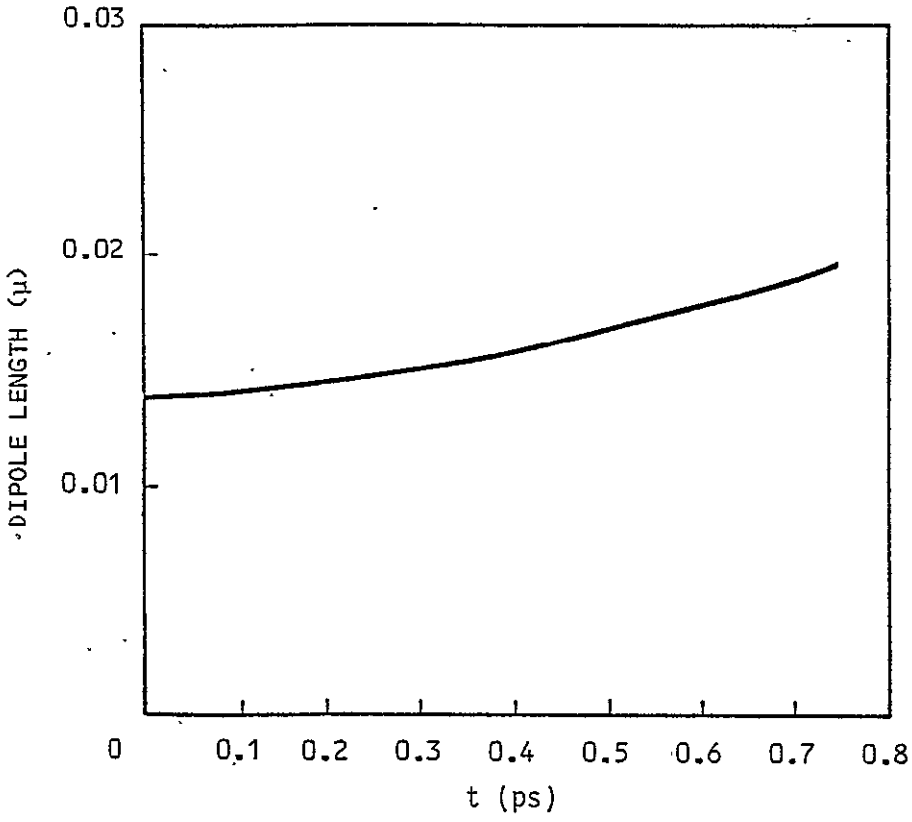

FIGURE 4.17. DIPOLE LENGTH vs. TIME-TEFLON

C-2

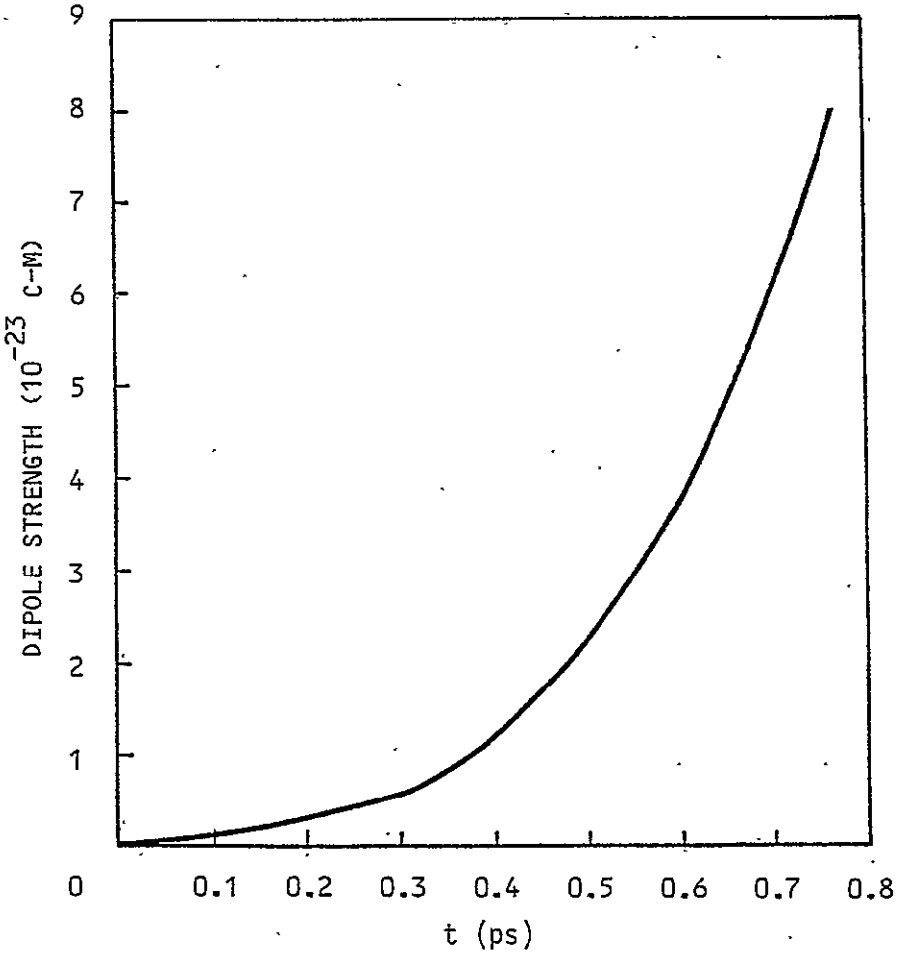

FIGURE 4.18. DIPOLE STRENGTH vs. TIME-TEFLON

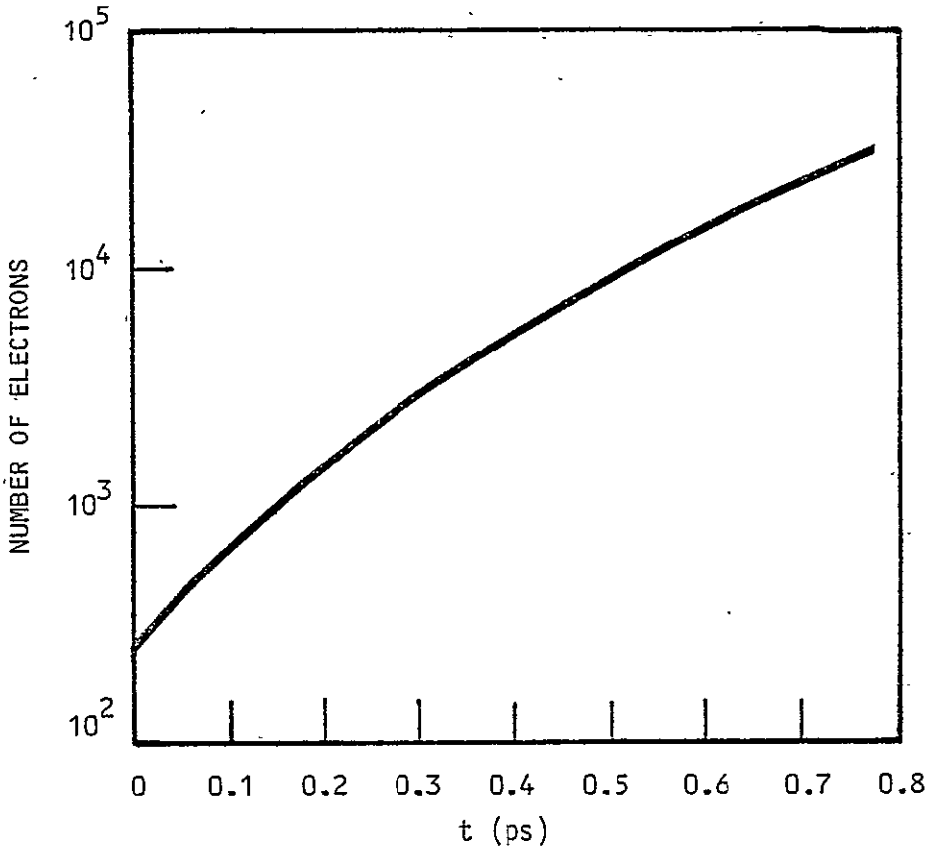

FIGURE 4.19. TOTAL NUMBER OF ELECTRONS vs. TIME-TEFLON

Section 5

SYNTHESIS

In the previous three sections, we have described the computational features of the basic elements of our model of dielectric breakdown in electron-irradiated solids. Basically, we have provided a mathematical description of what we perceive as the initiation stage of the breakdown development. It is the purpose of this section to attempt to interpret these results and to provide a conceptual model of the continued development and propagation of the discharge through tree formation.

We consider first the development of the negative streamer. This phenomenon has the following features:

(1) Drifting, avalanching electrons give rise to a space charge separation which leads to enhanced electric fields at the head of the avalanching region.

(2) The enhanced electric field gives rise to an enhanced avalanche rate through the field dependence of avalanche coefficients. This provides further enhancement of the field.

(3) The avalanche production of mobile electrons provides sufficient carrier number density to permit the relaxation of the electric fields internal to the streamer channel in very short times ($\lesssim 10^{-13}$ sec). This region of the solid locally appears to be a conductor.

(4) The acceleration process at the head of the streamer saturates. A space-charge ionization wave evolves which propagates with constant velocity in an essentially self-similar

fashion. This saturation velocity, together with the spatial character of the field and electron density in the front appear to be roughly independent of the initial conditions of the streamer development. That is, once a critical number density is reached in an avalanche, such that self-fields are important, the further development is driven by these self-fields.

(5) Very large fields are developed near the positive end of the streamer.

Strictly speaking, not all of the above items may be taken as conclusions from the results which have been computed to date. Rather, they represent extrapolations of the results based on reasonable theoretical expectations. Further work will be required to computationally verify these assertions. For now, we content ourselves with various theoretical arguments in support of these expectations.

The assumption that the electric field is derivable from an electrostatic potential means that $\vec{\nabla} \times \vec{E} = 0$. This, in turn, means that the magnetic field is negligible. From Ampere's law, with $\vec{\nabla} \times \vec{B} = 0$, we find:

$$\varepsilon \frac{\partial \vec{E}}{\partial t} \approx \vec{J} \qquad (5.1)$$

where $\vec{J}$ is the current density. [Relation (5.1) should not be taken too literally, since it would imply that the field can only change in the conducting region — It is useful for an estimate, however]. The current density $\vec{J}$ is given by Ohm's law, $\vec{J} = \sigma\vec{E}$, with the conductivity, σ, given by:

$$\sigma = n_e e \mu_e \qquad (5.2)$$

where n_e is the electron number density, e the electronic charge, and μ_e the electronic mobility. Relation (5.1) then represents the usual relaxation equation with relation time τ_r given by:

$$\tau_r = \frac{\varepsilon}{\sigma} = \frac{\varepsilon}{n_e e \mu_e} \tag{5.3}$$

Choosing the mobility to be roughly constant ($\mu_e \approx 1.6 \times 10^{-4}$ m^2/v-sec), as computed for Teflon in Section 2 above, we can see that this relaxation time depends only on the electron carrier density. A relaxation time of 10^{-13} secs is achieved for an electronic charge density of 1.1×10^6 C/m^3 ($n_e = 6.9 \times 10^{18}$ electrons/cm^3). This relaxation time is the dominant time of the problem, and should be kept in mind during the following discussion. Of course, this time depends critically on the density of electrons which are produced.

A reasonable estimate of the maximum value for this quantity may be developed. Denoting the convective time derivative by D/Dt ($D/Dt = \partial/\partial t + \bar{v} \cdot \bar{\nabla}$), eq. (4.18) for the electron dynamics may be written:

$$\frac{D}{Dt}\left(\ell n(n_e)\right) = (\beta - \vec{\nabla} \cdot \vec{v}_e) - \frac{1}{n_e} \vec{\nabla} \cdot (D \vec{\nabla} n_e), \tag{5.4}$$

Ignoring the diffusion term, we expect the electron density to level out when:

$$\beta - \vec{\nabla} \cdot \vec{v}_e \approx 0 \tag{5.5}$$

Assuming a roughly constant mobility, using the relation $\beta = \alpha|v_D|$, where α is the first Townsend coefficient, and invoking Gauss's law, eq. (5.5) may be rewritten as:

$$\rho_{MAX} \approx \frac{\varepsilon\beta}{\mu} = \varepsilon E\alpha \qquad (5.6)$$

Referring to Figure 2.6, we can see that this is a rather sharp function of the field strength. Taking the values indicated for the ambient field, this relation gives a value of $\rho \approx 1.1 \times 10^6$.

This number may be expected to be within a factor of two to three of that of the individual particle densities (i.e., ρ is achieved in a region where $\rho_+ \approx 0$). These estimates are entirely consistent with the numerical results.

The enhancement of the electric field at the negative streamer tip is apparent from the figures of Section 4. This enhancement is precisely that which may be expected from a dipole charge distribution and is similar to that seen in the primary avalanche of Section 3. The results of Section 4 also indicate that this enhanced electric field is accelerating the avalanching process, that the region of net negative charge is moving with a velocity faster than would be expected from the ambient electric field. What we see from Figure 4.6 is that the region of net negative electron density is propagating in an essentially self-similar (in the dZ direction) fashion, with radial growth due to diffusion. While some acceleration of this region is apparent from our results, the numerical computations have not been carried far enough to see an expected saturation of the tip velocity. We expect saturation near the tip for the following reasons.

The inverse ionization length (first Townsend coefficient) takes on a minimum value. The results of Section 2 for Teflon may be fit in the usual form $\alpha = \alpha_o \exp(-\mathcal{E}_o/E)$, with $\alpha_o \approx 1.85 \times 10^8\ m^{-1}$. This corresponds to the fact that at very high fields, the distance to achieve ionization must be at least $(N\sigma_I)^{-1}$ where N is an effective valence band electron number density, and σ_I is an effective ionization cross section. Thus, the distance between ionizations tends to a minimum value as the field increases. Similarly, the electron drift velocity tends to reach a maximum. This is given roughly by assuming no collisions other than ionization. The mean velocity is then roughly 1/2 that required to give an energy equal to the ionization threshold. For Teflon, we therefore expect the drift velocity to saturate at a value of about 7×10^5 m/sec.

The above two considerations imply that the ionization rate $\beta = \alpha|\vec{v}_D|$ also saturates. There is therefore a maximum electric field which could be sustained by this avalanching process, and is given roughly by the field at which the above quantities saturate. For Teflon, we estimate this field to be about 6×10^9 v/m. In practice, the effects of diffusion and multiple dimensions may be expected to lower this by as much as a factor of two. Nonetheless, the basic idea for the expected saturation is clear. We do not expect a completely runaway process. We do not have a good estimate at this time for the amount of propagation time required to achieve the expected saturation.

The important aspects of this negative streamer are that it propagates and is self-sustaining. That is, if a low probability event gives rise to an avalanche of sufficient

length that space charge effects become important, these effects will tend to maintain the effect through further generations. Further, the effects lead to an enhanced field which makes the process self-sustaining. Assuming the breakdown is initiated by the above streamer (to be discussed below), this phenomenon would explain why breakdown which is initiated at edges and weak spots at fields that are below bulk breakdown fields nonetheless can propagate into the bulk. That is, the low field initiated weak spot breakdown does not remain confined, but, in fact, can propagate throughout the region which is presumably not weak. We will return to this point below. Note the propagation velocity of the negative streamer ($\sim 2 \times 10^5$ m/sec) is sufficiently large that it can cover small macroscopic distances (1 mil $\sim$ 25μ) in very short times (125 ps).

This brings us to the next important feature of the above process. We are not suggesting that the propagation of the above negative streamer <u>is</u> the breakdown process. In fact, the rather small changes in lattice temperature noted in Section 4 above indicate that this is distinctly not the case. If the above developed streamer propagated to a conducting boundary, and no further source of current were made available, then the net effect of the process would be merely a rearrangement of electric field. Internal to the channel, recombination of the mobile carriers would quickly decrease the conductivity, and the process would be at end. For breakdown to occur, further processes must be at work on a timescale more rapid than the recombination process. To understand what these processes might be, we must shift our attention to the field rearrangement nature of the process, and concentrate our attention on the immobile positive tip of the streamer.

The region of net positive charge left behind occurs roughly on the outside and rear of the conducting central region. The field near this region is substantially perturbed from its ambient value. In particular, the field is enhanced and is directed toward the conducting region. The positive charge density falls off roughly as given by the considerations of Appendix 9. It is our hypothesis that the negative streamer process which has been modeled above now repeats, this time in the presence of the distorted positive tip field. To account for this occurrence, we must now take into account the discrete probabilistic nature of the process. In order for an avalanche and negative streamer to form, not only must the field be sufficiently large, but an initiating electron must be available in the conduction band. Let us estimate this probability. Consider a roughly spherical volume around the positive tip with radius of the order of 10^{-7} m (region of field enhancement). The volume of this region of space is about 4×10^{-21} m^3. In regions of dielectric which are uncharged, at most $\sim 10^{16}$ e/m^3 are expected to be found in the conduction band [Gross (1978)], so that on the average, only 4×10^{-5} electrons are expected to be found in this volume. In other words, the probability of finding an electron in this volume is quite small. However, in regions of the dielectric which have accumulated excess charge due to electron bombardment, the excess charge number density can be as high as $10^{21} - 10^{22}$ e/m^3 [Beers, et al. (1979)]. In regions such as this, the number of excess electrons to be found in the positive tip field region is on the average, from 4 to 40. Assuming that, on the time scales of interest (1-10 ps), one of these trapped electrons makes an excursion into the conduction band either via thermal processes, field assisted thermal processes (Poole-Frenkel), or direct beam processes, then the enhanced field in this region essentially guarantees that this elec-

electron will undergo avalanche in the direction of the local field. This direction is no longer determined by the ambient field.

The appearance of mobile electrons due to this second avalanche allows the charge to rearrange precisely as given in our above picture of the primary avalanche and streamer development. The net effect of the second process is to transport the positive tip in the opposite direction of the avalanche. That is, the positive tip appears to propagate. (It should be noted that probability arguments of the type invoked above have led researchers in gas breakdown to include photoionization processes in their description of positive point [cathode-directed streamer] propagation, this being necessary to account for the carriers necessary to permit the propagation. This photoionization process appears to be unnecessary to account for the behavior of positive point propagation in electron-irradiated solid dielectrics.) The propagation velocity is just that of the electron drift in the enhanced field. Repeated occurrence of the above process leads to a large scale propagation of the positive tip disturbance. Assuming that the controlling process is not the availability of avalanching electrons (the above estimates suggest it is not), then the positive tip also propagates at a velocity similar to the negative tip.

We believe that this process is intrinsically discrete and probabilistic. Thus, the direction that secondary avalanches take is determined by the probability of finding an electron at the location associated with the given field direction. Thus, the direction of the propagation no longer needs to follow the applied field, but is determined both by the field direction near the positive tip, and the density of available carriers in different directions.

Needless to say, this will provide for the preferential propagation of the positive tip into regions of high electron density. It is also quite clear that the probabilistic nature of the process is conducive to bifurcation i.e, treeing. In regions of high electron density, independent avalanches may be expected to develop at nearly concurrent times. These processes can continue without interfering until their space charge fields overlap and influence one another. Branching, and direction change, are thus intrinsic features of the model.

Insofar as the tree propagation also coincides with the regions of net excess charge density, each new avalanche/streamer contributes a net charge transfer out of the region. This net charge will be preferentially transferred along the entire conducting channel to the negative tip. This net charge transfer is important to the continued development of the breakdown, as it corresponds to the generation of net current to the system, thus extracting energy from the stored charge field.

It is clear how a computer model of the above process can be generated. A model of the trapped charge distribution is first developed. Then a probability function is ascertained for determining the probability of finding an electron in the conduction band during a sampling interval. This probability distribution is used to develop a sampling algorithm for choosing the location of the appearance of the next electron during the sampling interval. Having made the choice of the location of the next available electron, a stored description of the positive tip field developed in Section 4 above is consulted. The direction and magnitude of the ensuing avalanche/streamer from initiation to the

existing channel is determined. The positive tip field is transferred to the new initiation location. This process is repeated sequentially to generate many channel segments of a tree. The radius of each tree segment is updated at each time step to account for radial diffusion. The net charge transfer through each of the branches and trunk is scored. Ohmic heating of the lattice is determined in each channel segment. The overall driving field is relaxed globally according to external current transfer and circuit equation restrictions. Such a model would provide a reasonably complete description of the entire discharge process.

Before describing the predictions of such a model, we make one further note about Ohmic heating. On the time-scales of concern to this problem, lattice thermo-mechanical energy transfer is unimportant — these processes are far too slow. With the heating rates noted below, if the primary discharge streamer propagates to a conducting boundary, then subsequent positive point propagation will result in net current flow through the channel. For the field treated herein, the Ohmic heating rate is about 10^{20} watts/m^3. This corresponds to a 1000° K temperature rise in 20-30 ps. Clearly, this process cannot go on very long before our assumptions about the electronic mobility are no longer valid, i.e., the electronic transport model given above depends on the lattice temperature and structure. We believe that a rough estimate of the final temperature may be obtained by assuming that the electronic and lattice temperatures come to rough equilibrium. Assuming the mean energy of the electrons for this lattice temperature is not severely different from the mean electron energy in the cold solid, we may equate this final temperature to this preheating mean electron energy.

For the Teflon calculations of Section 2, the mean electron energy is approximately 0.8 eV. This corresponds to a temperature of about 6000° K. We believe this to be an upper bound on the temperature, and should be correct within a factor of two.

Based on this model, we make the following predictions of the model for the case of electron-beam irradiated Teflon. The sample is assumed to be circular, of radius R, and the beam deposition is assumed to be thin compared to the sample thickness, or R.

(1) Peak mobile electron density:

$$\rho_e \approx 10^6 \text{ C/m}^3$$

(2) Peak current density:

$$J \approx 10^{11} \text{ A/m}^2$$

(3) Channel temperature: 3000 - 6000° K.

(4) Roughly linear current rise in time with slope of $6\pi DJ$, or

$$I \approx 8 \times 10^8 \text{ t}$$

(5) Peak current proportional to sample radius with slope of $12\pi DJ/v_D$ or

$$I_{peak} \sim 8 \times 10^3 \text{ R(m)}$$

(6) Discharge pulse rise time given by the discharge length over the drift velocity or

$$\tau \approx 10^{-5} \text{ R(m)}$$

(7) Discharge tree in the plane of charge deposition.

(8) Maximum channel radius r_o proportional to the square root of the sample radius

$$r_o \approx 2 \times 10^{-4} R^{1/2} \text{ (m)} \quad .$$

Appendix 1

N_2 MODEL

The scattering and energy loss parameters needed by SEMC will be presented in this Appendix. SEMC is a single scattering Monte Carlo code and thus requires information on individual electron interaction processes in contrast to most Monte Carlo electron transport codes which use the continuous slowing down and small angle scattering approximations and thus require only a stopping power and multiple scattering formula. The interaction parameters needed by SEMC are the elastic scattering cross section, total excitation cross section, mean excitation energy and total ionization cross section. These will follow for molecular nitrogen (N_2) which was chosen for validating the newly developed code.

The elastic scattering cross section appears in Figure (A.1.1) versus the incident electron energy (see Strickland, et al. (1976) and Jasperse (1976) and references therein). Its differential form is assumed isotropic in angle which should be acceptable in the energy range of interest ($\tilde{<}$ 10 eV).

The excitation cross section is given in Figure (A.1.2). It contains contributions for several excitation processes starting with vibration excitation (which produces the feature peaking at 2.5 eV) and

extending through excitation of Rydberg states whose excitation energies are above 15 eV. The results shown above 8 eV are based on the individual cross sections given by Strickland et al. (1976). The vibrational excitation cross section was taken from Jasperse (1976). The differential form of the cross section is given by a delta function in angle and thus excitation does not lead to a change in direction of the electron.

The mean excitation energy is given in Figure (A.1.3). It is obtained from the formula

$$\bar{W}(E) = \sum_j W_j \sigma_j (E) \Big/ \sum_j \sigma_j (E) \qquad \text{eV}$$

where the sums are over excitation processes (ionization excluded), W_j is the j^{th} excitation energy, and σ_j is the j^{th} excitation cross section. The denominator gives the cross section appearing in Figure (A.1.2).

The total ionization cross section is given in Figure (A.1.4) and was taken from Strickland et al. (1976). This cross section serves to remove the electron from further transport. Thus, considerations regarding its differential form in energy loss (equivantly secondary electron energy) and angle are not required. The sum of all cross sections discussed above appears in Figure (A.1.5). This concludes the presentation of the atomic information needed by SEMC.

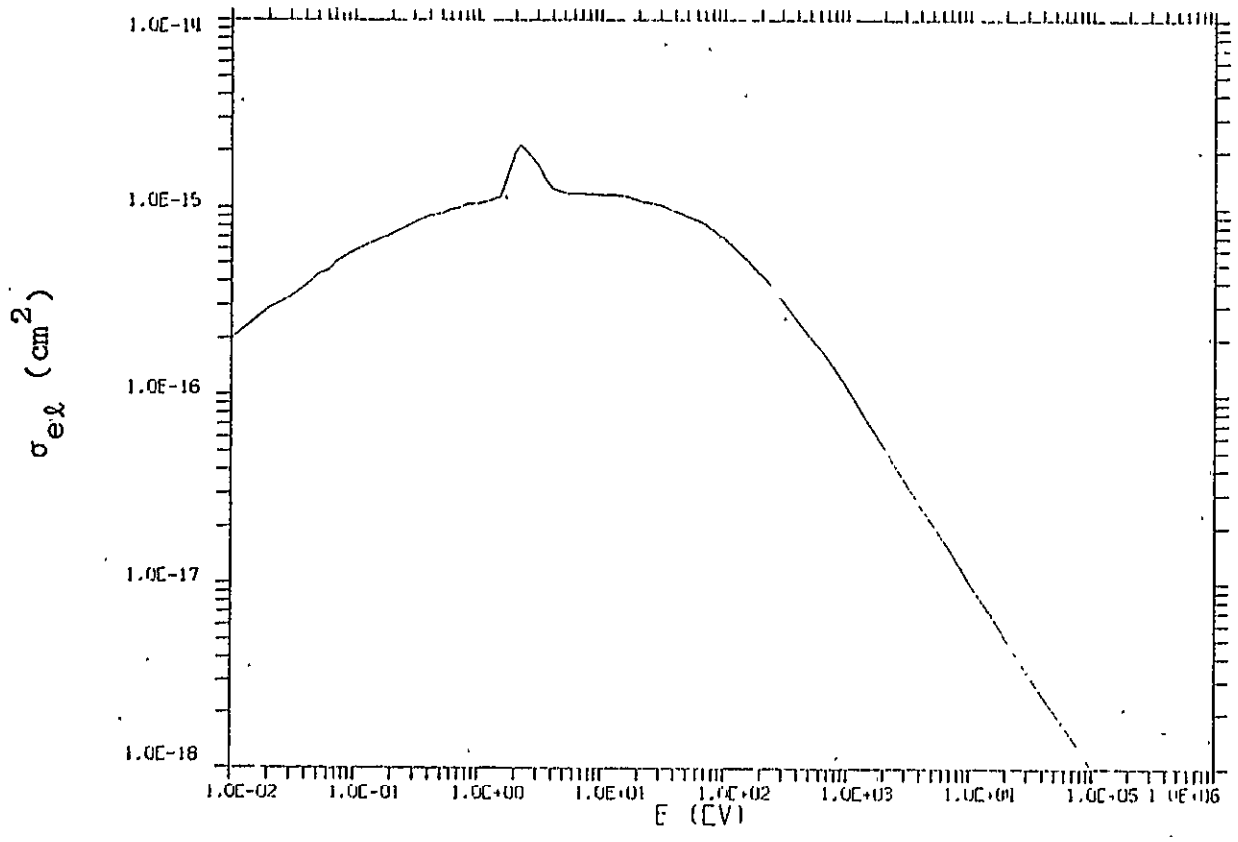

FIGURE A.1.1. ELASTIC SCATTER CROSS SECTION IN N_2

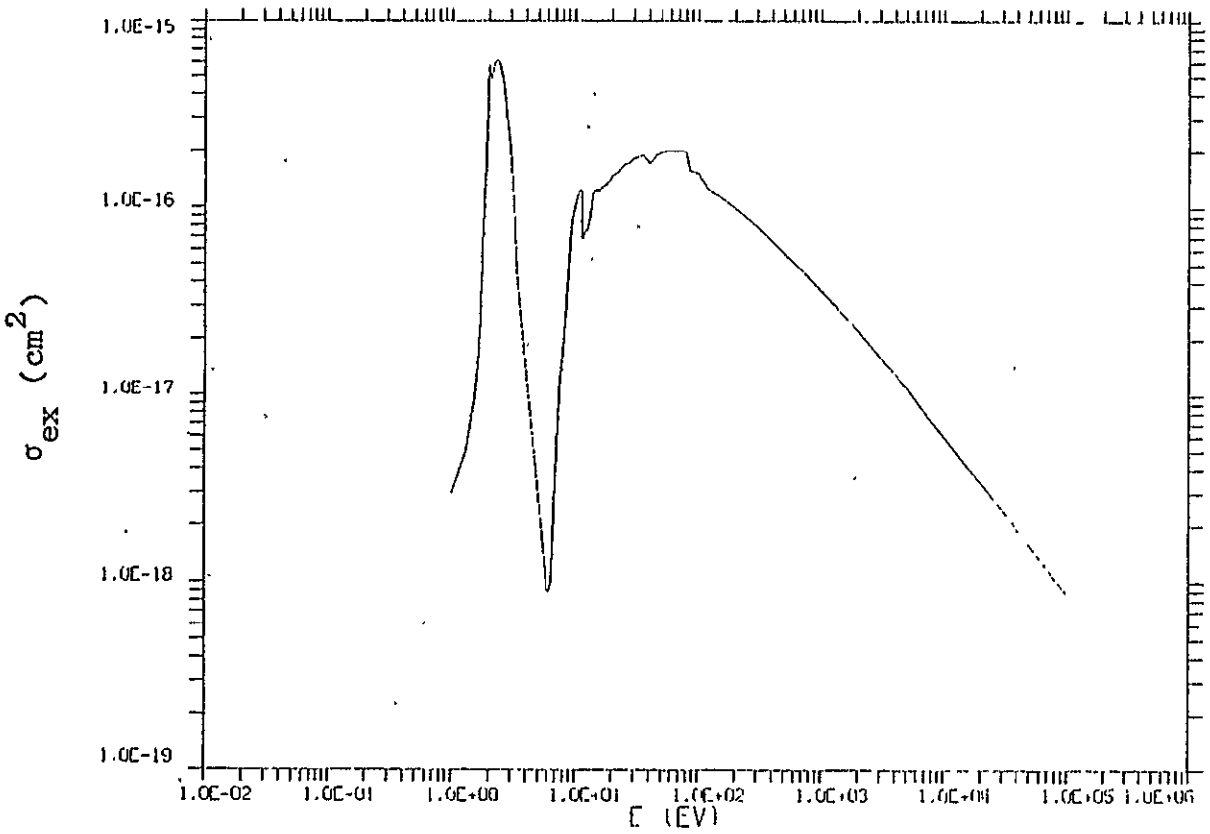

FIGURE A.1.2. EXCITATION CROSS SECTION IN N_2

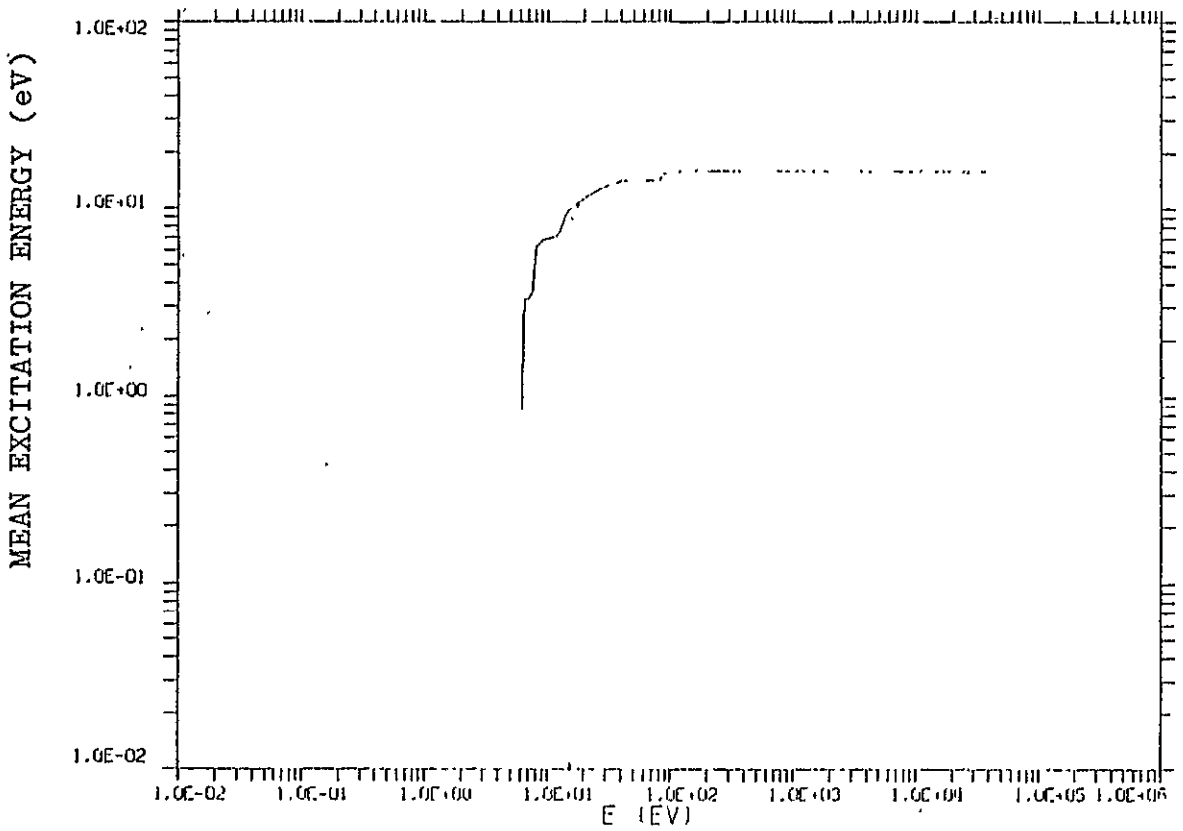

FIGURE A.1.3. MEAN EXCITATION ENERGY IN N_2

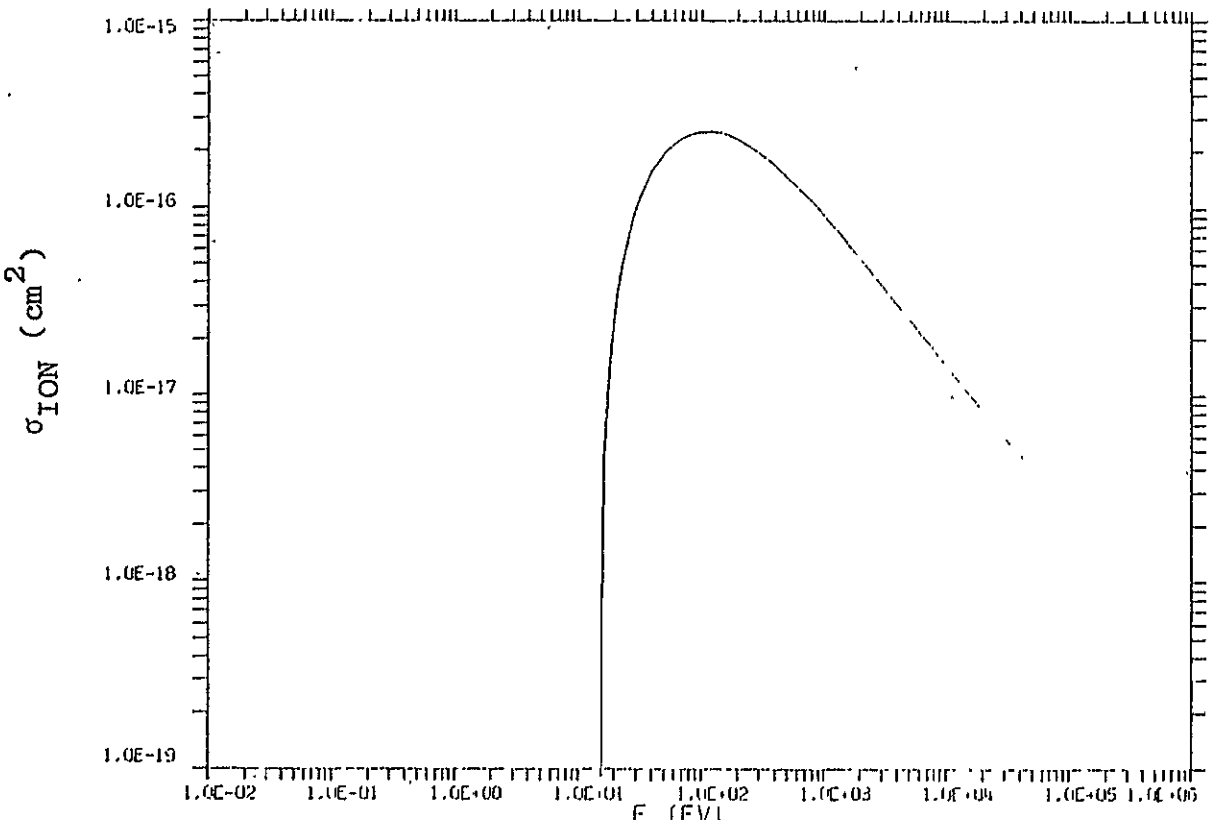

FIGURE A.1.4. TOTAL IONIZATION CROSS SECTION IN N_2

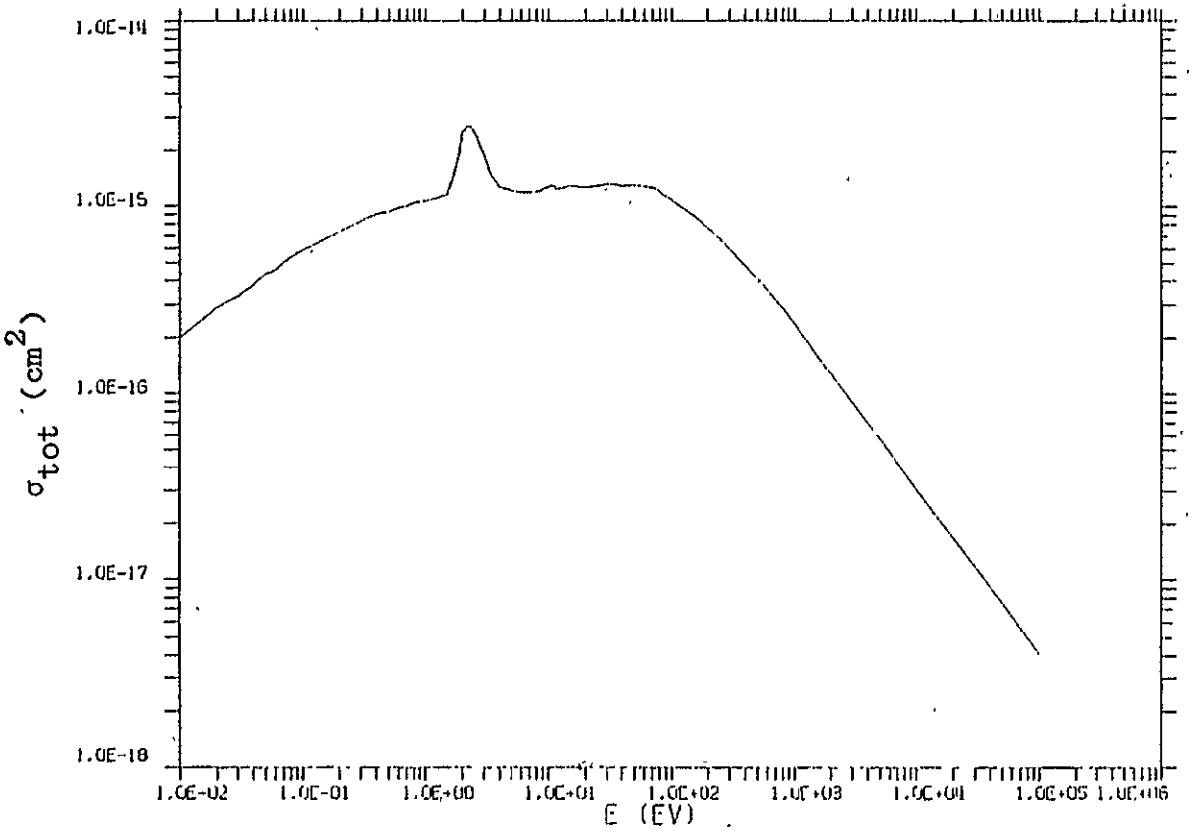

FIGURE A.1.5. TOTAL CROSS SECTION IN N_2

Appendix 2

TEFLON MODEL

The material model for Teflon (CF_2, with density 2.15 g/cm^3 and dieletric Constant 2.0) is described in this Appendix. In treating the electron multiplication in a material, the basic parameters consist of (a) the mean free path for acoustic phonon scattering, (b) the mean free path for optical phonon emission, (c) the quantum energy of the optical phonon, and (d) the threshold energy of pair production and the corresponding cross sections. We will describe briefly in the following the simple approaches we took in achieving this Teflon model.

A.2.1 ELECTRON MEAN FREE PATH FOR ACOUSTIC PHONON SCATTERING

We studied this quantity from two approaches:

Solid State Approach — The inverse mean free path of slow electrons for acoustic phonon scattering is given (Seitz, 1948; Ziman, 1960; O'Dwyer, 1973) by

$$\lambda_a^{-1} = \frac{4}{9\pi} C^2 \frac{kTm^{*2}}{\hbar^4 s^2 MN} \qquad (A.2.1)$$

where C represents the coupling constant, in units of eV, between the electron and the acoustic phonon, k is the Boltzman constant, T temperature, m* the effective

mass of electron, $\hbar$ Planck's constant, s sound speed of Teflon, M is the reduced mass of carbon and fluorine and N the number of unit cells per unit volume. The values used in Eq. (A.2.1) for Teflon are as follows:

C = 14 eV

T = 300°K

m* = free electron mass

s = 2×10^5 cm/sec

M = 7.2 times mass of proton

N = (3 times Bohr radius)$^{-3}$

Eq. (A.2.1) then gives $\lambda_a = 6$Å.

The choice of C=14 eV for Teflon is based on the general trend of C reported in literature (Seitz, 1948). C=31 eV for diamond, 10 eV for silicon and 5 eV for germanium. Kittel (1963) also used C 30 eV and s=5×10^5 cm/sec in discussing the phonon cloud around a slow electron.

The value for N (corresponding to a bond length of 1.5Å) is derived from a study of the Raman spectroscopy of polymer DUDF-PTFE (Latour, 1977).

Atomic Approach — If we consider Teflon as a gas with density the same as that of the solid, then the elastic scattering in the gaseous state will correspond tc acoustic phonon scattering in the solid state. We have carried out an analysis for elastic scattering mean free path based on a screened Rutherford scattering model. The elastic cross section for an electron with

$$V(r) = \frac{-Ze^2}{r} e^{-br} \qquad (A.2.2)$$

is given, in atomic units, by

$$\frac{d\sigma}{d\Omega} = \frac{Z^2}{4E^2} \frac{1}{[(1-\cos\theta) + 2\eta_o]^2} \qquad (A.2.3)$$

where

$$\eta_o = \frac{b^2}{8E} \qquad (A.2.4)$$

For the Thomas-Fermi model of atomic systems,

$$b = Z^{1/3}/0.885a_o \qquad (A.2.5)$$

where a_o is the Bohr radius.

The solid state effect on this atomic approach has been discussed (Nigam et al., 1959) and its result is effectively to replace η_o by $\eta \equiv \eta_o \mu^2$ where $\mu = 1.80$. The dimensionless η therefore becomes, with E in atomic units (27.21 eV is one atomic unit of energy),

$$\eta = 0.517 \frac{Z^{2/3}}{E} \qquad (A.2.6)$$

A slow electron of a few eV in a moderate Z material will have a very large η compared to the $(1-\cos\theta)$ factor in Eq. (A.2.3). The elastic scattering is therefore quite isotropic for slow electrons. Neglecting the $(1-\cos\theta)$, and integrating over the angles, one reaches the following formula for the total elastic scattering cross section

$$\sigma = 2.94\ Z^{2/3}\ a_o^2 \qquad (A.2.7)$$

A teflon gas (CF_2) of density 2.15 g/cm^3 contains 2.57×10^{22} carbon atoms and 5.15×10^{22} flourine atoms per cm^3. The mean free path of electron for elastic scattering in this gas is computed by Eq. (A.2.7) to be 4Å compared to 6Å from the solid state approach.

The agreement of the results from these two approaches is considered very satisfactory in the sense that many uncertainties are involved in either approach and yet the main physics in each approach is accurately maintained. In the calculation, we use 6Å.

A.2.2 ELECTRON MEAN FREE PATH FOR OPTICAL PHONON EMISSION

A detailed treatment for the mobility of electrons in pure non-polar insulators has been given by Seitz (1948). Besides the acoustic phonon, the non-acoustic phonons (optical phonons) were discussed according to the degree of symmetry in the insulator structure. For teflon, which we assume to possess minimal symmetry, the ratio of cross sections of the optical phonon emission to the acoustic phonon scattering is given by

$$R = \frac{\hbar\omega}{k_o T}\left(1 - \frac{\hbar\omega}{E}\right)^{1/2}\left(\frac{9}{8}\frac{D^2}{C^2}\right)\left(\frac{\hbar Ks}{\hbar\omega}\right)^2 \qquad (A.2.6)$$

In this equation, E is the energy of the slow electron capable of emitting an optical phonon of quantum energy $\hbar\omega$ ($E>\hbar\omega$). D and C, being almost equal (Seitz, 1948; Shockley, 1951), are the coupling constants of electrons with optical phonons and acoustic phonons respectively. K is the maximum wave number in the Brillouin zone.

For Teflon, the energy of the optical phonon, as will be seen in the next section, is quite large compared to that in semiconductor or diamond. It is therefore not suitable to put $\hbar Ks \sim \hbar\omega$ as Seitz (1948) did for diamond. In fact, using $s=2\times10^5$ cm/sec and $K=\pi/3a_o$, we obtain $\hbar Ks=0.026$ eV, almost identical to the thermal energy of 300°K. By putting $\hbar Ks \sim k_o T$ and $\frac{9}{8}\frac{D^2}{C^2} \sim 1$, Eq. (A.2.6) becomes

$$R = \frac{k_o T}{\hbar\omega}\left(1 - \frac{\hbar\omega}{E}\right)^{1/2} \qquad (A.2.7)$$

The mean free path for optical photon emission is then given by

$$\lambda_o = \lambda_a \frac{\hbar\omega}{k_o T} \left(1 - \frac{\hbar\omega}{E}\right)^{-1/2} \qquad \text{(A.2.8)}$$

A.2.3 QUANTUM ENERGY OF OPTICAL PHONON

Based on experimental Raman Spectroscopy results (Latour, 1977) of PVDF-PTFE we have determined the main vibrational frequency of the normal modes in Teflon to be $\sim$0.11 eV. There are three vibrational modes with energies close to this value: antisymmetric vibrations of CF_2 and CC, rocking mode of CF_2.

We also use another approach to check the reliability of the above value for optical phonon energy. From the polymer structure of Teflon, we assume the bond strength of CF is in between that of dimolecules HCl and CCl. We are then able to locate the symmetrical vibration frequency of CF_2 by the requirement that $\mu_A\omega^2$=constant for a given spring constant, where μ_A is the reduced mass and ω is the vibration frequency. $\mu_A\omega^2$=.141 and .099 $m_p(eV)^2$ respectively for HCℓ and CCℓ (Handbook of Chemistry and Physics, 1969). For symmetric vibration of CF_2, the mass of carbon can be set as infinite. The reduced mass of the system is then 19 m_p which in turn leads to 0.086 eV and 0.073 eV for CF_2 vibration. The use of 0.11 eV therefore seems reasonable.

A.2.4 IONIZATION THRESHOLD AND IONIZATION CROSS SECTION

The optical properties of TEFZEL (1973) indicates an energy gap between valance and conduction bands of about 7 eV. The sharp rise of the absorbence for smaller photon wavelengths corresponds to the fact that the edge of valance band is reached. For teflon, we adopt 6.5 eV as the energy gap.

We also roughly check, using the idea of bond strength, the order of magnitude of this 6.5 eV energy gap. From experimental data (Handbook of Chemistry and Physics, 1969), the bond strengths of HF and CF are respectively 153 and 107 Kcal/mole. From the ionization potential of HF, 17.7 eV, we infer that the ionization potential for CF is roughly 12 eV which is about a factor of two larger than the value we used.

The ionization cross section for electrons with energies above the threshold is not known. Fortunately, theories (Wolff, 1954; Baraff, 1962; DiStefano and Shatzkes, 1976) indicate this quantity is not important in the calculation of charge multiplications. We have chosen 10^{-15} cm^2, a large enough number, as the cross section for ionization.

A.2.5 SUMMARY OF PROPERTIES OF FEP TEFLON

The following summary of the physical properties of FEP Teflon have been taken in part from Dupont Technical Bulletin T-1C.

Density	2.15 gm/cm^3
Dielectric Constant	2.0
Volume Resistivity	10^{15} ohm-m

Appendix 3

DESCRIPTION OF XSCPRP

I. PURPOSE

XSCPRP is a computer code to prepare the cross section set for SEMC.

II.1 START-UP REQUIREMENT — INPUTS

The following inputs are needed for an XSCPRP run:

CARD TYPE 1 (12A6) COMMENT (I),I=1,12

A comment card defining the cross section set, e.g.,

N2 CROSS SECTION SET

CARD TYPE 2 (I3)

NDISC — number of discrete excitation levels.

CARD TYPE 3 (I3,F5.1)

NION — number of energy points in ionization cross section set.

THI ionization threshold (eV).

CARD TYPE 4 (8E9.2)

EION(I),I=1,NION — energy points for ionization cross section set.

CARD TYPE 5 (8E9.2)

SIGION(I),I=1,NION — cross section for ionization at the corresponding energies EION(I) (cm^2).

For each excitation level, K=1,NDISC, read

CARD TYPE 6 (I3,F5.1)

KDISC(K) — number of energy points in the K^{th} excitation level.

THDISC(K) — threshold for the K^{th} excitation level (eV).

CARD TYPE 7 (8E9.2)

EDISC(I,K),I=1,KDISC(K) — energy points for the K^{th} excitation level (eV).

CARD TYPE 8 (8E9.2)

SIGD(I,K),I=1,KDISC(K) — cross section for the K^{th} excitation level, at (cm^2) energies EDISC(I,K).

CARD TYPE 9 (I3)

NELAS — number of energy points in the elastic cross section set.

CARD TYPE 10 (8E9.2)

EEL(I),I=1,NELAS — energy points for the elastic cross section set (eV).

CARD TYPE 11 (8E9.6)

SIGEL(I),I=1,NELAS — cross section for elastic scattering at each of the energies EEL(I) (cm^2).

II.2 START-UP REQUIREMENTS — DISK FILES READ

No disk files are read.

III.1 CODE OUTPUTS — PRINTED OUTPUT

The code prints out the input data as read. The number of points in the energy grid for the total cross section and the master energy grid for the total cross section are printed. Finally, a tabulation of the total cross section, probability of ionization, probability of elastic scattering, probability of excitation, and the average energy loss per excitation event are printed at each energy point in the master energy grid.

III.2 CODE OUTPUTS — DISK FILES WRITTEN

The following information is written to file XSEC in binary format:

RECORD 1 HEADER(I),I=1,3,NEMG

HEADER(1)	—	material for which the cross section set is written.
HEADER(2)	—	date of preparation.
HEADER(3)	—	time of preparation.
NEMG	—	number of points in the master grid.

RECORD 2 EM(I),I=1,NEMG

master energy grid (eV).

RECORD 3 SIGTOT(I),I=1,NEMG

total cross section (cm^2).

RECORD 4 PELE(I),I=1,NEMG

probability of elastic scattering.

RECORD 5 PEX(I),I=1,NEMG

probability of excitation.

RECORD 6 AELE(I),I=1,NEMG

average loss per excitation event (eV).

V. PROGRAM LOGIC

The logic flow in XSCPRP proceeds as follows:

1) Input data read.

2) A master energy grid is defined to include all energies in all cross section sets, elastic, excitation, and ionization.

3) The total cross section at each point in the grid is calculated.

4) The probability of each event type, elastic, excitation, and ionization is determined.

5) The above results are printed and written to disk file XSEC.

Appendix 4

DESCRIPTION OF SEMC

I. PURPOSE

SEMC is a single scatter electron Monte Carlo code which calculates the drift velocity, ionization length, the diffusion coefficient parallel to the electric field, and the diffusion coefficient normal to the electric field. The spatial distributions of the ionization sites are also scored.

II.1 START-UP REQUIREMENTS — INPUTS

The inputs for the SEMC code are in namelist format. Two namelists $IV and $OF are needed for each data set. The run is terminated with the following card:

```
$IV MXHIST=-1$
```

The namelist format was chosen for ease of use, as well as for the ability to define default values for the variables in the namelist. The variables in namelist $IV are:

VARIABLE	DEFINITION	UNITS	DEFAULT VALUE
EZ	electric field	volts/m	10^7
RVMD	density of atomic bands	$/m^3$	5.14×10^{27}
ESTRT	initial energy of electron	eV	0.02
MXHIST	number of electron trajectories to be followed		200
DRBN	bin width for scoring radial location of ionization sites	m	1.0
DZBN	bin width for scoring axial location of ionization sites	m	1.0
DTBN	bin width for scoring temporal location of ionization site	sec	1.0
TSCORE	time to score the diffusion coefficients	sec	1.0

In order to get the values for variables DRBN, DZBN, and DTBN, it is usually necessary to make a preliminary run with a small number of electron trajectories ≈ 200. The information printed on the page of output labeled DIAGNOSTICS is used to determine the bin sizes. The values are chosen as:

DRBN > 0.1 * MAXIMUM RHO
DZBN > 0.1 * MAXIMUM Z
DTBN > 0.1 * MAXIMUM TIME

The value of TSCORE is determined from the value of ionization time printed on the first page of the output labeled RESULTS.

.25*IONIZATION TIME<TSCORE<.5*IONIZATION TIME

The variables in namelist $OF are:

VARIABLE	DEFINITION	DEFAULT
PRNTXS	logical variable to request, print of cross section set.	.FALSE.
PRNTMD	logical variable to request, print of the spatial and temporal distributions of ionization sites.	.FALSE.

II.2 START-UP REQUIREMENT — DISK FILES READ

SEMC reads the XSEC file prepared by XSCPRP.

III.1 CODE OUTPUTS — PRINTED OUTPUT

The code prints out the input data as read. The cross section identifiers as read from file XSEC are printed next. If PRNTXS is set to .TRUE. in namelist $OF, the cross section is printed. On the next page, labeled DIAGNOSTICS, only those values previously described are of general interest. On the following page, the drift velocity, ionization length, ionization time, mobility, the diffusion coefficient parallel to the electric field, the diffusion coefficient normal to the electric field, and the ratios of the diffusion coefficients to the mobility are printed. Finally, the spatial and temporal distributions of ionization sites is printed if PRNTMD is set to .TRUE. in $OF.

III.2 CODE OUTPUTS — DISK FILES

No output disk files are written.

IV. PROGRAM LOGIC

The logic flow in SEMC is as follows:

1) Input data read and printed.

2) Cross section set read and printed (if requested).

3) Random walk variables initiated.

4) Electron is started at energy ESTRT.

5) The distance and time to next collision site is determined.

6) The electron is moved to the site of the next collision and the electron energy updated.

7) The collision type is selected.

8) If collision is ionization, the ionization parameters are scored and a new electron begins at 4) if number of trajectories is less than MXHIST. If number of histories is equal to MXHIST, the results are printed.

9) If collision is elastic or excitation and the number of elastic scatters is less than 2000, then the next step of the random walk is taken at 5).

SAMPLE PROBLEM INPUT PARAMETERS

The sample problem was for one thousand electron histories incident on Teflon with an applied electric field of 10^9 volts/m. The inputs for this problem are

```
$IV
EZ      = 1.0E+9,
RVMD    = 5.14E+28,
MXHIST  = 1000,
DRBN    = 3.0E-9,
DZBN    = 3.0E-9,
DTBN    = 2.0E-14,
TSCORE  = 7.5E-14
#END

$OF
PRNTMD  = .T.
$END

$IV
MXHIST  = -1

$END
```

VI. SAMPLE PROBLEM OUTPUTS

Sample output from SEMC for the inputs listed in Section V are given below.

S E M C

SINGLE-SCATTER ELECTRON MONTE CARLO CODE

(032279 ,113702)

I N P U T S

ELECTRIC FIELD	1.00+009	(VOLTS/M)
MOLECULAR DENSITY	5.14+028	(/M**3)
E/N	1.95-020	(VOLTS-M**2)
INITIAL ENERGY	2.00-002	(EV)
NUMBER OF HISTORIES	1000	

BIN WIDTHS FOR SCORING

DELTA Z	3.00-009	(M)
DELTA RHO	3.00-009	(M)
DELTA TIME	2.00-014	(SEC)
TSCORE	7.50-014	(SEC)

PRINT FLAGS

CROSS SECTIONS	F
MAR. DISTRIBUTION	T
JOINT DISTRIBUTION	F

CROSS SECTION SET FOR CF2PREPARED 032079 ,111024

S E M C
SINGLE-SCATTER ELECTRON MONTE CARLO CODE
(032279 ,113702)
D I A G N O S T I C S

TOTAL OF 1000 HISTORIES
TOTAL OF 995 IONIZATIONS
TOTAL OF 0 RUNAWAY ELECTRONS
TOTAL OF 0 HISTORIES EXCEEDING 2000 ELASTIC SCATTERS
AVERAGE NUMBER OF ELASTIC SCATTERS PER HISTORY 108.059
AVERAGE NUMBER OF EXCITATIONS 23.681

MINIMUM Z =	5.549-009
MAXIMUM Z =	2.337-008
MINIMUM RHO =	5.455-011
MAXIMUM RHO =	2.858-008
MINIMUM TIME =	7.600-015
MAXIMUM TIME =	4.960-013
XBAR =	1.422-010
X2BAR =	2.342-017
YBAR =	-1.006-010
Y2BAR =	2.630-017
ZBAR =	8.750-009
Z2BAR =	8.196-017
RBAR =	5.810-009
R2BAR =	4.972-017
RZBAR =	5.629-017

S E M C

SINGLE-SCATTER ELECTRON MONTE CARLO CODE

(032279 ,113702)

R E S U L T S

DRIFT VELOCITY	1.63+005	(M/SEC)
IONIZATION LENGTH	1.26-008	(M)
IONIZATION TIME	1.15-013	(SEC)
MOBILITY	1.63-004	(M**2)/(VOLT-SEC)
DIFFUSION COEFF (PARALLEL)	3.97-005	(M**2/SEC)
DIFFUSION COEFF (NORMAL)	1.56-004	(M**2/SEC)
D (PARALLEL)/MOBILITY	2.44-001	(EV)
D (NORMAL)/MOBILITY	9.55-001	(EV)

S E M C
SINGLE-SCATTER ELECTRON MONTE CARLO CODE
(032279 ,113702)
R E S U L T S

MARGINAL DISTRIBUTION IN Z

Z (M)	PROB
1.50-009	.000
4.50-009	1.005-002
7.50-009	6.372-001
1.05-008	2.673-001
1.35-008	6.332-002
1.65-008	1.407-002
1.95-008	7.035-003
2.25-008	1.005-003
2.55-008	.000
2.85-008	.000

S E M C

SINGLE-SCATTER ELECTRON MONTE CARLO CODE

(032279 ,113702)

R E S U L T S

MARGINAL DISTRIBUTION IN RHO

RHO (M)	PROB
6.00-009	2.643-001
9.00-009	3.377-001
1.20-008	2.101-001
1.50-008	1.156-001
1.80-008	4.523-002
2.10-008	1.307-002
2.40-008	7.035-003
2.70-008	5.025-003
3.00-008	1.005-003
3.30-008	1.005-003

S E M C
SINGLE-SCATTER ELECTRON MONTE CARLO CODE
(032279 ,113702)
R E S U L T S

MARGINAL DISTRIBUTION IN TIME

TIME (SEC)	PROB
3.00-014	7.638-002
5.00-014	2.080-001
7.00-014	2.050-001
9.00-014	1.417-001
1.10-013	9.950-002
1.30-013	6.935-002
1.50-013	6.231-002
1.70-013	3.618-002
1.90-013	3.116-002
2.10-013	7.035-002

STOP 10

@FIN

Appendix 5

DESCRIPTION OF CASCAD

I. PURPOSE

CASCAD is a Monte Carlo code which calculates the electron avalanche process. A single electron is initiated; the location of the next ionization site is randomly sampled from the distribution of ionization sites calculated by SEMC. The process is repeated for all of the electrons in each generation. After a predetermined number of generations, the charge density, potential, and electric field are calculated. If the maximum electric field exceeds a pre-defined fraction of the electric field, the problem is terminated and the positive charge density and the electron density are separately written to disk.

II. START-UP REQUIREMENTS — INPUTS

The inputs for CASCAD are in namelist format. Three namelists, $CNTRL, $GEOM, and $DISTR, are needed for each run. The variables in namelist $CNTRL are:

VARIABLE	DEFINITION	DEFAULT
EPREL	relative dielectric permittivity.	1.0
ERRMAX	relative error for the iterative Poisson solution.	0.001
ITERMAX	maximum number of iterations for the iterative Poisson solution.	500
EFAC	fraction of the applied electric field for run termination.	0.5
NGEN	maximum number of generations.	13
NCHEK	generation to begin field calculation.	8

The variables in namelist $GEOM are:

VARIABLE	DEFINITION	UNITS	DEFAULT
IMAX	number of grid points in the radial direction.		20
JMAX	number of grid points in the axial direction.		21
L	axial length.	meters	--
A	maximum radius.	meters	--

The variables in namelist $DISTR are:

VARIABLE	DEFINITION	UNITS	DEFAULT
EAPP	value of the applied electric field for this data set.	volts/m	——
N1	number of points in the radial distribution of ionization sites.		10
N2	number of points in the axial distribution of ionization sites.		10
RMAX	maximum radial displacement for the distribution of ionization sites.	meters	——
ZMAX	maximum axial displacement for the distribution of ionization sites.	meters	——
PR(1)	radial distribution of ionization sites.		——
PZ(1)	axial distribution of ionization sites.		——

II.2 START-UP REQUIREMENTS — DISK FILES READ

No disk files are read.

III.1 CODE OUTPUTS — PRINTED OUTPUT

The code prints out the input data as read. Then the cumulative distribution of ionization sites are printed. The maximum values of the radial field, axial field, and maximum magnitude are printed for all generations greater than NCHEK.

When the maximum number of generations is reached or the maximum electric field exceeds EFRAC*EAPP, the spatial distribution of charge density RHO (in units of coul/m^3) is printed. Next, the electrostatic potential PHI (in units of volts) is printed. Then, the radial component of the electric field ER and the axial component of the electric field EZ (in units of volts/m) are printed. Finally, the number of positive and negative charges in each cell are printed.

III.2 CODE OUTPUTS — DISK FILES WRITTEN

The following three binary records are written to file COUT:

RECORD 1 IRS,IZS,DRS,DZS

- IRS — number of cells in the radial direction.
- IZS — number of cells in the axial direction.
- DRS — radial cell size in meters.
- DZS — axial cell size in meters.

RECORD 2 ((RHON(J,I),J=1,IRS),I=1,IZS)

- RHON — negative charge density in each of the cells (coul/m^3).

RECORD 3 ((RHOP(J,I),J=1,IRS),I=1,IZS)

RHOP — positive charge density in each of the cells (coul/m^3).

IV. PROGRAM LOGIC

The logic flow in CASCAD is as follows:

1) Input variables are read and printed.

2) Random walk variables are initialized.

3) Each electron in the present generation is moved to the next ionization site.

4) If the number of generations is less than NCHEK, go to 3).

5) Calculate the charge density, potential, and electric field. If the fields are less than EFRAC*EAPP, go to 3).

6) Print the charge density, potential, and electric field.

7) Write the positive and negative charge densities separately to disk.

V. SAMPLE PROBLEM INPUT PARAMETERS

The sample problem was for thirteen electron generations in Teflon for an applied electric field of 10^9 volts/m. The inputs for this problem are

```
$CNTRL
EPREL    = 2.0,
EFRAC    = .75,
NGEN     = 13
$END

$GEOM
$END

$DISTR
EAPP     = 1.0E+9,
N1       = 10,
N2       = 10,
RMAX     = 3.0E-8,
ZMAX     = 3.0E-8,
PR(1)    = .264, .338, .210, .116, .0452, .0131,
           .00704, .00525, .001, .001,

PZ(1)    = 0.0, .001, .637, .267, .0633, .01407,
           .00703, .001, 0.0, 0.6

$END
```

VI. SAMPLE PROBLEM OUTPUTS

Sample out from CASCAD for the inputs listed in Section V are given below.

```
[illegible]

[illegible]   = .2E+01,

ERRMAX   = .1E-02,

ITERMX   = 500,

EFRAC    = .75E+00,

NGEN     = 13,

NCHEK    = 8,

$END

[illegible]

IMAX     = 20,

JMAX     = 21,

L        = .6E-06,

A        = .15E-06,

$END

RECORD NO. 13       PZ(1)=0.,.001,.637,.267,.0633,.0141,.00703,.001,0.,0.
                   1234567890123456789012345678901234567890123456789O.........'1234567890123456789012345678901234567890

COMMA MISSING AT END OF RECORD - COMMA ASSUMED
ERROR NUMBER   49   DETECTED BY INCOM=  AT ADDRESS 000207
CALLED FROM NAMIN=  AT ADDRESS 000141
CALLED FROM CASCAD  AT  LINE 65

.1E+10,

10,

10,

.3E-07,

.5E-07,

.264E+00, .338E+00, .21E+00, .116E+00, .452E-01, .131E-01, .704E-02,  .525E-02, .1E-02, .1E-02, 0.0, 0.0,
0.0, 0.0, 0.0, 0.0, 0.0, 0.0, 0.0, 0.0,

0.0, .1E-02, .637E+00, .267E+00, .633E-01, .141E-01, .703E-02,        .1E-02, 0.0, 0.0, 0.0, 0.0, 0.0, 0.0,
0.0, 0.0, 0.0, 0.0, 0.0, 0.0,
```

ORIGINAL PAGE IS OF POOR QUALITY

DISTRIBUTIONS

I	Z	FUEL
1	0.	0.
2	5.00E-09	0.
3	1.00E-08	1.00E-03
4	1.50E-08	8.36E-01
5	2.00E-08	9.65E-01
6	2.50E-08	9.88E-01
7	3.00E-08	9.82E-01
8	3.50E-08	9.89E-01
9	4.00E-08	9.90E-01
10	4.50E-08	9.90E-01
11	5.00E-08	1.00E+00

J	RHO	FOFR
1	0.	0.
2	3.00E-09	2.64E-01
3	6.02E-09	8.62E-01
4	9.04E-09	9.12E-01
5	1.20E-08	9.28E-01
6	1.50E-08	9.73E-01
7	1.80E-08	9.86E-01
8	2.10E-08	9.93E-01
9	2.40E-08	9.99E-01
10	2.70E-08	1.00E+00
11	3.00E-08	1.00E+00

GENERATION 8

MAXIMUM RADIAL FIELD	3.242E+07
MAXIMUM AXIAL FIELD	4.592E+07
MAXIMUM MAGNITUDE	5.157E+07

GENERATION 9

MAXIMUM RADIAL FIELD	8.603E+07
MAXIMUM AXIAL FIELD	9.356E+07
MAXIMUM MAGNITUDE	1.107E+08

GENERATION 10

MAXIMUM RADIAL FIELD	1.071E+08
MAXIMUM AXIAL FIELD	1.741E+08
MAXIMUM MAGNITUDE	1.901E+08

GENERATION 11

MAXIMUM RADIAL FIELD	2.349E+08
MAXIMUM AXIAL FIELD	3.160E+08
MAXIMUM MAGNITUDE	3.670E+08

GENERATION 12

MAXIMUM RADIAL FIELD	3.173E+08
MAXIMUM AXIAL FIELD	6.211E+08
MAXIMUM MAGNITUDE	6.448E+08

GENERATION 13

MAXIMUM RADIAL FIELD	7.636E+08
MAXIMUM AXIAL FIELD	1.114E+09
MAXIMUM MAGNITUDE	1.220E+09

K(I)

I	K(I)	Z 0.	Z 3.00E-08	Z 6.00E-08	Z 9.00E-08	Z 1.20E-07	Z 1.50E-07	Z 1.80E-07	Z 2.10E-07	Z 2.40E-07	Z 2.70E-07
1	5.85E-09	0.	0.	0.	4.364E+04	8.607E+04	7.029E+05	2.640E+06	1.435E+06	-2.553E+06	-5.451E+06
2	1.15E-08	0.	9.563E+03	4.304E+04	7.775E+04	2.391E+05	6.177E+05	2.204E+06	-1.557E+06	-2.[illegible]	-[illegible]
3	1.72E-08	0.	0.	0.	0.025E+04	2.353E+05	7.029E+05	1.[illegible]	1.[illegible]	-1.[illegible]	-5.[illegible]
4	2.[illegible]	0.	0.	0.	0.197E+03	0.960E+04	5.[illegible]	1.[illegible]	-[illegible]	-1.[illegible]	-5.[illegible]
5	3.[illegible]	0.	0.	0.	0.	2.710E+04	1.456E+05	4.[illegible]	-1.[illegible]	-5.[illegible]	-1.[illegible]
6	4.23E-08	0.	0.	0.	0.	0.608E+03	4.175E+04	1.[illegible]	-0.[illegible]	-2.[illegible]	-7.[illegible]
7	5.00E-08	0.	0.	0.	0.	0.	2.207E+03	2.536E+04	-6.516E+04	-1.[illegible]	-5.310E+04
8	5.77E-08	0.	0.	0.	0.	0.	0.	4.782E+03	-1.148E+04	-1.817E+04	-1.913E+04
9	6.54E-08	0.	0.	0.	0.	0.	0.	0.	-1.[illegible]	-2.[illegible]	-1.[illegible]
10	7.31E-08	0.	0.	0.	0.	0.	0.	0.	-7.556E+02	-7.[illegible]	0.
11	8.08E-08	0.	0.	0.	0.	0.	0.	0.	0.	0.	0.
12	8.85E-08	0.	0.	0.	0.	0.	0.	0.	0.	0.	0.
13	9.62E-08	0.	0.	0.	0.	0.	0.	0.	0.	0.	0.
14	1.04E-07	0.	0.	0.	0.	0.	0.	0.	0.	0.	0.
15	1.12E-07	0.	0.	0.	0.	0.	0.	0.	0.	0.	0.
16	1.19E-07	0.	0.	0.	0.	0.	0.	0.	0.	0.	0.
17	1.27E-07	0.	0.	0.	0.	0.	0.	0.	0.	0.	0.
18	1.35E-07	0.	0.	0.	0.	0.	0.	0.	0.	0.	0.
19	1.42E-07	0.	0.	0.	0.	0.	0.	0.	0.	0.	0.
20	1.50E-07	0.	0.	0.	0.	0.	0.	0.	0.	0.	0.

I	K(I)	Z 3.00E-07	Z 3.30E-07	Z 3.60E-07	Z 3.90E-07	Z 4.20E-07	Z 4.50E-07	Z 4.80E-07	Z 5.10E-07	Z 5.40E-07	Z 5.70E-07
1	5.85E-09	-5.738E+04	-2.869E+04	0.	0.	0.	0.	0.	0.	0.	0.
2	1.15E-08	-5.738E+04	-9.563E+03	0.	0.	0.	0.	0.	0.	0.	0.
3	1.72E-08	-2.295E+04	0.	0.	0.	0.	0.	0.	0.	0.	0.
4	2.29E-08	-2.294E+04	0.	0.	0.	0.	0.	0.	0.	0.	0.
5	2.86E-08	-1.590E+04	0.	0.	0.	0.	0.	0.	0.	0.	0.
6	3.43E-08	-5.216E+03	0.	0.	0.	0.	0.	0.	0.	0.	0.
7	4.00E-08	-1.103E+03	0.	0.	0.	0.	0.	0.	0.	0.	0.
8	4.57E-08	0.	0.	0.	0.	0.	0.	0.	0.	0.	0.
9	5.14E-08	-8.458E+02	0.	0.	0.	0.	0.	0.	0.	0.	0.
10	5.71E-08	0.	0.	0.	0.	0.	0.	0.	0.	0.	0.
11	6.28E-08	0.	0.	0.	0.	0.	0.	0.	0.	0.	0.
12	6.85E-08	0.	0.	0.	0.	0.	0.	0.	0.	0.	0.
13	7.42E-08	0.	0.	0.	0.	0.	0.	0.	0.	0.	0.
14	1.00E-07	0.	0.	0.	0.	0.	0.	0.	0.	0.	0.
15	1.12E-07	0.	0.	0.	0.	0.	0.	0.	0.	0.	0.
16	1.19E-07	0.	0.	0.	0.	0.	0.	0.	0.	0.	0.
17	1.27E-07	0.	0.	0.	0.	0.	0.	0.	0.	0.	0.
18	1.35E-07	0.	0.	0.	0.	0.	0.	0.	0.	0.	0.
19	1.42E-07	0.	0.	0.	0.	0.	0.	0.	0.	0.	0.
20	1.50E-07	0.	0.	0.	0.	0.	0.	0.	0.	0.	0.

		6.00E+07
1	[illegible]	0.
2	1.1[illegible]	0.
3	1.9[illegible]	0.
4	[illegible]	0.
5	[illegible]	0.
6	4.23E+08	0.
7	5.06E+08	0.
8	5.77E+08	0.
9	6.54E+08	0.
10	7.31E+08	0.
11	8.04E+08	0.
12	8.65E+08	0.
13	9.62E+08	0.
14	1.04E+07	0.
15	1.12E+07	0.
16	1.19E+07	0.
17	1.27E+07	0.
18	1.35E+07	0.
19	1.42E+07	0.
20	1.50E+07	0.

I	R(I)	Z 0.	Z 3.00E-08	Z 6.00E-08	Z 9.00E-08	Z 1.20E-07	Z 1.50E-07	Z 1.80E-07	Z 2.10E-07	Z [illegible]	Z [illegible]
1	3.85E-09	1.956E+00	2.694E+00	4.153E+00	7.039E+00	1.294E+01	2.314E+01	3.171E+01	-1.701E+00	-3.105E+01	-1.955E+01
2	1.15E-08	1.956E+00	2.694E+00	4.153E+00	7.039E+00	1.294E+01	2.314E+01	3.171E+01	-1.702E+00	-3.109E+01	-1.955E+01
3	1.92E-08	1.940E+00	2.654E+00	3.975E+00	6.711E+00	1.212E+01	2.117E+01	2.825E+01	-1.465E+00	-2.852E+01	-1.801E+01
4	2.69E-08	1.917E+00	2.559E+00	3.780E+00	6.178E+00	1.075E+01	1.800E+01	2.278E+01	-1.773E+00	[illegible]	[illegible]
5	3.46E-08	1.887E+00	2.479E+00	3.566E+00	5.636E+00	9.521E+00	1.474E+01	1.721E+01	[illegible]	[illegible]	[illegible]
6	4.23E-08	1.850E+00	2.366E+00	3.338E+00	5.096E+00	8.014E+00	1.179E+01	1.259E+01	[illegible]	[illegible]	[illegible]
7	5.00E-08	1.808E+00	2.255E+00	3.100E+00	4.561E+00	6.605E+00	9.419E+00	9.166E+00	-1.563E+00	-1.182E+01	[illegible]
8	5.77E-08	1.761E+00	2.135E+00	2.857E+00	4.091E+00	5.844E+00	7.554E+00	6.677E+00	-1.250E+00	-8.250E+00	[illegible]
9	6.54E-08	1.709E+00	2.008E+00	2.613E+00	3.628E+00	4.993E+00	6.081E+00	4.970E+00	-9.567E-01	-6.283E+00	-6.225E+00
10	7.31E-08	1.654E+00	1.876E+00	2.371E+00	3.196E+00	4.236E+00	4.907E+00	3.751E+00	-7.485E-01	-4.782E+00	-5.076E+00
11	8.08E-08	1.596E+00	1.741E+00	2.132E+00	2.793E+00	3.577E+00	3.965E+00	2.863E+00	-5.879E-01	-3.694E+00	[illegible]
12	8.85E-08	1.537E+00	1.602E+00	1.898E+00	2.419E+00	3.003E+00	3.204E+00	2.203E+00	-4.636E-01	-2.874E+00	[illegible]
13	9.62E-08	1.476E+00	1.460E+00	1.670E+00	2.072E+00	2.502E+00	2.577E+00	1.703E+00	[illegible]	[illegible]	[illegible]
14	1.04E-07	1.415E+00	[illegible]	1.447E+00	1.750E+00	2.061E+00	2.064E+00	1.317E+00	[illegible]	[illegible]	[illegible]
15	1.12E-07	1.353E+00	1.166E+00	1.229E+00	1.451E+00	1.671E+00	1.632E+00	1.013E+00	[illegible]	-1.356E+00	[illegible]
16	1.19E-07	1.293E+00	1.011E+00	1.016E+00	1.171E+00	1.324E+00	1.267E+00	7.685E-01	-1.719E-01	-1.035E+00	-1.357E+00
17	1.27E-07	1.233E+00	8.467E-01	8.059E-01	9.095E-01	1.012E+00	9.523E-01	5.673E-01	-1.280E-01	-7.650E-01	-1.002E+00
18	1.35E-07	1.174E+00	6.704E-01	5.994E-01	6.632E-01	7.208E-01	6.769E-01	3.979E-01	-9.027E-02	-5.361E-01	-7.278E-01
19	1.42E-07	1.117E+00	4.763E-01	3.956E-01	4.305E-01	4.687E-01	4.314E-01	2.512E-01	-5.722E-02	-3.407E-01	-4.644E-01
20	1.50E-07	1.062E+00	2.565E-01	1.952E-01	2.098E-01	2.272E-01	2.079E-01	1.204E-01	-2.749E-02	-1.635E-01	-2.240E-01

I	R(I)	Z 3.00E-07	Z 3.30E-07	Z 3.60E-07	Z 3.90E-07	Z 4.20E-07	Z 4.50E-07	Z 4.80E-07	Z 5.10E-07	Z 5.40E-07	Z 5.70E-07
1	3.85E-09	-9.336E+00	-4.879E+00	-2.768E+00	-1.668E+00	-1.052E+00	-7.023E-01	-5.103E-01	[illegible]	[illegible]	[illegible]
2	1.15E-08	-9.339E+00	-4.879E+00	-2.769E+00	-1.669E+00	-1.053E+00	-7.030E-01	-5.108E-01	[illegible]	[illegible]	[illegible]
3	1.92E-08	-8.922E+00	-4.740E+00	-2.720E+00	-1.646E+00	-1.040E+00	-6.955E-01	[illegible]	[illegible]	[illegible]	[illegible]
4	2.69E-08	-8.311E+00	-4.536E+00	-2.635E+00	-1.605E+00	-1.018E+00	-6.815E-01	[illegible]	[illegible]	[illegible]	[illegible]
5	3.46E-08	-7.562E+00	-4.263E+00	-2.523E+00	-1.549E+00	-9.860E-01	-6.629E-01	[illegible]	-4.210E-01	[illegible]	[illegible]
6	4.23E-08	-6.751E+00	-3.958E+00	-2.387E+00	-1.480E+00	-9.479E-01	-6.390E-01	[illegible]	-4.068E-01	[illegible]	[illegible]
7	5.00E-08	-5.949E+00	-3.630E+00	-2.235E+00	-1.401E+00	-9.023E-01	-6.100E-01	-4.541E-01	-3.937E-01	[illegible]	-4.901E-01
8	5.77E-08	-5.192E+00	-3.293E+00	-2.070E+00	-1.312E+00	-8.508E-01	-5.781E-01	-4.317E-01	-3.767E-01	[illegible]	[illegible]
9	6.54E-08	-4.497E+00	-2.957E+00	-1.897E+00	-1.217E+00	[illegible]	-5.421E-01	[illegible]	-3.570E-01	-3.790E-01	[illegible]
10	7.31E-08	-3.865E+00	-2.628E+00	-1.720E+00	-1.116E+00	-7.331E-01	-5.029E-01	[illegible]	[illegible]	[illegible]	[illegible]
11	8.08E-08	-3.297E+00	-2.312E+00	-1.541E+00	-1.012E+00	[illegible]	[illegible]	[illegible]	[illegible]	[illegible]	[illegible]
12	8.85E-08	-2.790E+00	-2.011E+00	-1.364E+00	-9.050E-01	[illegible]	[illegible]	[illegible]	[illegible]	[illegible]	[illegible]
13	9.62E-08	-2.336E+00	-1.727E+00	-1.190E+00	-7.975E-01	[illegible]	-3.715E-01	[illegible]	[illegible]	[illegible]	[illegible]
14	1.04E-07	-1.935E+00	-1.460E+00	-1.021E+00	-6.901E-01	-4.652E-01	-3.247E-01	[illegible]	[illegible]	[illegible]	[illegible]
15	1.12E-07	-1.574E+00	-1.210E+00	-8.565E-01	-5.837E-01	[illegible]	-2.771E-01	-2.137E-01	[illegible]	-2.355E-01	[illegible]
16	1.19E-07	-1.250E+00	-9.754E-01	-6.980E-01	-4.790E-01	-3.261E-01	-2.292E-01	-1.776E-01	-1.658E-01	-2.004E-01	[illegible]
17	1.27E-07	-9.570E-01	-7.561E-01	-5.456E-01	-3.768E-01	-2.578E-01	-1.815E-01	-1.411E-01	-1.330E-01	-1.646E-01	[illegible]
18	1.35E-07	-6.896E-01	-5.507E-01	-4.000E-01	-2.775E-01	-1.901E-01	-1.343E-01	[illegible]	-9.917E-02	[illegible]	[illegible]
19	1.42E-07	-4.439E-01	-3.565E-01	-2.604E-01	-1.812E-01	-1.245E-01	[illegible]	[illegible]	[illegible]	[illegible]	[illegible]
20	1.50E-07	-2.152E-01	-1.735E-01	-1.271E-01	-8.803E-02	-6.097E-02	-4.321E-02	-3.362E-02	-3.245E-02	[illegible]	[illegible]

		e.66E-07
1	3.e5E-09	0.
2	1.15e-08	-e.5e7E-01
3	1.92E-08	-e.349E-01
4	2.69E-08	-e.323E-01
5	3.46E-08	-e.29eE-01
6	4.23E-08	-e.24eE-01
7	5.e0E-08	-e.195E-01
8	5.77E-08	-6.13PE-01
9	e.54E-08	-e.075E-01
10	7.31E-08	-6.005E-01
11	8.08E-08	-5.930E-01
12	8.e5E-08	-5.850E-01
13	9.62E-08	-5.765E-01
14	1.04E-07	-5.e76E-01
15	1.12E-07	-5.583E-01
16	1.19E-07	-5.4e6E-01
17	1.27E-07	-5.3e9E-01
18	1.35E-07	-5.287E-01
19	1.42E-07	-5.18:E-01
20	1.50E-07	-5.078E-01

I	R(I)	Z = 0.	Z = 3.00E-08	Z = 6.00E-08	Z = 9.00E-08	Z = 1.20E-07	Z = 1.50E-07	Z = 1.80E-07	Z = 2.10E-07	Z = [illegible]	Z = [illegible]
1	3.85E-09	0.	1.188E+04	1.972E+04	2.149E+04	1.659E+04	4.618E+03	-1.179E+04	-3.131E+04	-5.129E+04	-6.942E+04
2	1.15E-08	-2.043E+06	-7.733E+06	-2.315E+07	-4.265E+07	-1.055E+08	-2.561E+08	-4.449E+08	3.074E+07	4.385E+08	1.751E+08
3	1.92E-08	-3.013E+06	-9.758E+06	-2.537E+07	-6.935E+07	-1.514E+08	-4.114E+08	-7.115E+08	-4.007E+07	5.895E+08	2.528E+08
4	2.69E-08	-3.924E+06	-1.104E+07	-2.702E+07	-7.119E+07	-1.829E+08	-4.293E+08	-7.253E+08	-1.045E+07	[illegible]	[illegible]
5	3.46E-08	-4.759E+06	-1.326E+07	-2.970E+07	-6.946E+07	-1.699E+08	-3.761E+08	-6.015E+08	1.252E+07	[illegible]	[illegible]
6	4.23E-08	-5.506E+06	-1.460E+07	-3.092E+07	-6.695E+07	-1.494E+08	-3.004E+08	-4.524E+08	3.120E+07	[illegible]	2.025E+08
7	5.00E-08	-6.157E+06	-1.556E+07	-3.156E+07	-6.376E+07	-1.302E+08	-2.425E+08	-3.156E+08	4.330E+07	3.597E+08	2.214E+08
8	5.77E-08	-6.707E+06	-1.649E+07	-3.171E+07	-6.011E+07	-1.132E+08	-1.916E+08	-2.220E+08	3.550E+07	2.010E+08	1.825E+08
9	6.54E-08	-7.153E+06	-1.712E+07	-3.149E+07	-5.625E+07	-9.643E+07	-1.525E+08	-1.584E+08	2.700E+07	1.902E+08	1.491E+08
10	7.31E-08	-7.497E+06	-1.762E+07	-3.102E+07	-5.237E+07	-8.559E+07	-1.224E+08	-1.154E+08	2.087E+07	1.411E+08	1.219E+08
11	8.08E-08	-7.744E+06	-1.803E+07	-3.039E+07	-4.861E+07	-7.458E+07	-9.915E+07	-8.579E+07	1.016E+07	1.006E+08	1.003E+08
12	8.85E-08	-7.899E+06	-1.842E+07	-2.969E+07	-4.509E+07	-6.521E+07	-8.107E+07	-6.499E+07	1.271E+07	8.702E+07	8.514E+07
13	9.62E-08	-7.971E+06	-1.886E+07	-2.899E+07	-4.185E+07	-5.729E+07	-6.701E+07	-5.019E+07	1.010E+07	[illegible]	[illegible]
14	1.04E-07	-7.958E+06	-1.941E+07	-2.853E+07	-3.892E+07	-5.066E+07	-5.605E+07	-3.953E+07	6.243E+06	5.132E+07	5.775E+07
15	1.12E-07	-7.901E+06	-2.019E+07	-2.775E+07	-3.632E+07	-4.513E+07	-4.752E+07	-3.179E+07	6.603E+06	4.177E+07	5.021E+07
16	1.19E-07	-7.779E+06	-2.131E+07	-2.726E+07	-3.403E+07	-4.057E+07	-4.090E+07	-2.615E+07	5.716E+06	3.472E+07	4.550E+07
17	1.27E-07	-7.611E+06	-2.292E+07	-2.685E+07	-3.202E+07	-3.604E+07	-3.580E+07	-2.203E+07	4.901E+06	2.951E+07	5.027E+07
18	1.35E-07	-7.407E+06	-2.524E+07	-2.648E+07	-3.025E+07	-3.381E+07	-3.192E+07	-1.907E+07	4.297E+06	2.572E+07	5.425E+07
19	1.42E-07	-7.174E+06	-2.857E+07	-2.605E+07	-2.869E+07	-3.140E+07	-2.905E+07	-1.700E+07	3.864E+06	2.304E+07	5.125E+07

I	R(I)	Z = 3.00E-07	Z = 3.30E-07	Z = 3.60E-07	Z = 3.90E-07	Z = 4.20E-07	Z = 4.50E-07	Z = 4.80E-07	Z = 5.10E-07	Z = 5.40E-07	Z = 5.70E-07
1	3.85E-09	-8.382E+04	-9.324E+04	-9.713E+04	-9.558E+04	-8.917E+04	-7.878E+04	-6.541E+04	-5.065E+04	[illegible]	[illegible]
2	1.15E-08	5.428E+07	1.808E+07	6.386E+06	5.006E+06	1.023E+06	9.717E+05	6.459E+05	4.790E+05	[illegible]	[illegible]
3	1.92E-08	7.938E+07	2.741E+07	1.094E+07	5.301E+06	2.909E+06	1.703E+06	1.164E+06	8.626E+05	[illegible]	[illegible]
4	2.69E-08	9.743E+07	3.404E+07	1.403E+07	7.255E+06	4.033E+06	2.457E+06	1.607E+06	1.249E+06	[illegible]	[illegible]
5	3.46E-08	1.054E+08	[illegible]	1.759E+07	8.935E+06	5.637E+06	3.109E+06	2.118E+06	[illegible]	[illegible]	[illegible]
6	4.23E-08	1.052E+08	[illegible]	1.964E+07	1.035E+07	5.920E+06	3.694E+06	2.534E+06	[illegible]	[illegible]	[illegible]
7	5.00E-08	9.839E+07	4.382E+07	2.144E+07	1.151E+07	6.760E+06	4.221E+06	2.920E+06	2.245E+06	[illegible]	[illegible]
8	5.77E-08	9.039E+07	4.374E+07	2.247E+07	1.242E+07	7.357E+06	[illegible]	3.275E+06	2.546E+06	2.126E+06	1.620E+06
9	6.54E-08	8.219E+07	4.274E+07	2.302E+07	1.310E+07	7.900E+06	5.093E+06	3.595E+06	[illegible]	2.404E+06	[illegible]
10	7.31E-08	7.376E+07	4.111E+07	2.316E+07	1.357E+07	8.331E+06	5.435E+06	3.879E+06	3.107E+06	2.694E+06	2.158E+06
11	8.08E-08	6.590E+07	3.912E+07	2.302E+07	1.386E+07	8.659E+06	5.715E+06	4.125E+06	3.361E+06	2.993E+06	[illegible]
12	8.85E-08	5.876E+07	3.694E+07	2.262E+07	1.398E+07	[illegible]	[illegible]	4.353E+06	[illegible]	[illegible]	[illegible]
13	9.62E-08	5.242E+07	3.471E+07	2.205E+07	1.390E+07	9.010E+06	6.086E+06	4.499E+06	[illegible]	[illegible]	[illegible]
14	1.04E-07	4.689E+07	3.252E+07	2.130E+07	1.383E+07	9.056E+06	6.184E+06	4.623E+06	[illegible]	[illegible]	[illegible]
15	1.12E-07	4.214E+07	3.044E+07	2.059E+07	1.360E+07	9.025E+06	6.222E+06	4.704E+06	4.153E+06	[illegible]	[illegible]
16	1.19E-07	3.811E+07	2.852E+07	1.979E+07	1.330E+07	8.925E+06	6.205E+06	4.739E+06	4.275E+06	[illegible]	5.110E+06
17	1.27E-07	3.474E+07	2.676E+07	1.896E+07	1.293E+07	8.756E+06	6.133E+06	[illegible]	4.353E+06	[illegible]	[illegible]
18	1.35E-07	3.197E+07	2.516E+07	1.814E+07	1.250E+07	8.532E+06	6.010E+06	[illegible]	4.577E+06	5.302E+06	7.556E+06
19	1.42E-07	2.973E+07	2.379E+07	1.733E+07	1.203E+07	8.253E+06	5.817E+06	4.556E+06	[illegible]	5.524E+06	5.435E+06

		[illegible]
1	[illegible]	[illegible]
2	1.[illegible]E-06	2.311E+05
3	1.72E-06	3.43[illegible]E+05
4	2.[illegible]E-06	4.512E+05
5	3.4[illegible]E-06	5.5[illegible]E+05
6	[illegible]	[illegible]
7	[illegible]	[illegible]
8	5.77[illegible]E-06	8.27[illegible]E+05
9	6.54E-06	9.[illegible]E+05
10	7.31E-06	9.771E+05
11	[illegible]	1.042E+06
12	8.[illegible]E-06	1.102E+06
13	[illegible]	1.155E+06
14	[illegible]	[illegible]
15	[illegible]	[illegible]
16	1.19E-07	1.285E+06
17	1.27E-07	1.318E+06
18	1.35E-07	1.347E+06
19	1.42E-07	1.371E+06

I	R(I)	Z 0.	Z 3.00E-08	Z 6.00E-08	Z 9.00E-08	Z 1.20E-07	Z 1.50E-07	Z 1.80E-07	Z 2.10E-07	Z 2.40E-07	Z 2.70E-07
1	3.85E-09	2.459E+07	4.805E+07	9.620E+07	1.965E+08	3.401E+08	2.856E+06	-1.114E+09	-1.006E+09	4.179E+08	3.355E+08
2	1.15E-08	2.459E.07	4.805E+07	9.620E+07	1.955E+08	3.401E+08	2.852E+06	-1.114E+09	-1.006E+09	4.179E+08	3.335E+08
3	1.92E-08	2.313E+07	4.470E+07	9.120E+07	1.804E+08	3.014E+08	2.362E+06	-9.907E+08	-9.016E+08	3.594E+08	3.062E+08
4	2.69E-08	2.140E+07	4.070E+07	7.993E+07	1.517E+08	2.425E+08	1.592E+06	-8.184E+08	-7.493E+08	[illegible]	[illegible]
5	3.46E-08	1.942E+07	3.655E+07	6.601E+07	1.230E+08	1.793E+08	8.375E+07	-6.572E+08	-5.700E+08	[illegible]	[illegible]
6	4.23E-08	1.724E+07	3.233E+07	5.602E+07	9.720E+07	1.259E+08	2.649E+07	-4.797E+08	-4.200E+08	1.070E+08	1.541E+08
7	5.00E-08	1.491E+07	2.815E+07	4.938E+07	7.613E+07	8.514E+07	-1.043E+07	-3.557E+08	-3.151E+08	5.541E+07	1.135E+08
8	5.77E-08	1.247E+07	2.407E+07	4.112E+07	5.910E+07	5.655E+07	-2.924E+07	-2.636E+08	-2.340E+08	2.009E+07	8.124E+07
9	6.54E-08	9.967E+06	2.017E+07	3.384E+07	4.546E+07	3.627E+07	-3.703E+07	-1.975E+08	-1.762E+08	5.628E+05	5.762E+07
10	7.31E-08	7.410E+06	1.649E+07	2.749E+07	3.400E+07	2.239E+07	-3.854E+07	-1.500E+08	-1.348E+08	-9.940E+06	4.040E+07
11	8.08E-08	4.614E+06	1.305E+07	2.202E+07	2.614E+07	1.294E+07	-3.674E+07	-1.150E+08	-1.035E+08	[illegible]	2.812E+07
12	8.85E-08	2.176E+06	9.880E+06	1.755E+07	1.949E+07	6.640E+06	[illegible]	-8.889E+07	-8.035E+07	-1.650E+07	1.950E+07
13	9.62E-08	-5.226E+05	6.990E+06	1.340E+07	1.435E+07	2.572E+06	-2.919E+07	[illegible]	-6.258E+07	-1.621E+07	[illegible]
14	1.04E-07	-3.314E+06	4.592E+06	1.010E+07	1.037E+07	8.093E+04	-2.466E+07	-5.399E+07	[illegible]	-1.487E+07	[illegible]
15	1.12E-07	-6.249E+06	2.106E+06	7.366E+06	7.358E+06	-1.302E+06	-2.065E+07	-4.124E+07	-3.766E+07	-1.297E+07	[illegible]
16	1.19E-07	-9.400E+06	1.081E+05	5.188E+06	5.099E+06	-1.913E+06	-1.601E+07	-3.135E+07	-2.869E+07	-1.086E+07	3.354E+06
17	1.27E-07	-1.287E+07	-1.359E+06	3.453E+06	3.421E+06	-1.997E+06	-1.283E+07	-2.318E+07	-2.125E+07	-8.554E+06	2.173E+06
18	1.35E-07	-1.679E+07	-2.369E+06	2.129E+06	2.186E+06	-1.730E+06	-9.302E+06	-1.637E+07	-1.494E+07	-6.369E+06	1.269E+06
19	1.42E-07	-2.136E+07	-2.689E+06	1.163E+06	1.274E+06	-1.245E+06	-6.008E+06	-1.028E+07	-9.450E+06	-4.121E+06	6.636E+05
20	1.50E-07	-2.685E+07	-2.042E+06	4.602E+05	5.774E+05	-6.413E+05	-2.918E+06	-4.924E+06	-4.554E+06	-7.015E+06	2.920E+05

I	R(I)	Z 3.00E-07	Z 3.30E-07	Z 3.60E-07	Z 3.90E-07	Z 4.20E-07	Z 4.50E-07	Z 4.80E-07	Z 5.10E-07	Z 5.40E-07	Z 5.70E-07
1	3.85E-09	1.486E+08	7.034E+07	3.666E+07	2.054E+07	1.165E+07	6.202E+06	2.516E+06	-2.214E+05	[illegible]	[illegible]
2	1.15E-08	1.466E+08	7.035E+07	3.666E+07	2.055E+07	1.165E+07	6.206E+06	2.522E+06	-2.171E+05	-2.359E+06	[illegible]
3	1.92E-08	1.394E+08	6.736E+07	3.579E+07	2.619E+07	1.149E+07	6.122E+06	2.402E+06	-2.425E+05	[illegible]	[illegible]
4	2.69E-08	1.260E+08	6.318E+07	3.454E+07	1.958E+07	1.119E+07	5.973E+06	2.402E+06	[illegible]	[illegible]	[illegible]
5	3.46E-08	1.099E+08	5.602E+07	3.284E+07	1.875E+07	1.079E+07	5.766E+06	[illegible]	-3.553E+05	-2.672E+06	[illegible]
6	4.23E-08	9.309E+07	5.236E+07	3.022E+07	1.775E+07	1.036E+07	5.514E+06	2.152E+06	-4.370E+05	-2.574E+06	[illegible]
7	5.00E-08	7.729E+07	4.652E+07	2.779E+07	1.662E+07	[illegible]	5.216E+06	2.007E+06	-5.317E+05	-2.674E+06	[illegible]
8	5.77E-08	6.330E+07	4.078E+07	2.525E+07	1.538E+07	9.082E+06	4.883E+06	1.834E+06	-6.501E+05	-2.789E+06	-4.401E+06
9	6.54E-08	5.134E+07	3.533E+07	2.267E+07	1.409E+07	8.403E+06	4.520E+06	1.647E+06	-7.460E+05	-2.917E+06	-4.684E+06
10	7.31E-08	4.122E+07	3.067E+07	2.013E+07	1.275E+07	7.684E+06	4.136E+06	1.455E+06	[illegible]	-3.095E+06	-4.950E+06
11	8.08E-08	3.265E+07	2.588E+07	1.766E+07	[illegible]	6.941E+06	3.737E+06	1.256E+06	[illegible]	[illegible]	[illegible]
12	8.85E-08	2.598E+07	2.155E+07	1.531E+07	1.007E+07	6.107E+06	3.330E+06	1.059E+06	[illegible]	[illegible]	[illegible]
13	9.62E-08	2.032E+07	1.786E+07	1.310E+07	8.767E+06	5.432E+06	2.920E+06	8.697E+05	[illegible]	[illegible]	[illegible]
14	1.04E-07	1.584E+07	1.463E+07	1.102E+07	7.497E+06	4.662E+06	2.512E+06	6.925E+05	[illegible]	-3.577E+06	-6.550E+06
15	1.12E-07	1.216E+07	1.177E+07	9.093E+06	6.273E+06	3.946E+06	2.112E+06	5.310E+05	-1.190E+06	-3.635E+06	-7.174E+06
16	1.19E-07	9.159E+06	9.248E+06	7.303E+06	5.099E+06	3.228E+06	1.723E+06	3.965E+05	-1.151E+06	[illegible]	-7.902E+06
17	1.27E-07	6.696E+06	7.009E+06	5.630E+06	3.972E+06	2.531E+06	1.347E+06	2.717E+05	-1.054E+06	[illegible]	[illegible]
18	1.35E-07	4.652E+06	5.009E+06	4.067E+06	2.909E+06	1.868E+06	9.861E+05	1.701E+05	-8.895E+05	[illegible]	-1.019E+07
19	1.42E-07	2.512E+06	3.203E+06	2.641E+06	1.891E+06	1.212E+06	6.414E+05	1.020E+05	-6.523E+05	[illegible]	[illegible]
20	1.50E-07	1.386E+06	1.546E+06	1.284E+06	9.225E+05	5.920E+05	3.129E+05	4.552E+04	-3.476E+05	[illegible]	-1.365E+07

ORIGINAL PAGE IS OF POOR QUALITY

POSITIVE CHARGE LOCATIONS

0	0	0	5	3	46	166	264	48	4	2	0	0	0	0	0	0	0	0	0
0	2	7	8	42	129	458	755	144	10	2	0	0	0	0	0	0	0	0	0
0	0	0	21	61	184	691	1055	185	14	0	0	0	0	0	0	0	0	0	0
0	0	0	8	30	147	556	892	183	15	0	0	0	0	0	0	0	0	0	0
0	0	0	0	17	74	369	593	106	10	0	0	0	0	0	0	0	0	0	0
0	0	0	0	2	30	177	319	77	4	0	0	0	0	0	0	0	0	0	0
0	0	0	0	0	2	55	125	37	1	0	0	0	0	0	0	0	0	0	0
0	0	0	0	0	0	11	35	4	0	0	0	0	0	0	0	0	0	0	0
0	0	0	0	0	0	0	2	1	1	0	0	0	0	0	0	0	0	0	0
0	0	0	0	0	0	0	1	0	0	0	0	0	0	0	0	0	0	0	0
0	0	0	0	0	0	0	0	0	0	0	0	0	0	0	0	0	0	0	0
0	0	0	0	0	0	0	0	0	0	0	0	0	0	0	0	0	0	0	0
0	0	0	0	0	0	0	0	0	0	0	0	0	0	0	0	0	0	0	0
0	0	0	0	0	0	0	0	0	0	0	0	0	0	0	0	0	0	0	0
0	0	0	0	0	0	0	0	0	0	0	0	0	0	0	0	0	0	0	0
0	0	0	0	0	0	0	0	0	0	0	0	0	0	0	0	0	0	0	0
0	0	0	0	0	0	0	0	0	0	0	0	0	0	0	0	0	0	0	0
0	0	0	0	0	0	0	0	0	0	0	0	0	0	0	0	0	0	0	0
0	0	0	0	0	0	0	0	0	0	0	0	0	0	0	0	0	0	0	0

NEGATIVE CHARGE LOCATIONS

0	0	0	0	0	0	30	392	84	6	4	0	0	0	0	0	0	0	0	0
0	0	0	0	0	0	126	1120	236	20	4	0	0	0	0	0	0	0	0	0
0	0	0	0	0	0	226	1480	304	22	0	0	0	0	0	0	0	0	0	0
0	0	0	0	0	0	160	1308	320	26	0	0	0	0	0	0	0	0	0	0
0	0	0	0	0	0	140	888	174	20	0	0	0	0	0	0	0	0	0	0
0	0	0	0	0	0	72	486	130	8	0	0	0	0	0	0	0	0	0	0
0	0	0	0	0	0	34	204	66	2	0	0	0	0	0	0	0	0	0	0
0	0	0	0	0	0	6	52	6	0	0	0	0	0	0	0	0	0	0	0
0	0	0	0	0	0	0	4	2	2	0	0	0	0	0	0	0	0	0	0
0	0	0	0	0	0	0	2	0	0	0	0	0	0	0	0	0	0	0	0
0	0	0	0	0	0	0	0	0	0	0	0	0	0	0	0	0	0	0	0
0	0	0	0	0	0	0	0	0	0	0	0	0	0	0	0	0	0	0	0
0	0	0	0	0	0	0	0	0	0	0	0	0	0	0	0	0	0	0	0
0	0	0	0	0	0	0	0	0	0	0	0	0	0	0	0	0	0	0	0
0	0	0	0	0	0	0	0	0	0	0	0	0	0	0	0	0	0	0	0
0	0	0	0	0	0	0	0	0	0	0	0	0	0	0	0	0	0	0	0
0	0	0	0	0	0	0	0	0	0	0	0	0	0	0	0	0	0	0	0
0	0	0	0	0	0	0	0	0	0	0	0	0	0	0	0	0	0	0	0
0	0	0	0	0	0	0	0	0	0	0	0	0	0	0	0	0	0	0	0

Appendix 6

DESCRIPTION OF ACORN

I. PURPOSE

ACORN is a computer code to calculate streamer development initiated by electron avalanche.

II.1 START-UP REQUIREMENT — INPUTS

The following inputs are needed for an ACORN run:

CARD 1 (3I5) — contains three integer quantities:

- KMT = 1 — for starting from cards with new data.
  - = 0 — for restarting from magnetic tape (TAPE 3) at dump number KNR.
- KNR — writing on TAPE 3 commences at dump number KNR+1.
- KNL = 0 — if no enlargement of grid, spacing is required.
  - = 1 — if double spacing is required for consecutive run.

CARD 2 (3I5) — contains three integer quantities:

- NR — number of radial mesh points covering discharge volume.
- NZ — number of axial mesh points.
- NRR — number of radial mesh points used in calculation of potential.

CARDS 3-9 (1P3E15.8) — contains parameters for the dielectric avalanche.

P — gas pressure, Newton/m^2 — Vestigal.

GAP — imaginary gap length, M.

RAD — maximum radius at which charge density will be calculated, M.

FRA — fraction of distance between initial charge cloud origin and left-hand boundary to the gap length.

EPS — dielectric constant.

VG — voltage across the gap due to external field.

ALC1 - ALC3 — constants in formula for the primary ionization coefficient, α:
$\alpha/P=ALC1*EXP[-(ALC2)/(E/P)] + ALC3.$

DELTC1 — constant for detachment (for gas run purpose only).

WPC1 - WPC2 — constants for the ion drift velocity;
$\vec{V}_p = [WPC1(E/P) + WPC2] \cdot \vec{E}/E.$

WMC1 - WMC3 — constants for electron drift velocity:
$\vec{V}_e=[WMC1+WMC2/(E/P)] \cdot \vec{E}/P$ for $E/P > WMC3$;
$= const_1[1-const_2(E/P)] \cdot \vec{E}/P$ for $E/P < WMC3$.
(The constants are chosen so that the magnitude and slope of V_e are continuous at $E/P = WMC3$.)

D — material specific heat, J/M^3 - °K.

ZB — initial charge cloud length, M.

RML — avalanche length at the beginning of the calculation, M.

TOLPOT — fractional accuracy required in iterations for potential distortion.

TOLWM — fractional accuracy required in iterations for position of foot of characteristics.

DTMIN — minimum allowed time step.

CARD 10 (415) — contains four integers.

NT — number of detailed printouts between successive dumps to TAPE 3.

NTR — number of time steps between detailed printouts. (NT*NTR is therefore the number of time steps between dumps.)

IDIV — radial spacing of arrays in print-out.

JDIV — axial spacing of arrays in print-out (must be a power of two).

After each dump to TAPE 3, these four quantities are read again, as many times as desired.

LAST CARD — A blank card, or four zeros, in (4I5) terminates the run.

II.2 START-UP REQUIREMENTS

A magnetic tape is required to store the data for consecutive runs. For test runs, tape is not required.

III.1 CODE OUTPUTS — PRINTED OUTPUT

The code prints out first the input data, followed by a listing of the radii of radial mesh points. Next, the current values of NT, NTR, IDIV, and JDIV are printed.

At the end of each time step, a summary of the results is given comprising the present values of the time, the time step, and the number of iterations.

Every NTR time steps the following more detailed information is printed for every IDIVth radial mesh point and every JDIVth axial mesh point (in addition to the above summary):

a) axial electric field, V/m.

b) radial electric field, V/m

c) electron charge density, C/M^3.

d) positive ion charge density, C/M^3.

e) net charge density, C/M^3.

f) temperature, ^{o}K.

g) total electron charge, C.

h) dipole length, M.

i) electron charge center, M.

After NTR*NT time steps the record number of the dump to TAPE 3 is printed, followed by the next set of values of NT, NTR, IDIV, and JDIV.

The above sequence of output is repeated until a data card is encountered with NT=0.

III.2 CODE OUTPUTS — MAGNETIC TAPE 3

The time, time step, order of enlargement, electron density, positive ion density, net charge density, and temperature up to the present time are dumped to TAPE 3 in the form of an information record. The calculations may then be restarted at a later date.

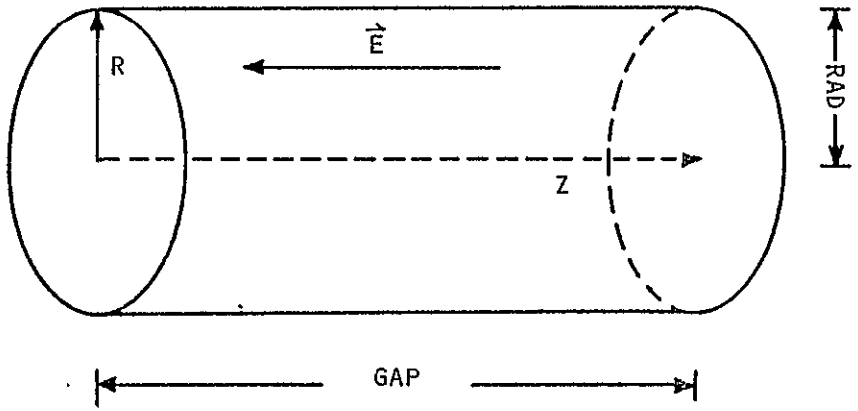

FIGURE A6.1. GEOMETRY OF CODE ACORN

IV. PROGRAM LOGIC

The logic flow in ACORN proceeds as follows:

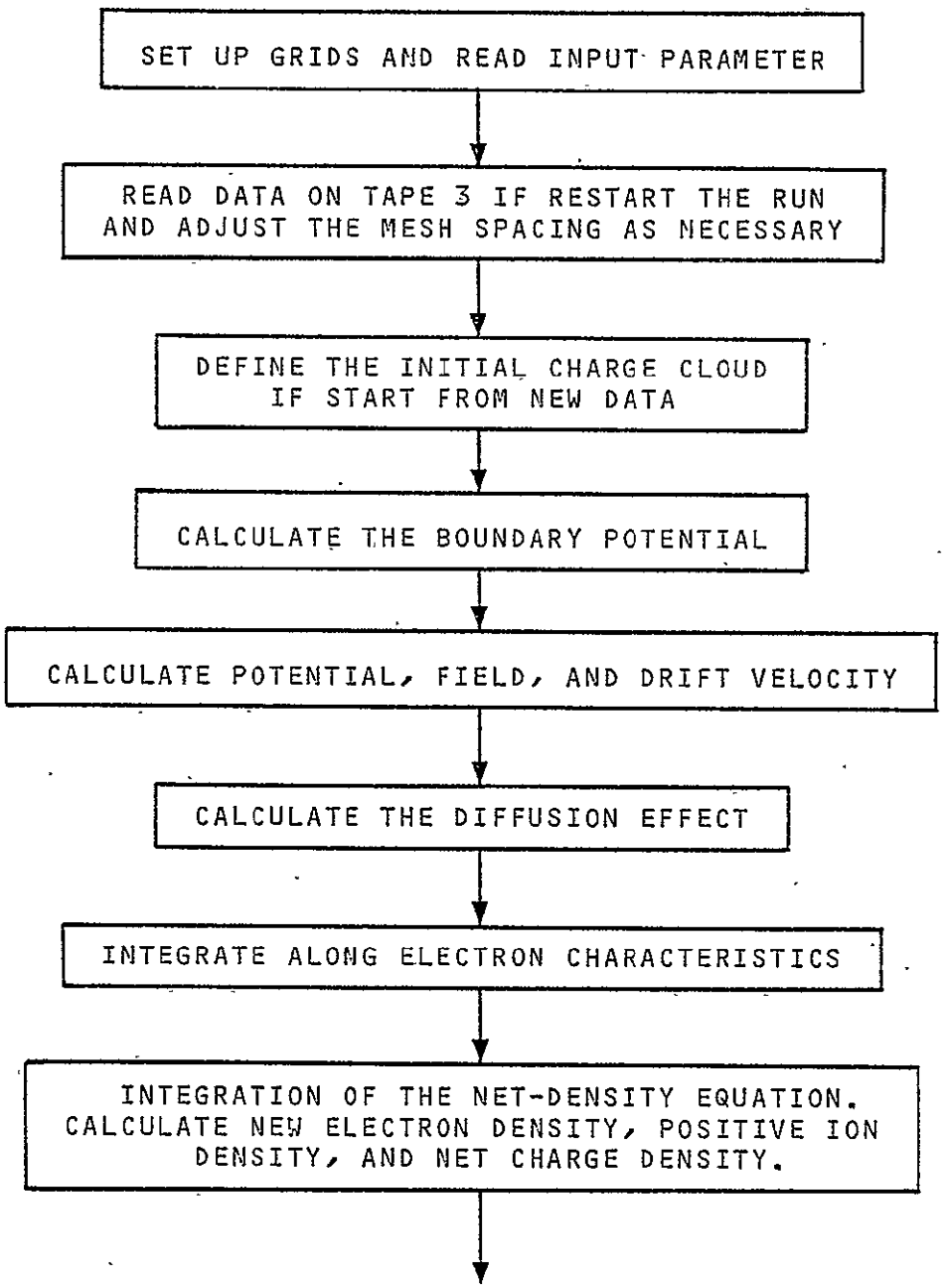

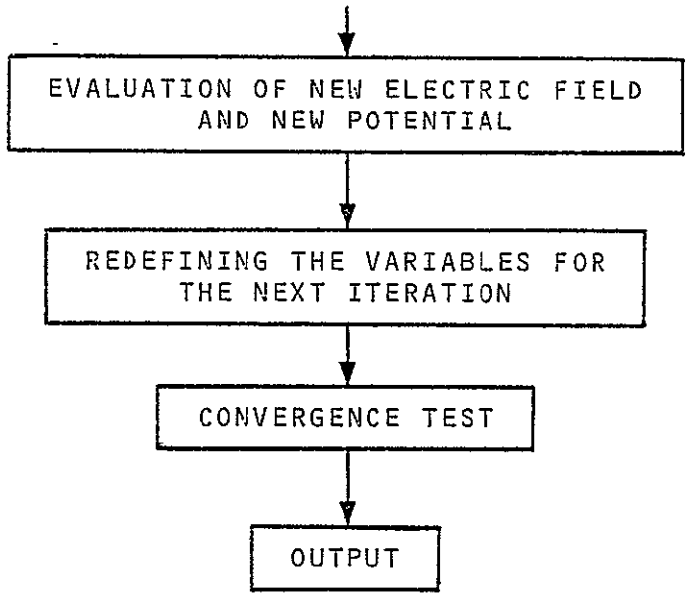
EVALUATION OF NEW ELECTRIC FIELD AND NEW POTENTIAL
REDEFINING THE VARIABLES FOR THE NEXT ITERATION
CONVERGENCE TEST
OUTPUT

TEST RUN OUTPUT

TEMPORAL GROWTH OF AVALANCHE- - TWO-DIMENSIONAL CALCULATION

INPUT DATA

KHT = 1, KHZ = 0, KHL = 0

NR = 21, NZ = 45, NRZ = 26

1.00000000E+00 GAS PRESSURE (TORR)

5.00000000E-07 GAP LENGTH (M)

1.54000000E-07 RADIUS OF DISCHARGE (M)

2.00000000E-01 FRACTION OF DISTANCE OF INITIAL CHARGE CLOUD TO THE GAP

1.77100000E-11 DIELECTRIC CONSTANT

4.00000000E+02 VOLTAGE ACROSS THE GAP

1.85400000E+08)
7.22000000E+08) CONSTANTS IN FORMULA FOR PRIMARY IONISATION COEFFICIENT
0.)

0. CONSTANT IN FORMULA FOR EXCITATION COEFFICIENT

0.)
0.) CONSTANTS IN FORMULA FOR ION DRIFT VELOCITY

1.60000000E-04)
0.) CONSTANTS IN FORMULA FOR ELECTRON DRIFT VELOCITY
1.00000000E+06)

2.50000000E+06 DENSITY OF THE SOLID MATERIAL(KG/M3)

1.06000000E-07 AXIAL RANGE OF INITIAL CHARGE CLOUD (M)

1.33000000E-08 AVALANCHE LENGTH (M)

1.00000000E-01 FRACTIONAL ACCURACY REQUIRED IN POTENTIAL

1.00000000E-02 FRACTIONAL ACCURACY REQUIRED IN SLOPE OF CHARACTERISTIC

5.00000000E-10 MINIMUM ALLOWED VALUE OF TIME STEP

1.00000000E+00 ORDER OF ENLARGEMENT

RADIAL MESH

1	0.
2	7.1000E-09
3	1.5400E-08
4	2.3400E-08
5	3.1200E-08
6	3.9000E-08
7	4.6800E-08
8	5.4600E-08
9	6.2400E-08
10	7.0200E-08
11	7.8000E-08
12	8.5800E-08
13	9.3600E-08
14	1.0140E-07
15	1.0920E-07
16	1.1700E-07
17	1.2480E-07
18	1.3260E-07
19	1.4040E-07
20	1.4820E-07
21	1.5600E-07
22	1.6380E-07
23	1.7160E-07
24	1.7940E-07
25	1.8720E-07
26	1.9500E-07

START OF CALCULATION

INITIAL CONDITIONS =
TIME = 0. SEC , GAP VOLTAGE = 4.80800E+02 VOLTS

NT = 1 NTR = 5 IDIV = 2 JDIV = 8

TIME SEC	TIME STEP SEC	NUMBER ITERATIONS
1.82873E-14	1.82873E-14	2
1.89726E-14	6.85256E-16	2
2.49760E-14	6.00340E-15	2
4.64130E-14	2.14370E-14	2
4.64180E-14	5.00600E-18	2

DISCHARGE VARIABLES AT TIME 4.64180E-14 SEC.

AXIAL ELECTRIC FIELD (VOLTS/ M)

8.01000E+08	8.03819E+08	8.20685E+08	7.33820E+08	8.34532E+08	8.85514E+08	8.81428E+08	8.00540E+08	8.08273E+08
8.00978E+08	8.03573E+08	8.18066E+08	7.46359E+08	8.28535E+08	8.85193E+08	8.81393E+08	8.00553E+08	8.08271E+08
8.00918E+08	8.02997E+08	8.09970E+08	7.69026E+08	8.15412E+08	8.84358E+08	8.81294E+08	8.00531E+08	8.08214E+08
8.00829E+08	8.02335E+08	8.04873E+08	7.83112E+08	8.05186E+08	8.83300E+08	8.81148E+08	8.00497E+08	8.08133E+08
8.00724E+08	8.01726E+08	8.02152E+08	7.90221E+08	8.00490E+08	8.82293E+08	8.80976E+08	8.00454E+08	8.08039E+08
8.00615E+08	8.01223E+08	8.00766E+08	7.94831E+08	7.99035E+08	8.81480E+08	8.80798E+08	8.00405E+08	8.07922E+08
8.00510E+08	8.00836E+08	8.00085E+08	7.96190E+08	7.98786E+08	8.80893E+08	8.80631E+08	8.00353E+08	8.07803E+08
8.00414E+08	8.00551E+08	7.99782E+08	7.97451E+08	7.98884E+08	8.80494E+08	8.80483E+08	8.00302E+08	8.07683E+08
8.00331E+08	8.00349E+08	7.99665E+08	7.98223E+08	7.99059E+08	8.80242E+08	8.80359E+08	8.00253E+08	8.07563E+08
8.00262E+08	8.00210E+08	7.99638E+08	7.98717E+08	7.99225E+08	8.80083E+08	8.80258E+08	8.00208E+08	8.07443E+08
8.00205E+08	8.00116E+08	7.99653E+08	7.98945E+08	7.99364E+08	7.99988E+08	8.80179E+08	8.00168E+08	8.07324E+08

RADIAL ELECTRIC FIELD (VOLTS/ M)

0.	0.	0.	0.	0.	0.	0.	0.	0.
0.	-7.47635E+05	-1.66608E+07	-3.04233E+07	1.69027E+07	1.09824E+06	1.99055E+05	5.54667E+04	0.
0.	-1.25811E+06	-1.29524E+07	-3.00682E+07	2.22127E+07	1.90857E+06	3.57819E+05	1.07729E+05	0.
0.	-1.47629E+06	-9.15245E+06	-1.61495E+07	1.75328E+07	2.29759E+06	4.86982E+05	1.53195E+05	0.
0.	-1.53092E+06	-6.45254E+06	-7.11934E+06	1.18177E+07	2.32052E+06	5.70053E+05	1.87651E+05	0.
0.	-1.44144E+06	-4.51555E+06	-3.26014E+06	6.48324E+06	2.18964E+06	6.08527E+05	2.16320E+05	0.
0.	-1.28784E+06	-3.15918E+06	-1.64215E+06	3.88217E+06	1.89003E+06	6.09877E+05	2.33113E+05	0.
0.	-1.11726E+06	-2.22494E+06	-1.83072E+05	2.47216E+06	1.47908E+06	5.84169E+05	2.40860E+05	0.
0.	-9.47771E+05	-1.58458E+06	-5.33412E+05	1.57444E+06	1.19007E+06	5.41327E+05	2.46921E+05	0.
0.	-7.93491E+05	-1.14388E+06	-3.33405E+05	1.06113E+06	9.47642E+05	4.89593E+05	2.34878E+05	0.
0.	-6.59110E+05	-8.37541E+05	-2.17838E+05	7.38038E+05	7.51876E+05	4.35015E+05	2.24483E+05	0.

ELECTRON DENSITY (COUL/M3)

1.13104E-18	5.91157E-07	7.74113E+01	2.92127E+05	5.64779E+04	2.16199E-01	4.03785E-11	1.07010E-23	4.77951E-34
7.94961E-20	2.94231E-08	2.07416E+01	2.08649E+05	4.66145E+04	1.99948E-01	3.66627E-11	3.84483E-23	4.65970E-34
9.50737E-23	2.51407E-11	8.30813E-01	5.38072E+04	2.15016E+04	1.18261E-01	2.36483E-11	2.55244E-23	3.14013E-34
1.19808E-25	3.09526E-14	1.09862E-02	6.60876E+03	5.96362E+03	4.45936E-02	1.13874E-11	1.28487E-23	1.40657E-34
1.93934E-28	5.02279E-17	5.45084E-05	1.54822E+02	1.00160E+03	1.25862E-02	4.10451E-12	4.92544E-24	4.30766E-35
2.92389E-31	7.54489E-20	1.58099E-07	9.12432E+00	1.62187E+02	2.48301E-03	1.11010E-12	1.44554E-24	1.96782E-35
3.73860E-34	9.54302E-23	2.95044E-10	1.21562E-01	4.48553E+00	3.42969E-04	2.25913E-13	3.25957E-25	4.46478E-36
4.04025E-37	1.01610E-25	4.01082E-13	9.04248E-04	2.47321E-01	3.32305E-05	3.46982E-14	5.17440E-26	8.12494E-37
3.75438E-40	9.28879E-29	4.30291E-16	4.00312E-06	5.96352E-03	2.26348E-06	4.83452E-15	7.66606E-27	1.15667E-37
3.06580E-43	7.46432E-32	3.85100E-19	1.11543E-08	9.13815E-05	1.08696E-07	3.58340E-16	5.86727E-28	1.21404E-38
9.61539E-48	2.03961E-33	1.09672E-20	5.15238E-10	1.08579E-05	2.16428E-08	9.83733E-17	2.43879E-28	3.94796E-39

POSITIVE ION DENSITY (COUL/M3)

-1.27030E-18 -4.19082E-10 6.34686E+04 4.62858E+05 1.54857E+04 2.59344E-02 1.13586E-12 1.76497E-25 -3.72437E-37
-4.06368E-20 -2.33674E-11 1.15094E+04 1.88448E+05 1.24317E+04 2.27250E-02 1.03597E-12 1.66345E-25 -1.59662E-37
-1.98128E-23 -5.60435E-14 1.57870E+02 8.69040E+04 5.44510E+03 1.33534E-02 6.79115E-13 1.11838E-25 -2.43785E-37
-3.65754E-26 -9.87161E-17 9.49125E+02 1.64377E+04 1.56312E+03 5.51000E-03 3.37046E-13 5.74527E-26 -1.26385E-37
-6.00428E-29 -1.36106E-19 1.53577E-06 5.34786E+02 2.64205E+02 1.59806E-03 1.26426E-13 2.26842E-26 -5.05451E-38
-7.80849E-32 -1.58568E-22 -3.17509E-09 1.17521E+01 2.77507E+01 3.26805E-04 3.59442E-14 6.90519E-27 -1.56444E-38
-8.15749E-35 -1.36717E-25 -3.69886E-12 1.11612E-01 1.76317E+00 4.68005E-05 7.74075E-15 1.62679E-27 -3.74203E-39
-6.99418E-38 -1.04193E-28 -3.87254E-15 4.41421E-04 6.83635E-02 4.72961E-06 1.27585E-15 2.97857E-28 -7.04031E-40
-5.02938E-41 -6.88120E-32 -2.05243E-18 8.28618E-07 1.61932E-03 3.36424E-07 1.59711E-16 4.25937E-29 -1.83924E-40
-3.18113E-44 -4.02980E-35 -1.17040E-21 5.94279E-10 2.35450E-05 1.68832E-08 1.52868E-17 4.78119E-30 -1.28542E-41
-9.17062E-45 -9.51431E-37 -2.70027E-23 -5.29184E-14 1.78179E-06 3.13851E-09 4.67447E-18 1.49153E-30 -7.14939E-42

NET CHARGE DENSITY (COUL/M3)

-2.37134E-18 -5.91576E-07 6.35912E+04 1.70731E+05 -4.09923E+04 -1.91864E-01 -3.92354E-11 -4.85245E-23 -4.78323E-34
-1.20133E-19 -2.94472E-08 1.34887E+04 9.97983E+04 -3.41748E+04 -1.67223E-01 -3.56317E-11 -3.82739E-23 -4.64356E-34
-1.14886E-22 -2.52167E-11 1.57044E+02 3.10968E+04 -1.58565E+04 -9.69879E-02 -2.29684E-11 -2.54125E-23 -3.14327E-34
-1.56384E-25 -3.10507E-14 8.48263E-02 3.82894E+03 -4.44050E+03 -3.90836E-02 -1.10503E-11 -1.27833E-23 -1.60784E-34
-2.53976E-28 -5.03660E-17 -5.29712E-05 1.29943E+02 -7.35394E+02 -1.09881E-02 -3.97888E-12 -4.96276E-24 -6.31271E-35
-3.70474E-31 -7.55985E-20 -1.61274E-07 2.42659E+01 -2.46364E+01 -2.15701E-03 -1.47415E-12 -1.43863E-24 -1.10939E-35
-4.55434E-34 -9.55670E-23 -2.98743E-10 -9.94973E-03 -4.64156E+00 -2.96161E-04 -2.18152E-13 -3.24332E-25 -4.46854E-36
-4.73967E-37 -1.01714E-25 -4.84135E-13 -4.42818E-04 -1.78958E-01 -2.85001E-05 -3.34232E-14 -5.64461E-26 -8.13200E-37
-4.25732E-40 -9.29567E-29 -4.32343E-16 -3.17450E-06 -4.34620E-03 -1.92685E-06 -3.87481E-15 -7.62347E-27 -1.15711E-37
-3.37391E-43 -7.46833E-32 -3.86271E-19 -1.85421E-01 -6.78345E-05 -9.18132E-08 -3.41059E-16 -8.83945E-28 -1.29524E-38
-9.18024E-45 -2.04058E-33 -1.01943E-20 -5.15297E-10 -8.27613E-06 -1.85842E-08 -9.34918E-17 -2.42388E-28 -3.95511E-39

TEMPERATURE (K)

3.01000E+02 3.01000E+02 3.00000E+02 3.00461E+02 3.00886E+02 3.00000E+02 3.00000E+02 3.00000E+02 3.01000E+02
3.00000E+02 3.00000E+02 3.01000E+02 3.00331E+02 3.00969E+02 3.00000E+02 3.00000E+02 3.00000E+02 3.01000E+02
3.00000E+02 3.00000E+02 3.01000E+02 3.00898E+02 3.00831E+02 3.00000E+02 3.00000E+02 3.00000E+02 3.01000E+02
3.00000E+02 3.00000E+02 3.00000E+02 3.00812E+02 3.00809E+02 3.00000E+02 3.00000E+02 3.00000E+02 3.01000E+02
3.00000E+02 3.01000E+02 3.00000E+02 3.00401E+02 3.00801E+02 3.00000E+02 3.00000E+02 3.00000E+02 3.01000E+02
3.00000E+02 3.00000E+02 3.00000E+02 3.00000E+02 3.00000E+02 3.00000E+02 3.00000E+02 3.00000E+02 3.00000E+02
3.00000E+02 3.00000E+02 3.00000E+02 3.00000E+02 3.00000E+02 3.00000E+02 3.00000E+02 3.00000E+02 3.01000E+02
3.00000E+02 3.00000E+02 3.00000E+02 3.00000E+02 3.00000E+02 3.00000E+02 3.00000E+02 3.00000E+02 3.01000E+02
3.00000E+02 3.00000E+02 3.00000E+02 3.00000E+02 3.00000E+02 3.00000E+02 3.00000E+02 3.00000E+02 3.01000E+02
3.00000E+02 3.00000E+02 3.00000E+02 3.00000E+02 3.00000E+02 3.00000E+02 3.00000E+02 3.00000E+02 3.01000E+02

TOTAL NET CHARGE = 4.53599215E-19 (COUL)

TOTAL ELECTRON CHARGE = 4.11222240E-17 (COUL)

DIPOLE LENGTH = 1.39206442E-08 (M)

CENTER OF ELECTRON CLOUD = 2.11967742E-07 (M)

CENTER OF DIPOLE = 2.65067419E-07 (M)

VARIABLES CORRESPONDING TO ABOVE TIME STEP DUMPED TO TAPE 3 AT RECORD 1

NT = 1 ITR = 5 IDIV = 2 JDIV = 8

TIME SEC	TIME STEP SEC	NUMBER ITERATIONS
1.98155E-13	1.05459E-14	2
2.09114E-13	1.09590E-14	2
2.18974E-13	9.80985E-15	2
2.28416E-13	9.49234E-15	2
2.37618E-13	9.20178E-15	2

DISCHARGE VARIABLES AT TIME 2.37618E-13 SEC

AXIAL ELECTRIC FIELD (VOLTS/ M)

8.03455E+08	8.18472E+08	8.58771E+08	7.77138E+08	6.78164E+08	8.53750E+08	8.19640E+08	8.03703E+08	8.01688E+08
8.03378E+08	8.10035E+08	8.45277E+08	7.74815E+08	6.87761E+08	8.49110E+08	8.10309E+08	8.03642E+08	8.01664E+08
8.03235E+08	8.08932E+08	8.31332E+08	8.00069E+08	7.13136E+08	8.37258E+08	8.09339E+08	8.03447E+08	8.01616E+08
8.02987E+08	8.07514E+08	8.11857E+08	7.88403E+08	7.41709E+08	8.24194E+08	8.07963E+08	8.03188E+08	8.01540E+08
8.02683E+08	8.06045E+08	8.11829E+08	7.84757E+08	7.63458E+08	8.13863E+08	8.06434E+08	8.02863E+08	8.01441E+08
8.02353E+08	8.04687E+08	8.06391E+08	7.86488E+08	7.76158E+08	8.07108E+08	8.04959E+08	8.02494E+08	8.01325E+08
8.02019E+08	8.03521E+08	8.03166E+08	7.89355E+08	7.84862E+08	8.03152E+08	8.03669E+08	8.02119E+08	8.01178E+08
8.01702E+08	8.02573E+08	8.01451E+08	7.91880E+08	7.81607E+08	8.00987E+08	8.02614E+08	8.01759E+08	8.01067E+08
8.01411E+08	8.01830E+08	8.00359E+08	7.93821E+08	7.92590E+08	7.99863E+08	8.01713E+08	8.01430E+08	8.00934E+08
8.01155E+08	8.01266E+08	7.99763E+08	7.95257E+08	7.94546E+08	7.99318E+08	8.01178E+08	8.01140E+08	8.00810E+08
8.00934E+08	8.00848E+08	7.99460E+08	7.96312E+08	7.95875E+08	7.99085E+08	8.00730E+08	8.00892E+08	8.00693E+08

RADIAL ELECTRIC FIELD (VOLTS/ M)

0.	0.	0.	0.	0.	0.	0.	0.	0.
0.	-1.69844E+06	-2.36020E+07	-1.37484E+08	1.68412E+07	1.32414E+07	1.62693E+06	4.85796E+05	0.
0.	-3.01141E+06	-2.39435E+07	-1.52481E+08	8.04826E+07	2.13478E+07	3.80681E+06	7.79243E+05	0.
0.	-3.84180E+06	-2.13585E+07	-1.57595E+07	7.68264E+07	2.30287E+07	3.95435E+06	1.09380E+06	0.
0.	-4.22372E+06	-1.71221E+07	-5.13052E+07	4.79364E+07	2.05824E+07	4.44630E+06	1.33211E+06	0.
0.	-4.25923E+06	-1.43695E+07	-2.79118E+07	2.54160E+07	1.44907E+07	4.53711E+06	1.49149E+06	0.
0.	-4.06011E+06	-1.12091E+07	-1.60453E+07	1.38494E+07	1.26107E+07	4.33857E+06	1.57251E+06	0.
0.	-3.72431E+06	-8.62194E+06	-9.71951E+06	8.03449E+06	9.43951E+06	3.96689E+06	1.58796E+06	0.
0.	-3.32575E+06	-6.59818E+06	-6.15736E+06	4.95057E+06	7.02807E+06	3.51627E+06	1.55155E+06	0.
0.	-2.91476E+06	-5.05580E+06	-4.06042E+06	3.20386E+06	5.24147E+06	3.05140E+06	1.47786E+06	0.
0.	-2.52188E+06	-3.88146E+06	-2.77145E+06	2.15876E+06	3.95071E+06	2.61070E+06	1.38011E+06	0.

ELECTRON DENSITY (COUL/M3)

7.59543E-14	3.17091E-05	2.13218E+02	3.42208E+05	9.65719E+05	1.91330E+03	1.16367E-04	1.81556E-14	1.74847E-24
2.98835E-14	1.31071E-05	7.57374E+01	1.14444E+05	8.65538E+05	1.62473E+03	1.84302E-04	1.67469E-14	1.66422E-24
1.27512E-15	6.33965E-07	2.15641E+00	3.52381E+04	5.09189E+05	8.31111E+02	6.36620E-05	1.98633E-14	1.18944E-24
1.91598E-17	1.08454E-08	5.71317E-02	4.19133E+03	1.68968E+05	2.82134E+02	2.79803E-05	5.24430E-15	5.56494E-25
1.44787E-19	1.35056E-11	1.03294E-03	3.09259E+02	2.78826E+04	6.59124E+01	8.92840E-06	1.98141E-15	2.12564E-25
6.69841E-22	5.02595E-13	1.81051E-05	1.36090E+01	2.59318E+03	1.06542E+01	2.08117E-06	5.28196E-16	6.21481E-26
2.18630E-24	2.02039E-15	2.52239E-07	3.74438E-01	1.58463E+02	1.20192E+00	3.56682E-07	1.07972E-16	1.31743E-26
5.69561E-27	7.22811E-18	2.60314E-09	6.18818E-03	5.75821E+00	9.52617E-02	4.52376E-08	1.71043E-17	2.43155E-27
1.32121E-29	2.34441E-20	2.80941E-11	9.19142E-05	1.51315E-01	5.35576E-03	4.27542E-09	2.08138E-18	3.29328E-28
2.92536E-32	8.63084E-23	1.19344E-13	8.94224E-07	2.83392E-03	2.16789E-04	3.84573E-10	1.96942E-19	3.51685E-29
2.13872E-33	5.08351E-24	8.13825E-15	8.61820E-08	1.82279E-04	4.41080E-05	8.31814E-11	6.22465E-20	1.59871E-29

POSITIVE ION DENSITY (COUL/M3)

-2.77983E-13 -5.47089E-06 6.43264E+04 1.00111E+06 7.38913E+05 4.41681E+02 1.76952E-05 2.23417E-15 -1.11544E-25
-9.43639E-14 -1.29576E-06 1.36515E+04 4.66797E+05 6.40774E+05 3.91204E+02 1.58727E-05 2.86281E-15 -1.09641E-25
-2.97201E-15 -3.73177E-07 1.40611E+02 1.68614E+05 3.38583E+05 2.06797E+02 9.71178E-06 1.13926E-15 -7.31573E-26
-3.42079E-17 -6.38301E-10 1.25279E-01 1.98313E+04 1.01324E+05 6.88573E+01 4.28400E-06 6.47528E-16 -3.46095E-26
-2.06141E-19 -5.82141E-12 2.66382E-04 1.08333E+03 1.64837E+04 1.62423E+01 1.37544E-06 2.35272E-16 -1.31732E-26
-7.96838E-22 -3.28655E-14 2.13981E-06 2.88148E+01 1.55814E+03 2.66883E+00 3.22983E-07 6.45493E-17 -4.07917E-27
-2.22928E-24 -1.41519E-16 1.28918E-08 1.26405E-01 9.01377E+01 3.07906E-01 5.58504E-08 1.34312E-17 -9.15886E-28
-5.23273E-27 -5.57119E-19 2.97021E-11 4.30541E-03 3.48380E+00 2.48427E-02 7.15776E-09 2.13681E-18 -1.51967E-28
-1.13227E-29 -2.13230E-21 -2.83560E-13 3.46482E-05 8.44548E-02 1.42448E-03 6.84397E-10 2.61130E-19 -2.14654E-29
-2.37001E-32 -7.48252E-24 -3.69846E-15 2.26593E-07 1.44168E-03 5.86654E-05 4.93830E-11 2.48235E-20 -2.28183E-30
-1.76230E-33 -4.39600E-25 -3.32149E-16 1.78785E-08 1.81285E-04 1.19681E-05 1.35598E-11 7.45165E-21 -1.45503E-30

NET CHARGE DENSITY (COUL/M3)

-3.53938E-13 -3.71808E-05 6.41133E+04 6.58103E+05 -2.27806E+05 -1.45161E+03 -9.84713E-05 -1.59215E-14 -1.88501E-24
-1.24247E-13 -1.44031E-05 1.35757E+04 4.66333E+05 -2.24742E+05 -1.23352E+03 -8.84292E-05 -1.46843E-14 -1.77388E-24
-4.24713E-15 -6.71283E-07 1.37655E+02 1.33384E+05 -1.70687E+05 -6.39314E+02 -5.39502E-05 -9.52484E-15 -1.18270E-24
-5.33677E-17 -1.14837E-08 8.81471E-02 1.56400E+04 -6.67436E+04 -2.13977E+02 -2.34943E-05 -4.59677E-15 -5.91014E-25
-3.50928E-19 -9.73244E-11 -7.66582E-04 7.74075E+02 -1.13187E+04 -4.96701E+01 -7.55256E-06 -1.66613E-15 -2.26540E-25
-1.44068E-21 -5.35460E-13 -1.59453E-05 1.52058E+01 -1.63564E+03 -7.98542E+00 -1.75818E-06 -4.35656E-16 -4.42280E-26
-4.41558E-24 -2.16191E-15 -2.31407E-07 4.99673E-02 -5.95249E+01 -8.94913E-01 -3.80832E-07 -1.15324E-17 -1.48912E-26
-1.09283E-26 -7.78605E-18 -2.37344E-09 -2.48257E-03 -1.35520E+00 -7.04196E-02 -3.80818E-08 -1.49674E-17 -2.59052E-27
-2.45348E-29 -2.75784E-20 -2.03797E-11 -5.72461E-05 -4.68518E-02 -3.13128E-03 -3.59102E-09 -1.82025E-18 -3.56713E-28
-5.21545E-32 -1.37905E-23 -1.21034E-13 -6.67431E-07 -1.39224E-03 -1.58123E-04 -2.55210E-10 -1.72138E-19 -3.74583E-29
-3.90103E-33 -5.52311E-24 -9.27048E-15 -6.83435E-08 -2.80195E-04 -3.21378E-05 -6.76216E-11 -5.43948E-20 -1.71421E-29

TEMPERATURE (K)

3.00000E+02 3.00000E+02 3.00002E+02 3.02725E+02 3.63391E+02 3.00002E+02 3.00000E+02 3.00000E+02 3.00000E+02
3.00000E+02 3.00000E+02 3.00001E+02 3.01843E+02 1.92153E+02 3.00002E+02 3.00000E+02 3.00000E+02 3.00000E+02
3.00000E+02 3.00000E+02 3.00000E+02 3.00448E+02 3.01569E+02 3.00001E+02 3.00000E+02 3.00000E+02 3.00000E+02
3.00000E+02 3.00000E+02 3.00001E+02 3.00454E+02 3.00473E+02 3.00000E+02 3.00000E+02 3.00000E+02 3.00000E+02
3.00000E+02 3.00000E+02 3.00000E+02 3.00003E+02 3.00077E+02 3.00001E+02 3.00000E+02 3.00000E+02 3.00000E+02
3.00000E+02 3.00000E+02 3.00000E+02 3.00000E+02 3.00007E+02 3.00000E+02 3.00000E+02 3.00000E+02 3.00000E+02
3.00000E+02 3.00000E+02 3.00000E+02 3.00000E+02 3.00000E+02 3.00000E+02 3.00000E+02 3.00000E+02 3.00000E+02
3.00000E+02 3.00000E+02 3.00000E+02 3.00000E+02 3.00000E+02 3.00000E+02 3.00000E+02 3.00000E+02 3.00000E+02
3.00000E+02 3.00001E+02 3.00000E+02 3.00000E+02 3.00000E+02 3.00000E+02 3.00000E+02 3.00000E+02 3.00000E+02
3.00000E+02 3.00000E+02 3.00000E+02 3.00000E+02 3.00000E+02 3.00000E+02 3.00000E+02 3.00000E+02 3.00000E+02
3.00000E+02 3.00000E+02 3.00000E+02 3.00000E+02 3.00000E+02 3.00000E+02 3.00000E+02 3.00000E+02 3.00000E+02

TOTAL NET CHARGE = 1.12205654E-18 (COUL)

TOTAL ELECTRON CHARGE = 2.86649018E-14 (COUL)

DIPOLE LENGTH = 1.46510677E-08 (M)

CENTER OF ELECTRON CLOUD = 1.37335770E-07 (M)

CENTER OF DIPOLE = 2.30010236E-07 (M)

VARIABLES CORRESPONDING TO ABOVE TIME STEP DUMPED TO TAPE 3 AT RECORD 4

NI = 0 NIR = 1 IDIV = 1 JDIV =

Appendix 7

ANALYTIC APPROACH TO THE CALCULATION OF IONIZATION COEFFICIENTS

The interest of calculating ionization coefficients α_i in semiconductors dates back to about three decades ago. McKay (1954) derived from experimental data a curve of α_i versus applied electric field. Wolff (1954) has developed a method to compute α_i by expanding the electron distribution function in terms of Legendre polynomials and keeping the first two terms in solving the Boltzmann transport equation in steady-state. This approximation is justified at high electric fields. Shockley (1961) has conjectured that the steady-state electron distribution function must have a spike in the direction of the electric field and, by neglecting all other electrons not in this spike, he was able to obtain an α whose logarithm is inversely proportional to the electric field. This approach is reasonable for low electric fields. Baraff (1962) solved numerically the Boltzmann equation and obtained an important plot of $\alpha\lambda$ versus $E_i/e\mathcal{E}\lambda$ for various $\hbar\omega/E_i$ values. Here, λ is the optical mean free path, E_i, the energy gap between the valance band and the conduction band, $\hbar\omega$ the energy of the optical phonon, and $\mathcal{E}$ the external electric field. Further publication by Baraff (1964) concentrated on the high field case in which spherical harmonics expansion was made and a truncation procedure was used to obtain a closed system of equations. Temperature consideration was also given later on (Okuto and Crowell, 1972; Crowell and Sze, 1966). Finally, macroscopic ionization rates from theory were studied and found to be generally different due to the possible field dependence of the carrier's drift velocities in the avalanche regime (Beni and Capasso, 1979).

In this appendix, we will approach the problem of computing ionization coefficients from a point of view different from that of solving Boltzmann equation numerically (Baraff, 1962, 1964). Specifically, we treat the collision processes as Markov processes. If λ is the mean free path of a collision, then the probability of no collision for an electron traveling a distance x is $\exp(-x/\lambda)$; the probability of one collision in dx is dx/λ. The mean distance of a collision is therefore:

$$\bar{x} = \int_0^\infty x e^{-x/\lambda} \frac{dx}{\lambda} = \lambda \qquad \text{(A7.1)}$$

In the following, we will concentrate on the application of the concept of Markov processes to the calculation of the ionization coefficient in the case that scattering effect is neglected.

An electron is released at E=0, gaining energy from the constant electric field $\mathcal{E}$, losing energy $\hbar\omega$ by emitting an optical phonon with a constant mean free path λ. What is the mean distance in which the electron will reach the ionization energy E_i? This is the question we would like to address analytically.

Shockley's (1961) conjecture about the aforementioned spike is based on the Markov concept in a very trivial way, as follows. The number of electrons, per unit volume, which have survived the transport to energy E_i without collisions is proportional to $\exp(-E_i/e\mathcal{E}\lambda)$ where $E_i/e\mathcal{E}$ is the distance traveled by the electron to reach energy E_i. Those are the electrons which can ionize electrons in the valance band. The number of ionizations in a unit length is therefore proportional to $\exp(-E_i/e\mathcal{E}\lambda)$:

$$\alpha = c \exp(-E_i/e\mathcal{E}\lambda) \qquad \text{(A7.2)}$$

Results from our analysis, on the other hand, possess more complicated dependence on $(E_i/e\mathcal{E}\lambda)$.

We choose $E_i = (n+1)\hbar\omega$ for simplification of the analysis. Let λZ_ℓ be the mean distance in which an electron released with $E = \ell\hbar\omega$ at origin will reach E_i. Define $R \equiv \hbar\omega/E_i$, $X = E_i/e\mathcal{E}\lambda$, $Y = \alpha\lambda$, $\alpha = \exp(-RX)$, $\beta = RX$, and $\Delta Z \equiv \hbar\omega/e\mathcal{E}\lambda = \beta$. Apparently, $Z_1 = Z_o - \Delta Z$. We define K(i) by:

$$Z_i = Z_o - K(i)\Delta Z \qquad \text{(A7.3)}$$

Obviously, K(1) = 1. The recursive formula for K(i+1) can be obtained by considering the probabilities of possible final states the electron with energy $i\hbar\omega$ at origin can end up with. As shown in Figure (A7-1), it has probability α to go up to $(i+1)\hbar\omega$ and then reaches E_i at $(Z_{i+1} + \Delta Z)$. It has $\alpha P(i,j)$ probability to go to energy $j\hbar\omega(j\neq 1)$, and then reaches E_i at $(Z_j + \Delta Z)$ where $P(i,j) = \beta^{i-j+1}/(i-j+1)!$ Finally, the remaining probability is to drop down to below $\hbar\omega$ and reaches E_i at $(Z_1 + \Delta Z)$.

$$Z_i = \alpha(Z_{i+1} + \Delta Z) + \alpha \sum_{j=2}^{i} P(i,j)\,(Z_j + \Delta Z)$$

$$+ \left(1 - \alpha - \alpha \sum_{j=2}^{i} P(i,j)\right)(Z_1 + \Delta Z) \quad . \qquad \text{(A7.4)}$$

By substituting $Z_k = Z_o - K(k)\Delta Z$ into the above equation, one gets:

$$\alpha K(i+1) = 1 + K(i) - \alpha \sum_{j=2}^{i} P(i,j)K(j)$$

$$- (1 - \alpha - \alpha \sum_{j=2}^{i} P(i,j)K(1) \qquad \text{(A7.5)}$$

This equation and $K(1) = 1$ thus determine all $K(k)$'s. It is noted that eq. (A7.5) depends only on the two dimensionless quantities $R \equiv \hbar\omega/E_i$ and $X \equiv E_i/e\mathcal{E}\lambda$.

At energies greater than $E_i = (n+1)\hbar\omega$, the electron is assumed to be capable of ionizing electrons from the valance band with a mean free path λ_i. We also assume infinite mean free path for optical phonon emission when the electron energy is greater than E_i. Under these circumstances, $Z_{n+1} = \lambda_i/\lambda$. Eqs. (A7.3) and (A7.5) then determine Z_o as a function of R and X.

The ionization coefficient per unit length is given by

$$\alpha = \frac{1}{Z_o \lambda}$$

$$\alpha\lambda = 1/Z_o = f(R,X)$$

i.e.,

$$Y = f(R,X) \qquad \text{(A7.6)}$$

We have carried out the calculation for a number of R's. Fig. (A7-2) shows the results with $\lambda_i = \lambda$. The curve for R=0 (n=∞ in this case) is obtained differently as follows. In the limit of zero energy for the optical phonon, the electron does not lose energy. $Z_o\lambda = E_i/e\mathcal{E} + \lambda_i$, i.e.,

$$Y = \frac{1}{1+X} \quad \text{for } \lambda_i = \lambda.$$

The curves in Fig. (A7-2) do not have the simple behavior (a straight line in semi-log plot) of eq. (A7.2), except for R ∿ 0.5. This is anticipated because there are terms of the type e^{mRX} in eq. (A7.5) for m = 1,...,n+1. It is only when m=n+1 does $e^{mRX} = e^{X}$, as eq. (A7.2).

Compared with Baraff's (1962) work in which the isotropic scattering effect is included, our results agree with his only for the small X where the electric field is so high that the direction of the electron after an isotropic scattering almost immediately goes back to that of the applied field. For large X (small electric field), the scattering effect should be very important and our results do deviate greatly from Baraff's (1962) work.

For the case of Teflon, we have put $\lambda = 26$ Å, independent of the electron energy [eq. (A.2.8) does depend on energy, however], for the optical phonon mean free path. $E_i = 6.5$ eV, $\hbar\omega = 0.11$ eV. The calculated ionization length by this model is plotted in Fig. (A7.3) as a function of the applied electric field. The region for which the electric field is above 10^9 V/m is characterized as high field region and the present model is more reliable. Comparison with Fig. 2.6 which is obtained by the Monte Carlo approach with energy-dependent λ and with scattering, shows reasonable agreement between the two approaches; the ionization lengths being within a factor of two of each other for $E \gtrsim 10^9$ V/m.

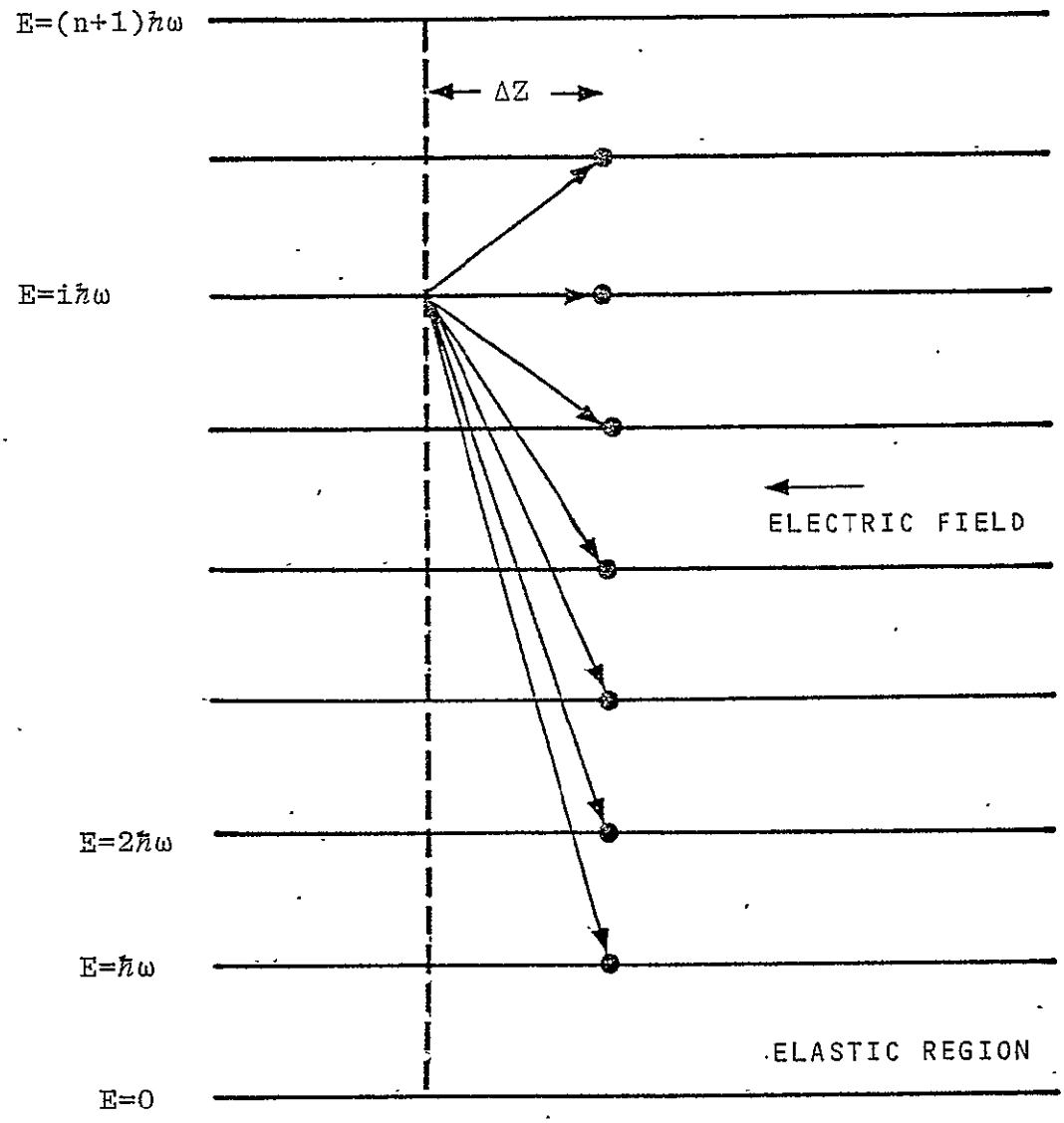

FIGURE A7.1. ALL POSSIBLE STATES OF AN ELECTRON RELEASED WITH E=iħω AT ORIGIN

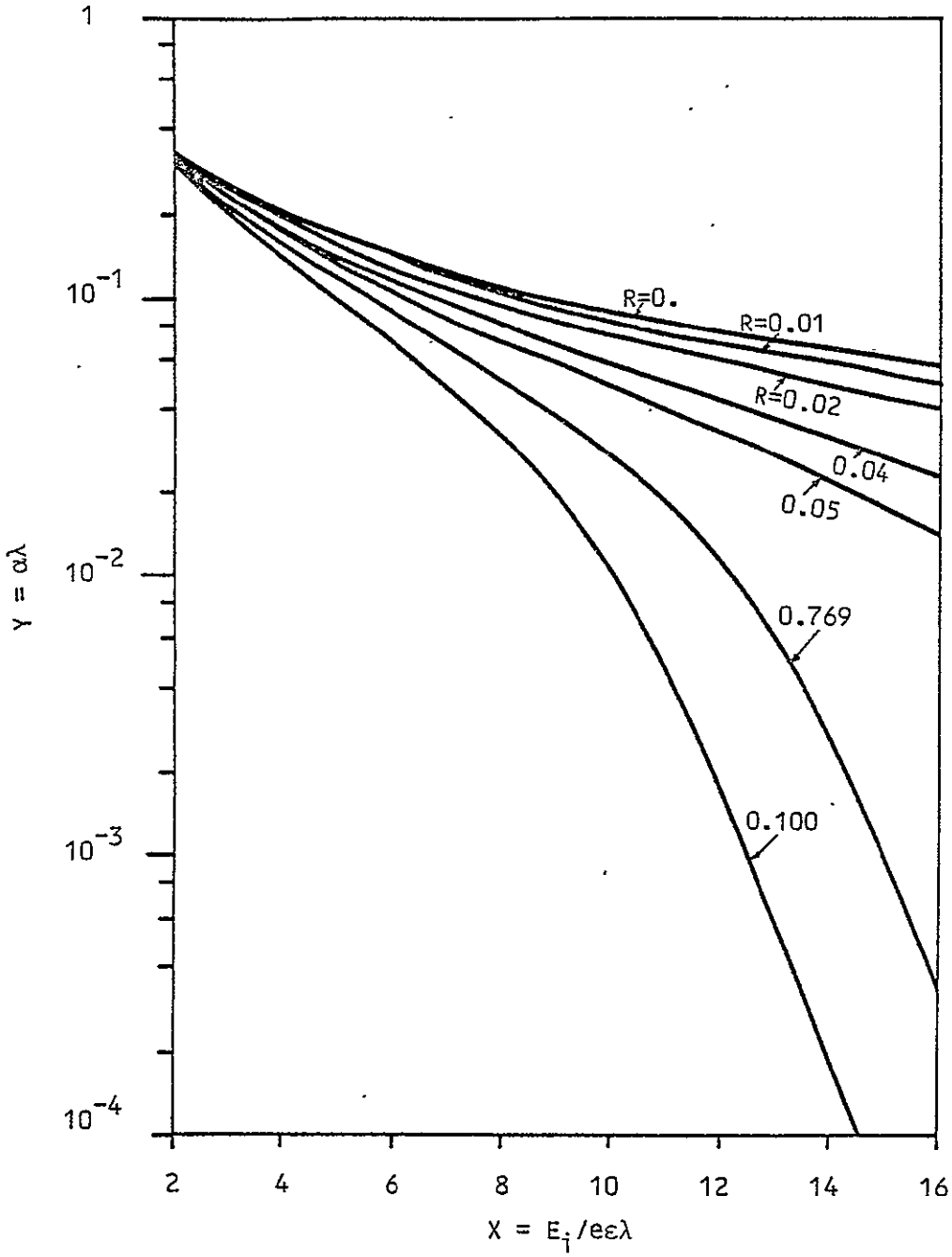

FIGURE A7.2. IONIZATION COEFFICIENT AS A FUNCTION OF ELECTRIC FIELD FOR VARIOUS R

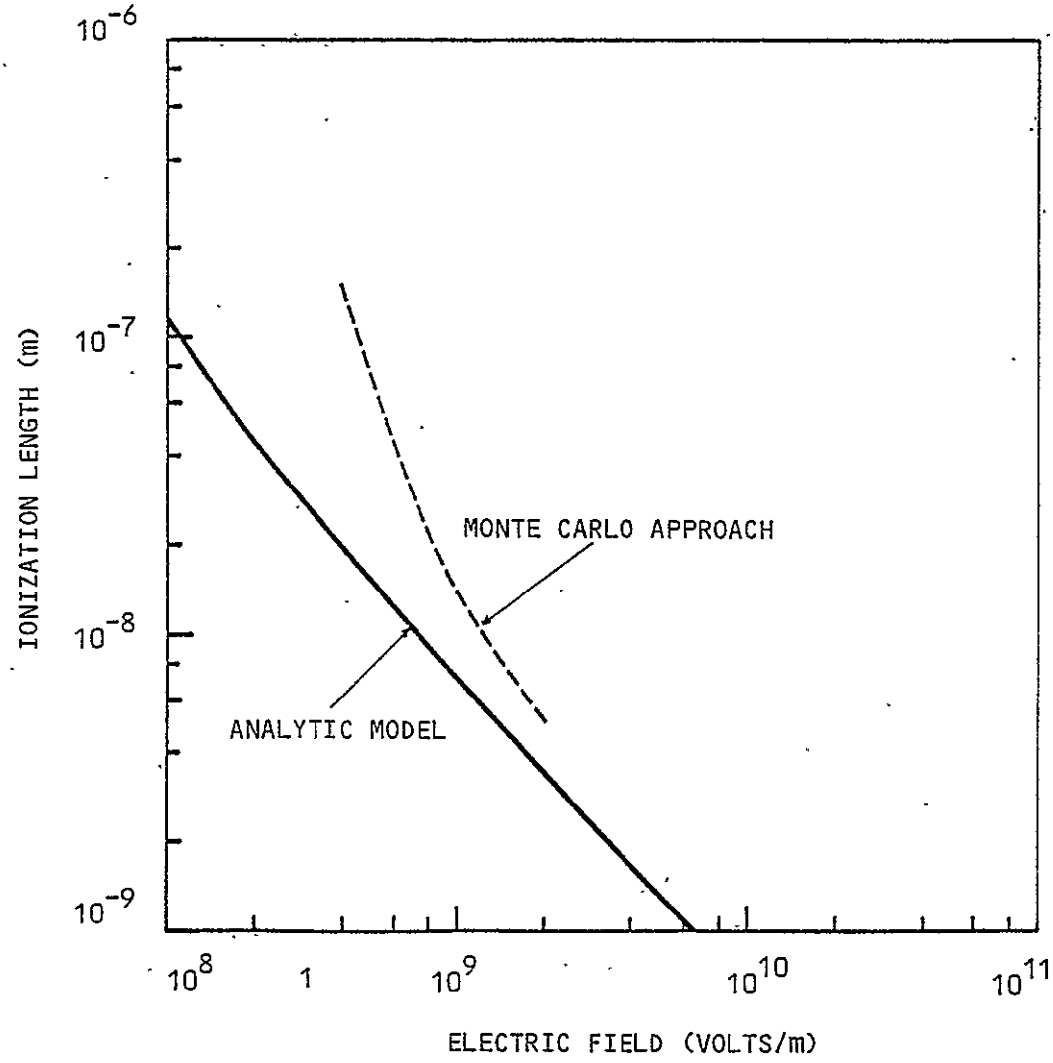

FIGURE A7.3. IONIZATION LENGTH AS A FUNCTION OF EXTERNAL ELECTRIC FIELD FOR CF_2 (SCATTERING IS NEGLECTED)

Appendix 8

ELECTRIC FIELD PENETRATION INTO AN ISOTROPIC PLASMA

In one dimension the equations that describe the steady state penetration of an electric field into an isotropic plasma with fixed ions are:

$$0 = \mu n(x)E(x) - D\frac{\partial n(x)}{\partial x} \qquad (A.8.1)$$

$$\frac{\partial E(x)}{\partial x} = \frac{e}{\varepsilon_o}(n(\infty) - n(x)) \qquad (A.8.2)$$

where $n(x)$ is the electron number density, $E(x)$ is the electric field, μ is the charge mobility for electrons, D is the diffusion coefficient for electrons, e is the charge on an electron ($e<0$), and ε_o is the permittivity of free space.

Equation (A.8.1) is a statement of the balance of particle current due to diffusion and due to E field drifting. Equation (A.8.2) is Poisson's equation. Here, we will assume that μ and D are constant, although in general this is not a restriction to the numerical solutions of Eqs. (A.8.1) and (A.8.2).

We are interested in the problem of a plasma with a density n_∞ and electron temperature kT, existing from $x=0$ to $x=\infty$, where at $x=0$ the electric field has a known value. Equations (A.8.1) and (A.8.2) are easily nondimensionalized by the following substitutions:

$$\left.\begin{aligned} n(x) &= n_\infty \hat{n}(x) \\ E(x) &= E_o \hat{E}(x) \\ x &= x_o \hat{x} \end{aligned}\right\} \quad (A.8.3)$$

where:

$$n_\infty = n(\infty)$$

$$E_o = E(0)$$

$$x_o = \sqrt{\frac{E_o D}{n_\infty |e| \mu}} = \sqrt{\frac{E_o kT}{n_\infty e^2}}$$

In the definition of x_o we have used the Einstein relation that states:

$$\frac{\mu}{D} = \frac{e}{kT}$$

x_o is the standard definition for a Debye length.

In nondimensional "hat" variables Eqs. (A.8.1) and (A.8.2) become:

$$\frac{\partial \hat{n}}{\partial \hat{x}} = \zeta \hat{n} \hat{E} \quad (A.8.4)$$

$$\frac{\partial \hat{E}}{\partial \hat{x}} = -\frac{1}{\zeta}(1-\hat{n}) \quad (A.8.5)$$

where:

$$\zeta = \left(\frac{\varepsilon_o E_o^2}{n_\infty kT} \right)^{1/2}$$

The parameter ζ is the square root of the ratio of the electric field energy density at x=0 to the electron thermal energy density at x=∞. In what follows we drop the "hat" notation and assume all variables to be non-dimensional.

Refering to Eq. (A.8.3) the boundary conditions for the problem we wish to solve are:

$$n(\infty) = 1$$

$$E(0) = \pm 1 \qquad \text{(A.8.6)}$$

Before we solve Eqs. (A.8.4) and (A.8.5) with boundary conditions Eq. (A.8.6) it is profitable to look at the first integral. If we multiply Eq. (A.8.5) by E and replace nE and $\dot{E}$ by derivatives of n using Eq. (A.8.4) it is simple to show:

$$\frac{d}{dx} \left[\frac{\zeta^2}{2} E^2 + \ell n(n) - n \right] = 0$$

Integrating this expression we immediately get:

$$\frac{\zeta^2}{2} E^2 + \ell n(n) - n = \text{const.}$$

Applying the boundary conditions at x=∞ (we tacitly assume for the moment E(∞)=0, that is the plasma shields the E field) we get:

$$\frac{\zeta^2}{2} E^2 + \ell n(n) + 1 - n = 0$$

which is valid for all x. In particular for x=0 we have:

$$\frac{\zeta^2}{2} + \ell n(n_o) + 1 - n_o \doteq 0 \qquad \text{(A.8.7)}$$

where:

$$n_o = n(0)$$

Figure (A.8.1) is a plot of left hand side of Eq. (A.8.7) versus n_o. It is obvious from the plot that for $\zeta^2>0$ there are always two solutions which make the left hand side of Eq. (A.8.7) zero. One solution is always less than 1 corresponding to the case where the E field is repeling electrons from the surface. The other solution is always greater than 1 corresponding to the situation where the E field attracts electrons to the surface.

If $\zeta>>1$, from Eq. (A.8.7) we can estimate the two solutions for n_o to be:

$$n_o \cong \begin{cases} e^{-\left(1 + \frac{\zeta^2}{2}\right)} \\ 1 + \frac{\zeta^2}{2} \end{cases}$$

For $\zeta<<1$ the corresponding solutions would be:

$$n_o \cong \begin{cases} 1 - \zeta \\ \\ 1 + \zeta \end{cases}$$

Figures (A.8.2a) and (A.8.2b) are plots of n_o versus ζ for both branches. The dotted lines correspond to the estimates for large and small ζ.

Knowing n_o makes Eqs. (A.8.4) and (A.8.5) straight forward to integrate, since by the first integral we know two boundary conditions at x=0. If we divide Eq. (A.8.4) by n and differentiate we obtain:

$$\frac{\partial^2}{\partial x^2} \ell n(n) = \zeta \frac{\partial E}{\partial x} \qquad (A.8.8)$$

Substituting Eq. (A.8.5) into Eq. (A.8.8) and letting $\alpha(x) = \ell n(n)$ Eq. (A.8.8) becomes:

$$\frac{\partial^2 \alpha}{\partial x^2} = (e^{\alpha} - 1) \qquad (A.8.9)$$

with boundary conditions

$$\alpha(0) = \ell n(n_o)$$

$$\left.\frac{d\alpha}{dx}\right|_{x=0} = \pm\zeta \qquad (A.8.10)$$

Eq. (A.8.9) with boundary condition Eq. (A.8.10) is in standard form for numerical integration. Once the solution to $\alpha(x)$ is obtained the profiles n and E are simply computed by:

$$n(x) = e^{\alpha(x)}$$

$$E(x) = \frac{1}{\zeta}\frac{d\alpha(x)}{dx}$$

Figure (A.8.4) shows a numerical solution to Eq. (A.8.9) for $\zeta=2$, for both attracting and repelling E fields. The profile E(x) really does fall away to zero at $x=\infty$, verifying our assumption about the first integral.

As a measure of the penetration of the E field we define an E field penetration depth as the first moment of the E field profile:

$$\lambda_E = \frac{\int_0^\infty xE(x)dx}{\int_0^\infty E(x)dx}$$

Likewise we define the distance over which the density varies appreciably as:

$$\lambda_N = \frac{\int_0^\infty x|n(x) - 1|dx}{\int_0^\infty |n(x) - 1|dx}$$

Figures (A.8.4) and (A.8.5) are a plot of λ_E and λ_N versus ζ for the cases where the E field attracts and repels the electrons from the surface, respectively. λ_E and λ_N were computed from the numerical solution of Eq. (A.8.10). The x integration was terminated when both λ_E and λ_N were changing by less than a hundredth of a percent.

In Figure (A.8.4), the case where the E field attracts electrons to the surface, the penetration depth decreases with increasing E (recall $\zeta \sim E$ for constant

thermal energy). This reflects the fact that as E increases more and more electrons migrate to the surface, more effectively shielding the E field. For small E (no matter how small) the penetration depth is fixed at one Debye length. The density damps more quickly than the E field.

In Figure (A.8.5), the case where electrons are repelled from the surface, the penetration depth increases with increasing E. This happens because as E increases the density can only decrease to zero effectively letting the E field penetrate undamped in this very low density region. For this case the E field is damped more effectively than the density.

Finally, we present an actual physical case of interest in this paper. For the following parameters:

$$E_o = 2 \times 10^8 \text{ volts/m}$$

$$kT = 1 \text{ ev.}$$

$$n_o = 1 \times 10^{18}/\text{cm}^3$$

Figure (A.8.6) is a plot of the E field and density vs. distance for both the attracting and repelling cases. The penetration lengths are computed as:

$$\left.\begin{aligned} \lambda_n &= 52.9 \text{ Å} \\ \lambda_E &= 59.1 \text{ Å} \end{aligned}\right\} \text{ attracting}$$

$$\left.\begin{aligned} \lambda_N &= 97.7\ \text{Å} \\ \lambda_E &= 82.9\ \text{Å} \end{aligned}\right\} \text{ repelling}$$

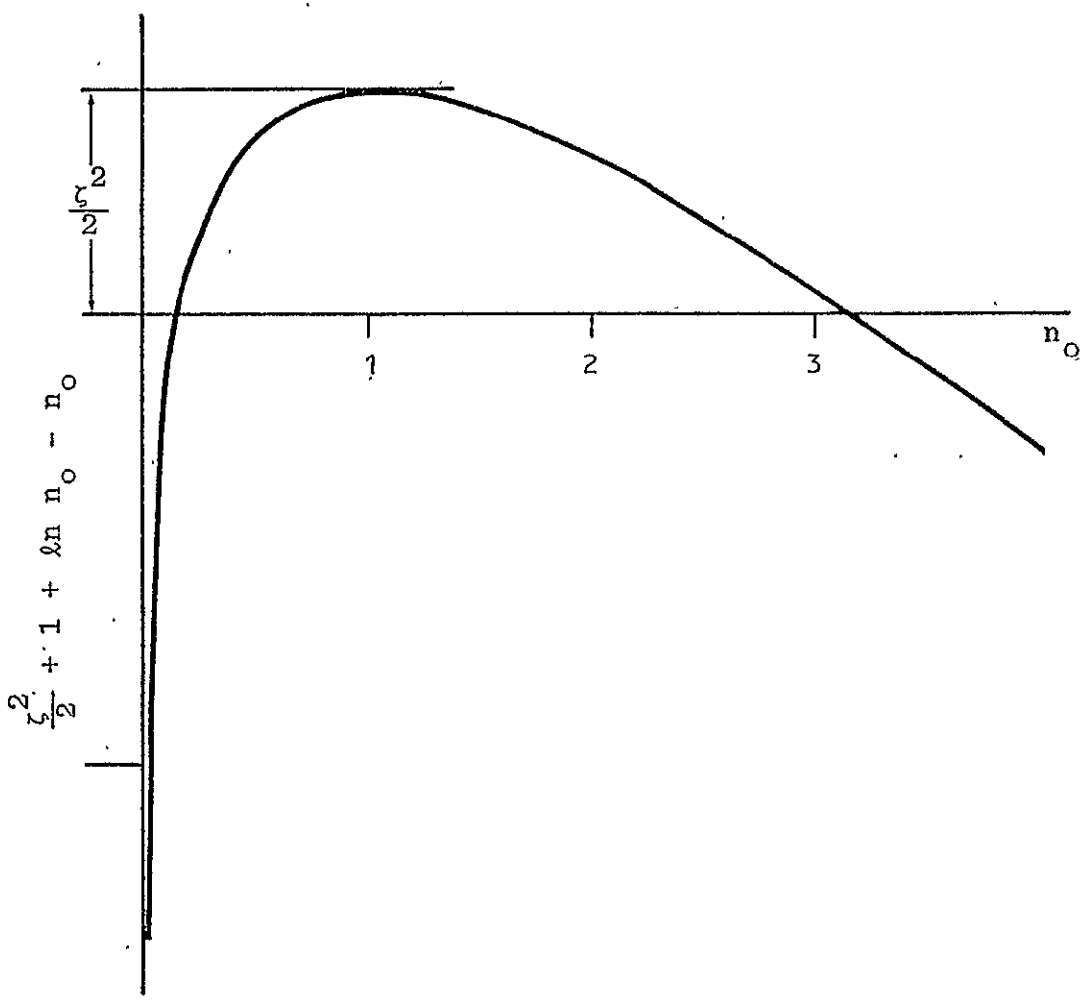

FIGURE A.8.1. FIRST INTEGRAL OF EQS. (A.8.4) AND (A.8.5) vs. n_o. THE VALUES OF n_o FOR WHICH THE FIRST INTEGRAL IS ZERO GIVE THE BOUNDARY CONDITION AT x=o NEEDED TO SOLVE EQS. (A.8.4) AND (A.8.5) NUMERICALLY.

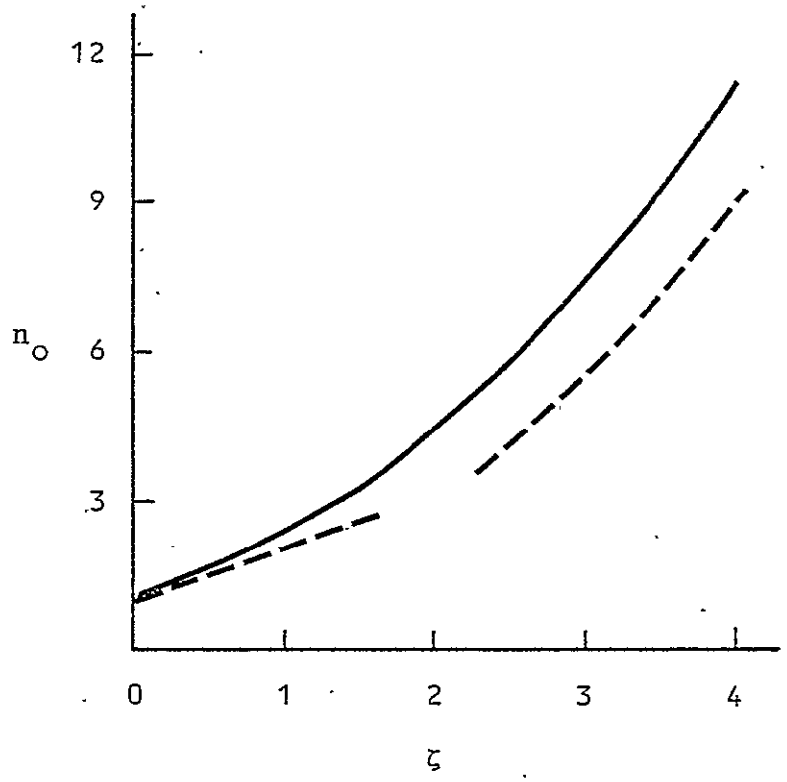

FIGURE A.8.2A. n_o vs. ζ FOR THE CASE WHERE THE E FIELD IS ATTRACTING ELECTRONS TO THE SURFACE. DOTTED LINES ARE ANALYTIC APPROXIMATIONS.

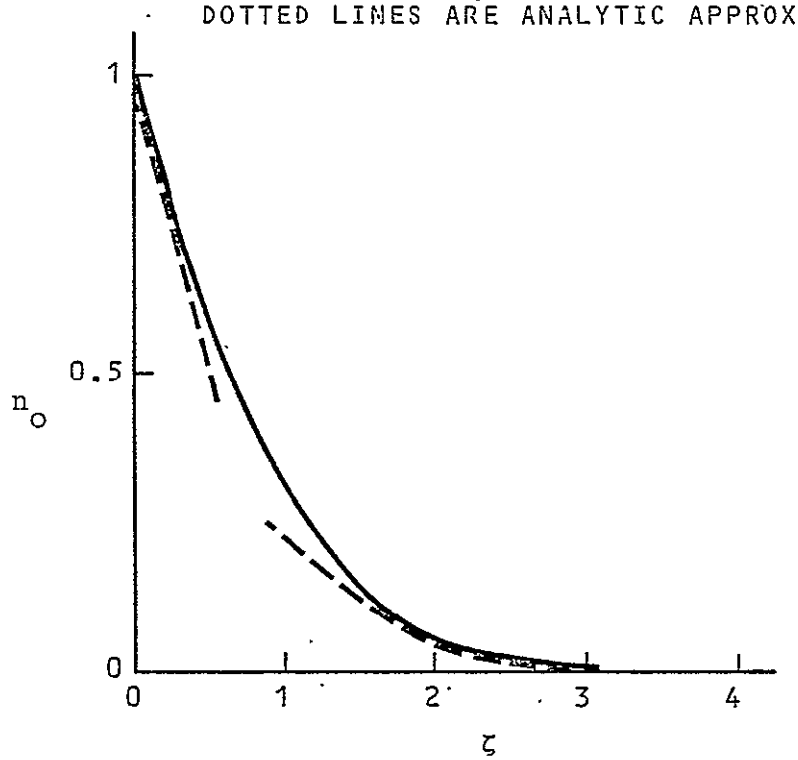

FIGURE A.8.2B. n_o vs. ζ FOR THE CASE WHERE THE E FIELD REPELS ELECTRONS FROM THE SURFACE. DOTTED LINES ARE ANALYTIC APPROXIMATIONS.

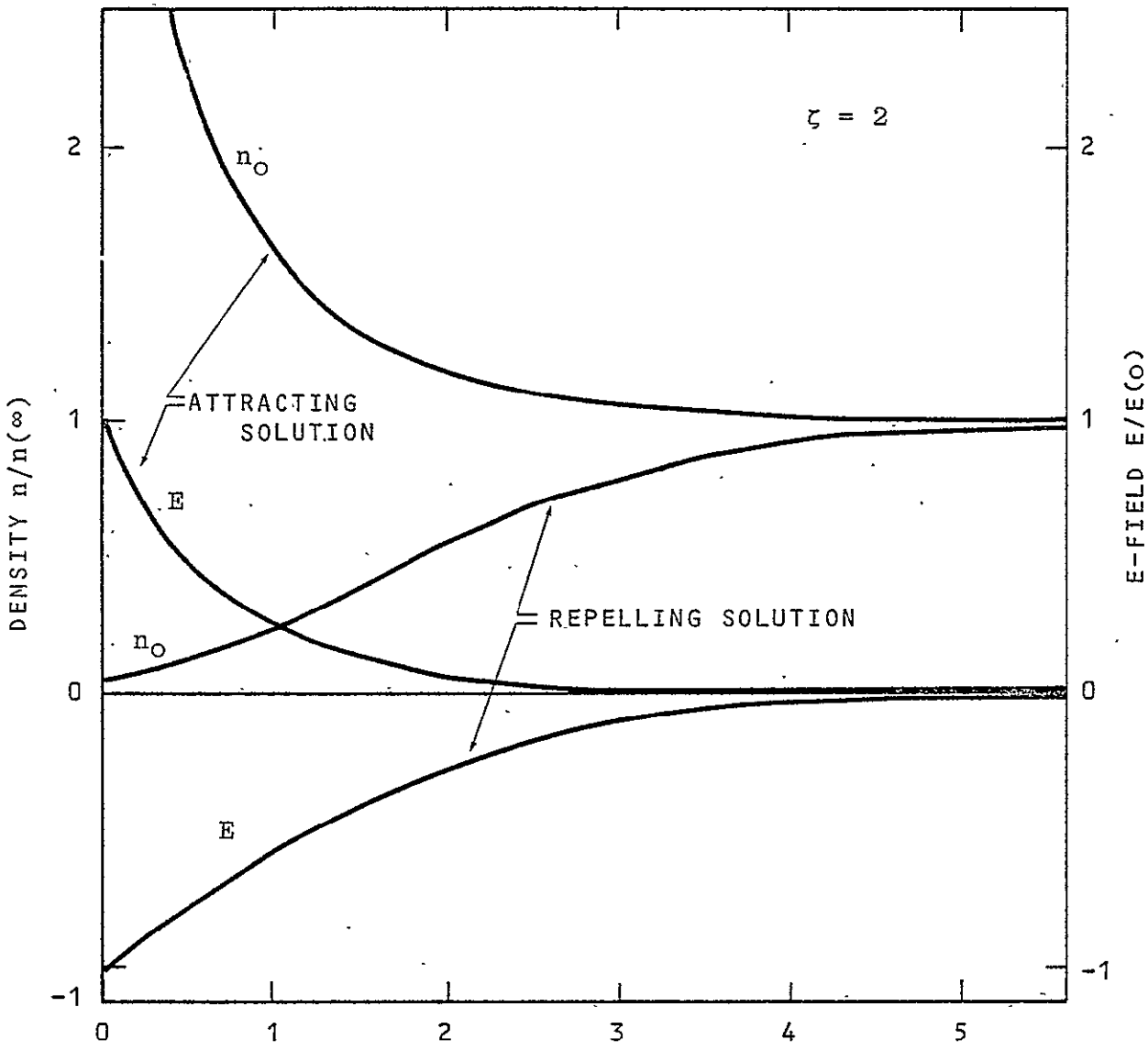

FIGURE A.8.3. TYPICAL SOLUTIONS TO EQUATIONS (A.8.4) AND (A.8.5)

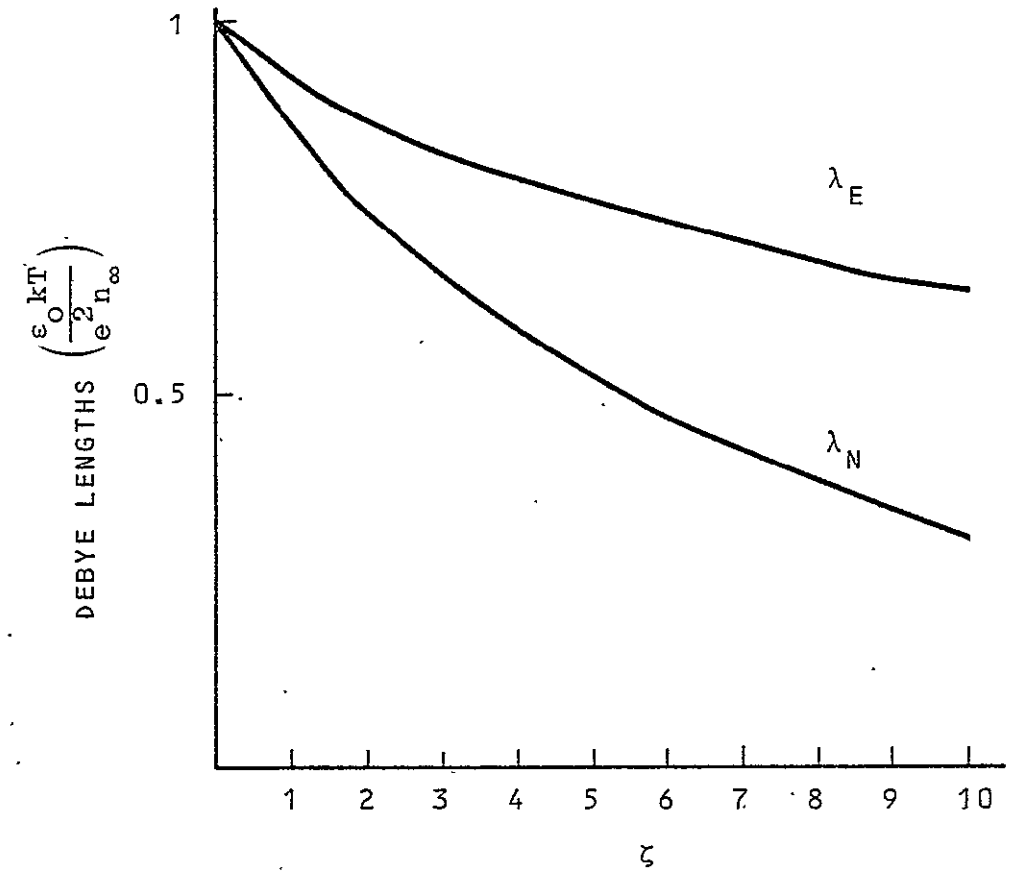

FIGURE A.8.4. E FIELD PENETRATION LENGTH (λ_E) AND DENSITY SCALE LENGTH (λ_N) FOR ATTRACTING SOLUTION

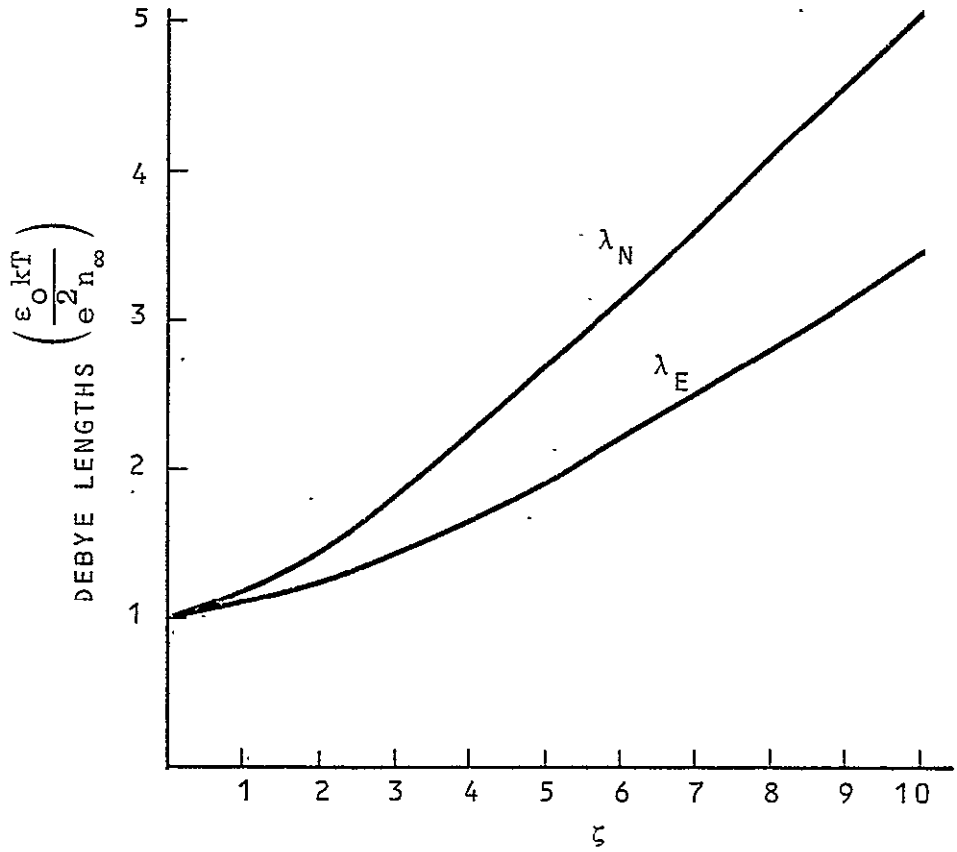

FIGURE A.8.5. E FIELD PENETRATION LENGTH (λ_E) AND DENSITY SCALE LENGTH (λ_N) FOR REPELLING SOLUTION

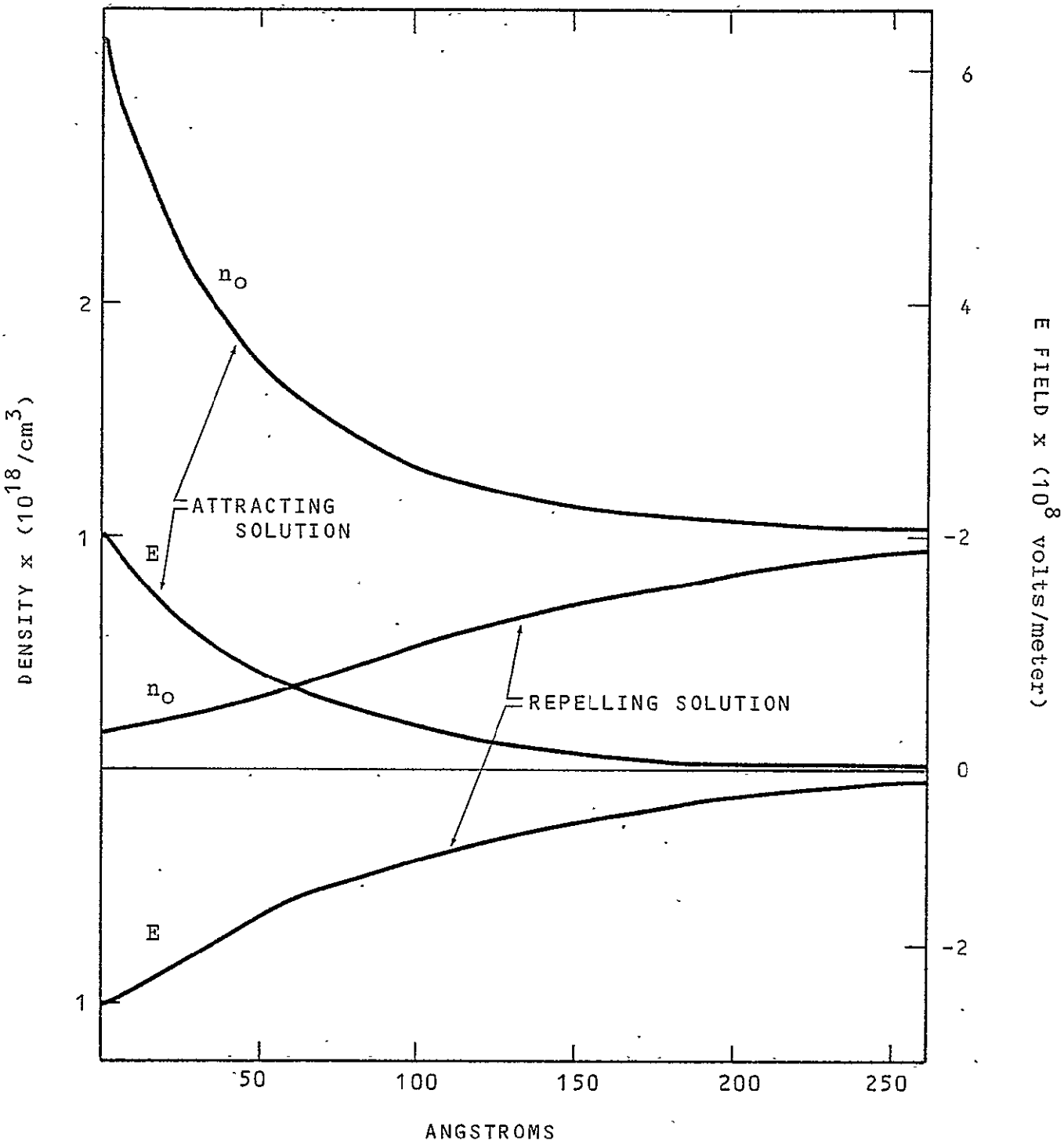

FIGURE A.8.6. THE ELECTRIC FIELD AND DENSITY vs. DISTANCE FOR A TYPICAL PHYSICAL CASE OF INTEREST IN THIS PAPER

Appendix 9

CHAPMAN-ENSKOG THEORY

The Boltzmann equation can be written in the following form:

$$\frac{\partial f}{\partial t} + \vec{v} \cdot \nabla_{\vec{x}} f - \frac{e\vec{E}}{m} \cdot \nabla_{\vec{v}} f = \int d\vec{v}_o \, K(\vec{v},\vec{v}_o) f \quad . \quad (A.9.1)$$

Let ε be the expansion parameter according to the standard Chapman-Enskog procedure (Ferziger and Kaper, 1972), and expand f

$$f = f_o + \varepsilon f_1 + \ldots . \quad (A.9.2)$$

In order to include the effects of the electric field, as well as the scattering process in the lowest order solution f_o, we formally order these two terms of $O(1/\varepsilon)$. The equation of order $1/\varepsilon$ is, therefore:

$$- \frac{e\vec{E}}{m} \cdot \nabla_{\vec{v}} f_o = \int d\vec{v}_o K(\vec{v},\vec{v}_o) f_o \quad (A.9.3)$$

The solution of this equation determines f_o. The equation of order one is the following equation:

$$\frac{\partial f_o}{\partial t} + \vec{v} \cdot \nabla_{\vec{x}} f_o = \frac{e\vec{E}}{m} \cdot \nabla_{\vec{v}} f_1 + \int d\vec{v}_o \, K(\vec{v},\vec{v}_o) f_1 \quad . \quad (A.9.4)$$

According to the Chapman-Enskog procedure, the time dependence of the distribution function is determined through the dependence of f on the density, drift velocity, and temperature, and this is determined by the solution to the lowest order equation. If we restrict our attention to the case of constant drift velocity and temperature, we can write:

$$\frac{\partial f_o}{\partial t} = \frac{\partial f_o}{\partial n}\frac{\partial n}{\partial t} \qquad \text{(A.9.5a)}$$

$$\frac{\partial f_o}{\partial \vec{x}} = \frac{\partial n}{\partial \vec{x}}\frac{\partial f_o}{\partial n} \qquad \text{(A.9.5b)}$$

$$f_o = ng_o \qquad \text{(A.9.5c)}$$

To lowest order in ε:

$$\frac{\partial n}{\partial t} + \vec{v}_D \cdot \nabla_{\vec{x}} n = 0 \qquad \text{(A.9.6)}$$

where

$$\vec{v}_D = \frac{1}{n}\int f\vec{v}d\vec{v} \qquad \text{(A.9.7)}$$

Therefore, eq. (A.9.4) can be written:

$$g_o[(\vec{v}-\vec{v}_D)\cdot\nabla_{\vec{x}} n] = \int d\vec{v}_o K(\vec{v},\vec{v}_o)f_1 + \frac{e\vec{E}}{m}\cdot\nabla_{\vec{v}} f_1 \qquad \text{(A.9.8)}$$

We can obtain a particular solution of this equation by taking the first velocity moment:

$$[\langle v_i v_j \rangle - \langle v_i \rangle \langle v_j \rangle] \frac{\partial n}{\partial x_i} = \int d\vec{v}_o d\vec{v}\ v_j K f_1 \qquad \text{(A.9.9)}$$

where

$$\langle v_i v_j \rangle = \int g_o v_i v_j d\vec{v} \qquad \text{(A.9.10)}$$

$$\langle v_i \rangle = \int g_o v_i d\vec{v} \qquad \text{(A.9.11)}$$

Define:

$$\int d\vec{v}_o d\vec{v}\ v_j K(\vec{v},\vec{v}_o) f_1(\vec{v}_o) \qquad \text{(A.9.12)}$$

$$\equiv \int d\vec{v}_o\ v_{jo}\ K_1\ (v_o^2)\ f_1\ (\vec{v}_o)$$

A solution of eq. (A.9.9) is the following:

$$f_1 = \frac{g_o}{K_1} [\vec{v} - \vec{v}_D] \cdot \nabla_{\vec{x}} n \qquad \text{(A.9.13)}$$

A knowledge of f_1 allows us to compute the average electron velocity to order 1:

$$\langle\vec{v}\rangle = \vec{v}_D + \frac{1}{n}\int d\vec{v} f_1(\vec{v})\vec{v}d\vec{v} \qquad \text{(A.9.14)}$$

and we can write:

$$\langle\vec{v}\rangle - \vec{v}_D = \bar{\bar{D}} \cdot \nabla n \qquad \text{(A.9.15)}$$

where $\bar{\bar{D}}$ is the diffusion coefficient and can be written:

$$\bar{\bar{D}} = \frac{1}{n}\int d\vec{v} \frac{g_o}{K_1} [\vec{v}(\vec{v}-\vec{v}_D)] \qquad \text{(A.9.16)}$$

Because of the symmetry of the scattering process, $\bar{\bar{D}}$ is diagonal, but with different values parallel and perpendicular to the E field.

REFERENCES

1. Anderson, P. W., "Absence of Diffusion in Certain Random Lattices," Phys. Rev. 109, 1492 (1958).

2. Baraff, G. A., "Distribution Functions and Ionization Rates for Hot Electrons in Semiconductors," Phys. Rev. 128, 2507 (1962).

3. Bayle, P. and M. Bayle, "Simulation of Secondary Processes in Breakdown in Air," Z. Physik, 266, 275 (1974).

4. Beni, G. and F. Capasso, "Effects of Carrier Drift Velocities on Measured Ionization Coefficients in Avalanching Semiconductors," Phys. Rev. B (1979).

5. Crowell, C. R. and S. M. Sze, "Temperature Dependence of Avalanche Multiplication in Semiconductors," Appl. Phys. Lett. 9, 242 (1966).

6. Davies, A. J., C. J. Evans and P. M. Woodison, "Simulation of the Growth of Axially Symmetric Discharges Between Plane Parallel Electrodes," Computer Physics Communications 14, 287 (1978).

7. DiStefano, T. H. and M. Shatzkes, "Dielectric Instability and Breakdown in S_iO_2 Thin Films," J. Vac. Sci. Technol. 13, 50 (1976).

8. Dutton, J., "A Survey of Electron Swarm Data," J. Phys. and Chem. Reference Data, 4, 577 (1975).

9. Ferzinger, J. H. and H. G. Kaper, Mathematical Theory of Transport Processes in Gases, North-Holland, Amsterdam (1972).

10. Frost, L. S. and A. V. Phelps, "Rotational, Excitation and Momentum Transfer Cross Sections for Electrons in H_2 and N_2 from Transport Coefficients," Phys. Rev. 127, 1621 (1962).

11. Geary, J. M., Ph.D. Thesis (Carnegie-Mellon University, Pittsburgh, Pa., 1973) (unpublished).

12. Geary, J. M. and G. W. Penney, "Charged-Sheath Model of Cathode-Directed-Streamer Propagation," Phys. Rev. A17, 1483 (1978).

13. Hake, R. D. and A. V. Phelps, "Momentum-Transfer and Inelastic-Collision Cross Sections for Electrons in O_2, CO and CO_2," Phys. Rev. 158, 70 (1967).

14. Handbook of Chemistry and Physics, 49th Ed. (1969).

15. Heller, W. R., "Kinetic-Statistical Theory of Dielectric Breakdown in Nonpolar Crystals," Phys. Rev. 84, 1130 (1951).

16. Jasperse, J. R., "Boltzmann-Fokker-Planck Model for the Electron Distribution in the Earth's Ionosphere," Planet. Space Sci. 24, 33 (1976).

17. Kittel, C., Quantum Theory of Solids, John Wiley (1963), p. 135.

18. Kline, L. E., "Effect of Negative Ions on Current Growth and Ionizing Wave Propagation in Air," J. Appl. Phys. 46, 1994 (1975).

19. Kline, L. E. and J. G. Siambis, "Computer Simulation of Electrical Breakdown in Gases: Avalanche and Streamer Formation," Phys. Rev. A5, 794 (1971).

20. Kubo, R., Lectures in Theoretical Physics, Vol. 1, Boulder, Colorado, Interscience, New York, 1959.

21. Latour, M. in "International Symposium on Electrets and Dielectrics," pp. 239-254, published by Academia Brasileira Ciencias, Rio de Janeiro (1977).

22. Loeb, L. B., Basic Processes of Gaseous Electronics, University of California Press, Berkeley (1955).

23. McKay, K. G., "Avalanche Breakdown in Silicon," Phys. Rev. 94, 877 (1954).

24. Meek, J. M. and J. D. Craggs, editors, "Electrical Breakdown of Gases," John Wiley & Sons, New York (1978).

25. Mott, N. F. and E. A. Davis, Electronic Processes in Non-Crystalline Materials, Clarendon Press, Oxford, 1971.

26. Nigam, B. P., M. K. Sundaresan and T. Y. Wu, "Theory of Multiple Scattering: Second Born Approximation and Corrections to Moliere's Work," Phys. Rev. 115, 491 (1959).

27. O'Dwyer, J. J., The Theory of Electrical Conduction and Breakdown in Solid Dielectrics, Clarendon Press, Oxford, 1973.

28. Okuto, Y. and C. R. Crowell, "Energy-Conservation Considerations in the Characterization of Impact Ionization in Semiconductors," Phys. Rev. B8, 3076 (1972).

29. Raether, H., Electron Avalanches and Breakdown in Gases, Butterworths, Washington, (1964).

30. Reininghaus, W., "Calculation of Streamers in Gaseous Discharges," J. Phys. D., 6, 1486 (1973).

31. Seitz, F., "On the Mobility of Electrons in Pure Non-Polar Insulators," Phys. Rev. 73, 549 (1948).

32. Shockley, W., "Hot Electrons in Germanium and Ohm's Law," Bell. System Tech. J. 30, 990 (1951).

33. Shockley, W., "Problems Related to p-n Junctions in Silicon," Solid State Electron. 2, 35 (1961).

34. Strickland, D. J., D. L. Book, T. P. Coffey and J. A. Fedder, "Transport Equation Techniques for the Deposition of Auroral Electrons," J. Geophys. Res. 81, 2755 (1976).

35. TEFZEL Fluoropolymer, DuPont Design Handbook (1973), p. 23.

36. Ward, A. L., "Calculations of Electrical Breakdown in Air and Near-Atmospheric Pressure," Phys. Rev. 138A, 1357 (1965).

37. Ward, A. L., "An Electro-Thermal Model of Second Breakdown," IEEE Trans. Nuc. Sci., Vol. NS-23, 1679 (1976).

38. Wolff, P. A., "Theory of Electron Multiplication in Silicon and Germanium," Phys. Rev. 95, 1415 (1954).

39. Yoshida, K. and H. Tagashira, "Computer Simulation of a Nitrogen Discharge at High Overvoltages," J. Phys. D., 9, 491 (1976).

40. Ziman, J. M., Electrons and Phonons; The Theory of Transport Phenomena in Solids, Clarendon Press, Oxford, 1960.